NOVEL PHOTONICALLY CONTROLLED REFLECTARRAY ANTENNAS FOR BEAM STEERING FOR MILLIMETER WAVE APPLICATIONS

BY

MOHAMMAD REZA CHAHARMIR

A thesis

Submitted to the Faculty of Graduate Studies of the

University of Manitoba

in Partial Fulfillment of the Requirement for the Degree of

Doctor of Philosophy in Electrical Engineering

THE UNIVERSITY OF MANITOBA

FACULTY OF GRADUATE STUDIES

*****

COPYRIGHT PERMISSION

Novel Photonically Controlled Reflectarray Antennas for Beam Steering for Millimeter Wave Applications

BY

Mohammad Reza Chaharmir

A Thesis/Practicum submitted to the Faculty of Graduate Studies of The University of Manitoba in partial fulfillment of the requirement of the degree

Of

DOCTOR OF PHILOSOPHY

This thesis is dedicated to my parents, whose constant support and encouragement made this possible

ABSTRACT

The overall contribution of the research presented in this dissertation is to introduce a novel method for generating a reconfigurable reflectarray that is based on the creation of photoinduced plasma inside the semiconductor. An optically controlled variable slot located on the ground plane of a reflectarray antenna is utilized in the suggested scheme to change the distribution of phase on the surface of the reflectarray. This property can be used for dynamic beam scanning and beam shaping.

A class of novel reflectarray antenna topologies is proposed in this dissertation. The common features of these topologies are the presence of microstrip patches of similar size arranged into a regular lattice configuration on the top layer, and a periodic configuration of slots of variable size on the lower layer that are utilized to adjust the phase shift of the incoming wave.

A method is outlined for the calculation of the plasma profile in the semiconductor and an equivalent uniform plasma profile model is introduced and used throughout the design process. The parameters of this model such as effective conductivity and effective thickness have been evaluated. Two techniques for the calculation of the reflection coefficient of an incident plane wave on a photoinduced plasma structure are presented. An optically controlled three-layer reflectarray is designed and fabricated. A measurement setup based on an optical pulse excitation is presented for the measurement of the reflectarray radiation pattern. The fabrication process of this antenna is presented and the sources of phase error and loss in efficiency are studied. The measurement results demonstrate the potential of the proposed reflectarray antenna to collimate the beam at boresight.

ACKNOWLEDGMENT

It is my pleasure to acknowledge the many people who have contributed to the preparation of this thesis. In particular, I would like to thank my advisor Professor A. Sebak for his continuous support, encouragement and advice throughout the course of this study. Special thanks also goes to Dr. L. Shafai and Dr. D. Thomson for their contribution and their valuable suggestions.

I wish to express my gratitude to my thesis co-advisor Dr J. Shaker for his invaluable comments and for his inspiring and encouraging way of guiding me towards a deeper understanding of physical concepts, during the whole work with this dissertation.

I also would like to express my sincere appreciation to Mr. Cuhaci for all his professional assistance and for providing me with the opportunity and financial support necessary to complete this work. My special thanks goes to all my colleagues in the Radio Science Advanced Antenna Technology branch at CRC for providing a warm and friendly working environment, especially Dr. Ittipiboon and Dr. Petosa for the many useful discussions and taking their time to review my papers and thesis. I would also like to thank Mr. D. Lee and Mr. J. Bradley for their help in fabricating the measurement setups and the reflectarray antennas.

I would like to thank my parents for giving me life in the first place, for educating me in all aspects of the arts and sciences, for unconditional support and encouragement to pursue my interests, even when the interest went beyond boundaries of language and geography.

Finally, I wish to give a very special thanks and all my love to my beautiful wife Katayon. Without her, I doubt that this thesis would ever have been written.

TABLE OF CONTENTS

LIST OF FIGURES

LIST OF TABLES

CHAPTER 1

INTRODUCTION

Intelligent scanning antenna systems have wide applications in millimeter wave radar, imaging and wireless telecommunications. Phased array antenna technology can be a viable candidate for this purpose and has been utilized widely in communications and radar systems due to its flexibility and agility in pointing a highly collimated beam onto an arbitrarily specified direction. One of the important features of the phased array antennas is their electronic beam steering capability that precludes the need for mechanical movement of the antenna. This feature is especially important for large antenna systems where the physical motion of the antenna is impractical. By proper excitation of the individual elements, it is also possible to generate shaped beams. Shaped beams are particularly useful for satellite broadcasting to cover terrestrial regions by a desired footprint.

Despite the increased use of electronically steerable phased arrays and the extensive research into this area, such systems suffer from numerous drawbacks especially in millimeter wave (MMW) band applications. Some of the more generic drawbacks include high loss, cost, complexity, size and weight. Opto-electronic technologies are being proposed as an alternative to overcome these drawbacks. For example, fiber optics could replace the conventional waveguides or coaxial cable for signal distribution and this would not only result in a considerable reduction of the weight and size of the antenna but also allows for lower losses in the signal distribution network, and provides better

interference immunity and wider bandwidth. Also some of the signal processing tasks are benefited from the parallel processing capability of optical systems.

Many different methods have been reported in the literature for beam scanning through the application of optical technology. In 1985, Daryoush *et. al.*[1] introduced the concept of using an optically controlled PIN diode to tune a patch antenna. They suggested shining light directly onto the device to change the PIN diode's impedance characteristics. This approach removed the wire connection and allowed the control device to be placed in the plane of the antenna itself. However application of direct optical illumination of a PIN diode has the disadvantage of the variation of the quality factor (Q) of device as a function of the optical illumination. Cohen and Y. Chang [2], [3] introduced other techniques based on the true-time delay (TTD) method. This method is based on the utilization of optical dispersion as a variable delay line. Variations have been proposed which use multiple wavelength source and switch in different length of dispersive fiber or by using a wavelength tunable laser and single length of dispersive fiber. This method suffers from a number of difficulties including system complexity, optical power loss, signal stability, and system cost.

Currently, an intense effort is being made to reduce the cost and increase power handling capability for commercial applications especially in MMW band. Photo-induced plasma excited in a semiconductor medium is a promising solution for inexpensive beam steering in MMW band [4]-[9]. The key element in these antennas is interaction of MMW with an electron-hole plasma grating created by optical means.

Several antenna designs utilizing this approach have been fabricated and tested. All of these designs are based on one of the following structures:

a) Preliminary attempts to build a photo-controlled MMW antenna employed a leaky wave semiconductor waveguide with a photoinduced plasma grating [10]-[12]. A schematic of this antenna is shown in Fig. (1-1). The antenna consists of a semiconductor substrate and an illumination system. The MMW propagates along the semiconductor substrate. The output beam angle can be controlled by varying the grating period Λ. This is accomplished by changing the grating pattern of photo-masks [13]-[14]. The drawback of this method is that it produces only 1-D beam scanning and also suffers from low diffraction efficiency.

b) The other method is based on first-order diffraction beam generated by photo-induced plasma grating [15]-[17], when a MMW beam passed through a semiconductor plate. By changing period and/or rotating the grating, the output beam can be steered in two dimensions (see Fig. (1-2)). The disadvantage of this method is low diffraction efficiency and narrow beam scanning.

c) The photoinduced plasma can be utilized for generation of reconfigurable antenna [18]. In this method the size and shape of the antenna can be dynamically modified by generating the photoinduced plasma inside the semiconductor. Various antenna shapes could be created in the same wafer by merely reconfiguring the illumination pattern. Since the whole antenna is generated by photoinduced plasma, the antenna is very lossy and efficiency is low for this method.

1.1 Problem description

Since the photoinduced plasma is a lossy material, the loss is the main issue in all conventional optically beam scanning methods based on photoinduced plasma [15]. Beside since all radiating elements are generated by the photoinduced plasma, a high

power optical source is required to generate the photoinduced plasma inside the semiconductor. Also these antennas can steer the beam in one or two dimensions with a narrow beam scanning angle. The main motivation and purpose of this thesis is to introduce a new photonically technique for beam scanning and beam shaping in MMW band antenna based on photoinduced plasma in silicon. The proposed technique in this thesis is based on varying the slot length by photoinduced plasma, which establishes the phase shift mechanism in a reflectarray configuration [19]. In this scheme an optically controlled slot located on the ground plane of a reflectarray antenna is utilized to change the phase distribution on the surface of the reflectarray that can be used for dynamic beam scanning and beam shaping. This method overcomes many of the limitations associated with the conventional approaches. In this technique since the reflectarray partially exists, and optical illumination in each cell is used to perturb or modify an existing conductive pattern therefore, less area of photoinduced plasma compared to conventional photoinduced plasma grating (PIPG) methods will be generated and lower loss and higher efficiency can be achieved. Also, less area for the photoinduced plasma implies lower optical power requirements. A wide variety of beam shapes can be achieved by controlling the phase distribution on the surface of the optically controlled reflectarray.

In this thesis also a theoretical framework is introduced to investigate optical-microwave interaction in semiconductor substrate for antenna applications. Our objective is to introduce photoinduced plasma profile inside the silicon to analyze photoinduced plasma periodic structures.

1.2 Document outline

This thesis is organized into 7 chapters. The first chapter states the research motivation and presents the problem description. Chapter 2 gives an overview of the reflectarray. The existing theoretical frameworks in the analysis of periodic structures will be discussed in this chapter. A method for the calculation of the reflectarray radiation pattern is presented and different techniques for designing the reflectarray antenna are introduced. The chapter will be closed by studying some of the main characteristics of the reflectarray such as efficiency, bandwidth and polarization.

A novel method for controlling the phase distribution in reflectarray antenna based on slot of varying size in ground plane is introduced in chapter 3. In the chapter three novel techniques for the design of this class of reflectarrays are presented and an investigation is carried out on their performance characteristics such as bandwidth, gain, and phase sensitivity. A mechanically controlled method for beam scanning based on slots of varying size is also presented. Chapter 4 describes the photoconductivity and methods for analyzing the plasma profile inside the semiconductor. An equivalent uniform profile for plasma is derived and the parameters of this model such as effective conductivity and effective thickness is calculated. A non-destructive method for the measurement of the carrier recombination lifetime in silicon based on a waveguide technology is introduced and measurement results are presented in this chapter. Two techniques for the calculation of reflection coefficient of an incident plane wave in the photoinduced plasma structures are presented in chapter 5. A measurement method based on waveguide technology is introduced for the measurement of the profile of plasma inside a silicon wafer. In this chapter a surface impedance method based on MOM is introduced for analyzing the

photoinduced plasma grating structures. A novel photonically technique for changing the slots beneath the patches and adjusting the phase shift of the radiating elements of reflectarray is presented in chapter 6. In this method the slot length size in each unit cell is changed by generating the photoinduced plasma beneath the slot. A prototype is designed for the measurement of the radiation pattern of this antenna. In this prototype an optical pulse source is used for the illumination of the reflectarray and the effect of optical illumination density on radiation pattern and efficiency of the antenna are studied. Finally chapter 7 summarizes the thesis, provides conclusion for this research work, presents our contributions and outlines future study on this topic.

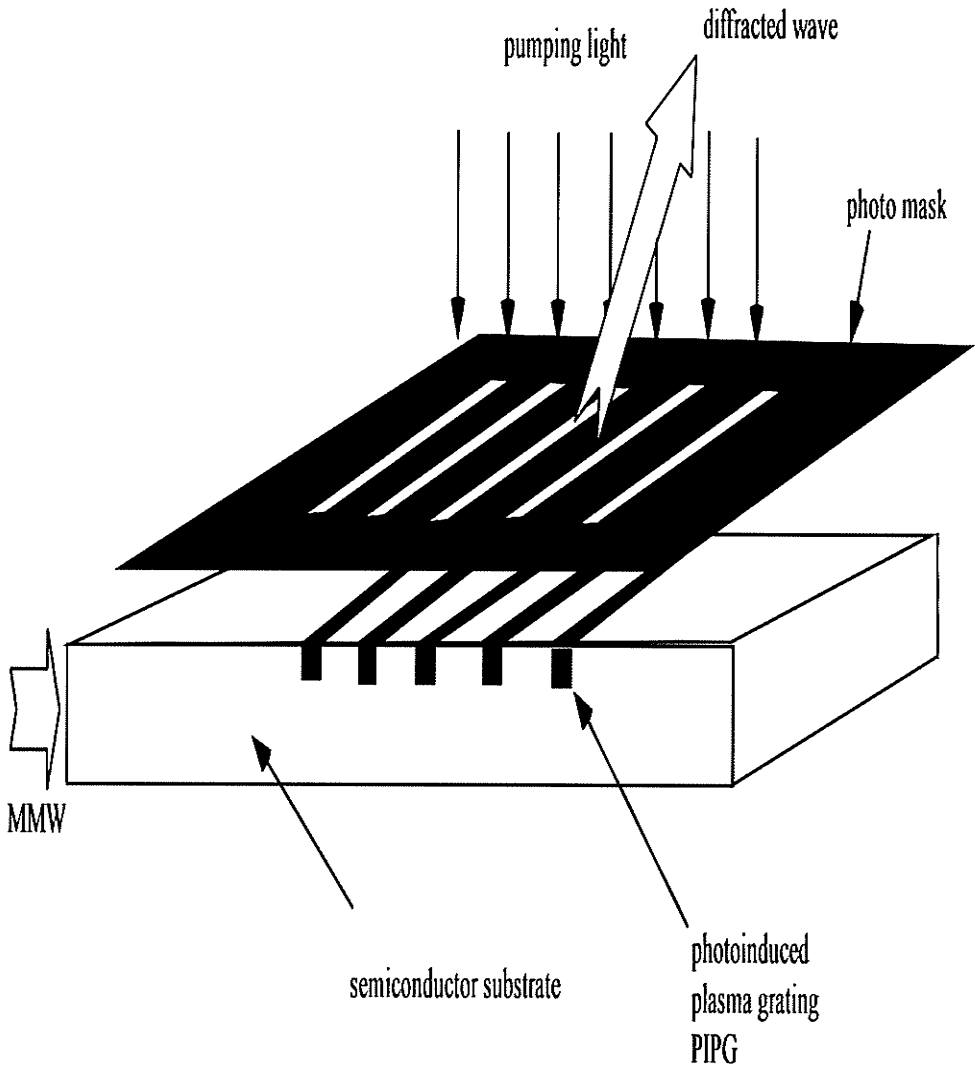

Figure1-1: Leaky wave semiconductor waveguide with photoinduced plasma grating

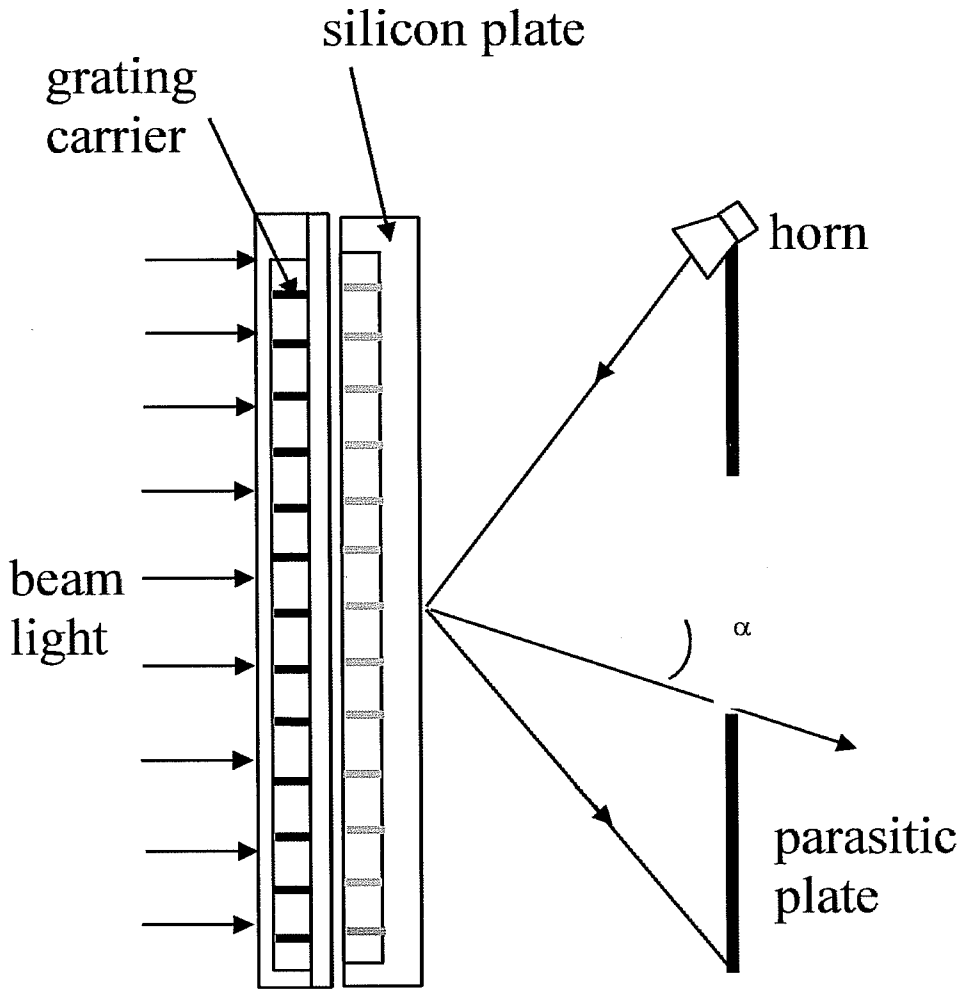

Figure1-2: Schematic of optical -control MMW scanning antenna based on first-order diffraction by photo-induced plasma grating

CHAPTER 2

MICROSTRIP REFLECTARRAY ANTENNAS, ANALYSIS AND DESIGN

Introduction

High gain antennas are widely used in microwave and millimeter wave applications. Only quasi-optical antennas, such as parabolic reflectors, lenses, array antennas and planar reflectarray antennas meet most of these requirements. A reflector antenna utilizes a primary feed to illuminate a reflective surface. In this case the reflective surface transforms the energy from the primary horn into a desired shaped beam, which can be a plane wave in its simplest implementation. The direction and shape of the radiation pattern is determined by the shape of the reflector surface.

In contrast an array utilizes discrete elements to sample the aperture amplitude and phase distribution. Typically, corporate feed network is used as a mean of combining the signals that are received by the array elements.

A planar reflectarray combines the features of reflector and array technologies and was first introduced in 1963 by Berry et al. [20]. A reflectarray is an array of antenna elements, which is illuminated by a primary feed horn instead of a conventional transmission line network that is used in the case of array antennas. The reflective surface consists of an array of discrete radiating elements that receive and then re-radiate the

incident energy. The geometry of the constituent antenna elements is adjusted to achieve the required phase transformation for the realization of the desired antenna radiation pattern. Reflectarray technology demonstrates several advantages as compared to phased array or conventional reflector technologies. The absence of the complex feed network as opposed to conventional phased arrays removes the feed loss that can be quite significant in the millimeter frequency band. Also the parabolic reflector can be replaced by a planar reflectarray surface that is composed of elementary radiators such as microstrip patch or waveguide, which reduces the mechanical complexity of the structure and entails added functionalities such as multifrequency, multipolarization, power combining, etc., features.

Microstrip patch, spiral, and waveguide are among the radiating elements that have been used in the past as the constituent elements of reflectarrays. However, the low-profile printed reflectarray is a fairly new concept, and consists of a very thin flat-grounded substrate onto which a lattice of microstrip patches is etched and illuminated by feed [21]. A feed antenna illuminates the array whose individual elements are designed to scatter the incident field with the appropriate phase to form a planar or any other desired phase front.

In this chapter, subsequent to a review of the existing methods of analysis of the reflectarray antenna, general configurations for the implementation of such an antenna are described. A method for the calculation of the reflectarray radiation pattern is presented. This chapter is closed by considering the efficiency and losses in reflectarrays.

2.1 Review of the existing methods for analysis of periodic structures

Since reflectarray antenna is a quasi-periodic structure, the analytical tools that have been developed for the characterization of periodic structures can be used in its analysis. Methods for the computational characterization of periodic structures have been a subject of continued interest in recent years. The formulation for scattering by periodic structures usually invokes Floquet's theorem leading to an equation for the patch current upon enforcement of the required boundary conditions on the array elements. Initially, Floquet modes were used to decompose the scattered field into discrete component in the angular spectrum [22]. The boundary conditions are used to obtain the amplitude of each individual Floquet mode. In other words, the modal field equations defining the field quantities satisfy Helmholtz wave equation exactly and are solved subject to boundary conditions. Incorporation of this assumption into various computational schemes will lead to different methods for the analysis of periodic structures that are outlined briefly in the following:

2.1.1 Green's function method

Electromagnetic scattering from periodic structures may be formulated in term of an integral equation that has periodic Green's function as its kernel [23], [24]. The resulting integral equation is converted into a matrix equation using the method of moment. This approach is appealing due to its generality and versatility in the analysis of multilayer double periodic structures. Green's function can be used for the analysis of finite array. For moderate sized arrays (up to a few hundred elements), it is possible to use a rigorous element-by-element analysis, where the computation of the interaction between elements has been optimized in order to keep the numerical effort reasonable [25], but this

technique can not be extended to larger arrays. The usual approach for large periodic structures is based on an infinite array approach. However, this method does not give good predictions of the behavior of radiating elements close to an edge or a corner of the array as edge effects are neglected. Some methods have been developed to include the edge effects in the infinite array approach, through the convolution of the infinite array solution with an appropriate window function [26].

The choice of basis functions is critical for the accuracy and convergence of Green's function method. Various types of basis function can be used to represent the unknown current distribution of the cell elements. In order to minimize the number of basis functions it is desirable that these functions satisfy the appropriate edge condition. In general there are two categories of basis functions in the context of method of moment: the entire domain and subdomain basis function [27], [28]. The entire domain basis function can be used for cell elements such as dipole, square patch, circular patch, cross and Jerusalem cross, etc. However to handle periodic structure that are compromised of arbitrary-shaped aperture or patches, subdomain basis functions have been found to be more versatile than entire domain functions. It is also demonstrated in [29] that a proper choice of basis functions will accelerate the convergence of the algorithm.

The accuracy of Green's function methods is very good, since approximation only occurs when the integral equation governing the current distribution is solved using method of moment. However, the formulation of this method is difficult if the structure is nonplanar or does not exhibit the kind of geometry that is compatible with the three commonly used coordinate systems. This method is also relatively inefficient for handling inhomogeneous substrates.

2.1.2 Finite difference method

The finite different method has strong appeal for modeling periodic structures. However, there are fundamental difficulties in applying periodic boundary conditions in the time domain. Several techniques have been proposed for this problem [30]. Some methods approximate the problem by using multiple unit cells, while others use a single frequency to allow the periodic boundary condition to be applied in the frequency domain. Because of its versatility, the finite difference algorithm appears to be attractive for analyzing the periodic structures with inhomogeneous and complex geometries.

As compared to the Green's function method, the finite difference approach approximates both Helmholtz and the boundary conditions using difference quotients at discrete points. This discretization of the various equations governing the field behavior can be less accurate when compared to Green's function method of moment approach.

Several techniques have been proposed in the context of finite difference method for the analysis of periodic structures. These techniques can be divided into two classes [31]. In first class, which is called field transformation method, a field transformation is carried out to eliminate the need for time-advance data. The transformed field equations are then quantized and solved using finite different techniques. All of the other techniques are listed in second category and called direct field method. These methods work directly with Maxwell's equations subject to periodic boundary conditions. The issue of numerical stability has received significant attention in all of these methods.

2.1.3 Finite element method

Over the last thirty years, the finite element method has been established as a powerful and widely employed numerical technique for solving electromagnetic problems. A very vigorous activity has been recorded in the area of applying the finite element method to various 2-D and 3-D electromagnetic field computations promoting this method as a powerful and versatile numerical technique for electromagnetic analysis. However this method suffers from some drawbacks such as long computation time and large memory requirements.

There are several techniques for analyzing periodic structures using the finite element method. One approach has been proposed by Lou et al. [32], which combines the finite element method with Fourier modal expansion. However it should be noted that this method is not general as it is only allows one to analyze those directions of propagation of the incident wave plane wave that are related to the periodicity of the structure. The method that was proposed by Polosi [33], employs the FEM but uses the Floquet modal expansion, instead of Fourier modal expansion. In this method the periodic structure can be completely arbitrary as to its form and material properties.

Linked Boundary Conditions (LBCs) is one of the more recent techniques which addresses a new class of problems such as the inclusion of active devices, by specifying a relationship in the fields between two or more boundaries. By imposing these boundary conditions, it is sufficient to model only one radiating element. The periodicity of the array is maintained through the imposition of boundary conditions. LBCs save computer time and memory in modeling long, uniform structures and periodic structures. Periodic LBCs allow multiple master-slave boundaries dictated by a phasor relationship.

Designers can now analyze a unit cell of a phased array to extract the active element factor and impedance and explore new designs to detect array blind zones, polarization behavior, and grating lobes.

2.1.4 Waveguide simulator

A classical experimental procedure for determining the active element impedance, or equivalently the embedded element factor, is known as the waveguide simulator technique. By placing one or more elements within a waveguide one can simulate an infinite array due to the imaging properties of the metallic waveguide walls.

Recently an equivalent unit cell waveguide approach (WGA) has been presented for the analysis of the multilayer periodic structure. [34]. Problem set-up using periodic boundaries follows closely that of the waveguide simulator. In this method one or more elements are placed within a unit cell and the walls of the unit cell are defined as perfect electric conductors (PEC) and perfect magnetic conductors (PMC) as shown in Fig. (2-1).

Symmetry planes, orthogonal to the E-field, which run horizontally, can be replaced with perfect electric walls. This can be justified by considering that identical currents flowing above and below these planes would result in the cancellation of the tangential electric field. Similarly, vertical symmetry planes, parallel to the E-field can be replaced with perfect magnetic walls. A plane wave traveling in the z-direction with the electric field polarized along the y-axis will induce a current on the unit-cell as describe. Therefore, the unit cell can be utilized to analyze the structure. This method was utilized in this dissertation and finite element method was used to analyze this waveguide simulator in the context of HFSS^{TM} [35], which is commercial software.

2.2 Radiation analysis of the microstrip reflectarray

Different methods have been introduced for the calculation of the radiation pattern of a microstrip reflectarray. In this dissertation a fairly accurate method presented by Huang [36] is used.

Consider a planar reflectarray consisting of M×N microstrip patch elements that are illuminated non-uniformly by a low-gain feed located at R_f as shown in Fig. (2-2). The radiation pattern of the structure along the $\hat{u}$ direction will be of the form:

$$E(\hat{u}) = \sum_{m=1}^{M}\sum_{n=1}^{N} F(\vec{r}_{mn}.\vec{r}_f) A(\vec{r}_{mn}.\hat{u}) A(\hat{u}.\hat{u}_0) e^{\{-jk[|\vec{r}_{mn}-\vec{r}_f|+r_{mn}.\hat{u}]+j\alpha_{mn}\}} + \vec{E}_r + \vec{E}_d \qquad (2\text{-}1)$$

where "$F(r_{mn}.r_f)$" represents the feed radiation pattern on the *mnth* element, "$A(r_{mn}.\hat{u})$" is the radiation pattern expression for the microstrip patch on the flat plate, r_{mn} is the position vector of *mn*th patch, u_0 is the main beam direction, and α_{mn} is the phase shift introduced by *mn*th element. E_r and E_d are, the specular reflected field from the flat ground plane and diffracted field from the edges of the ground plane, respectively [37].

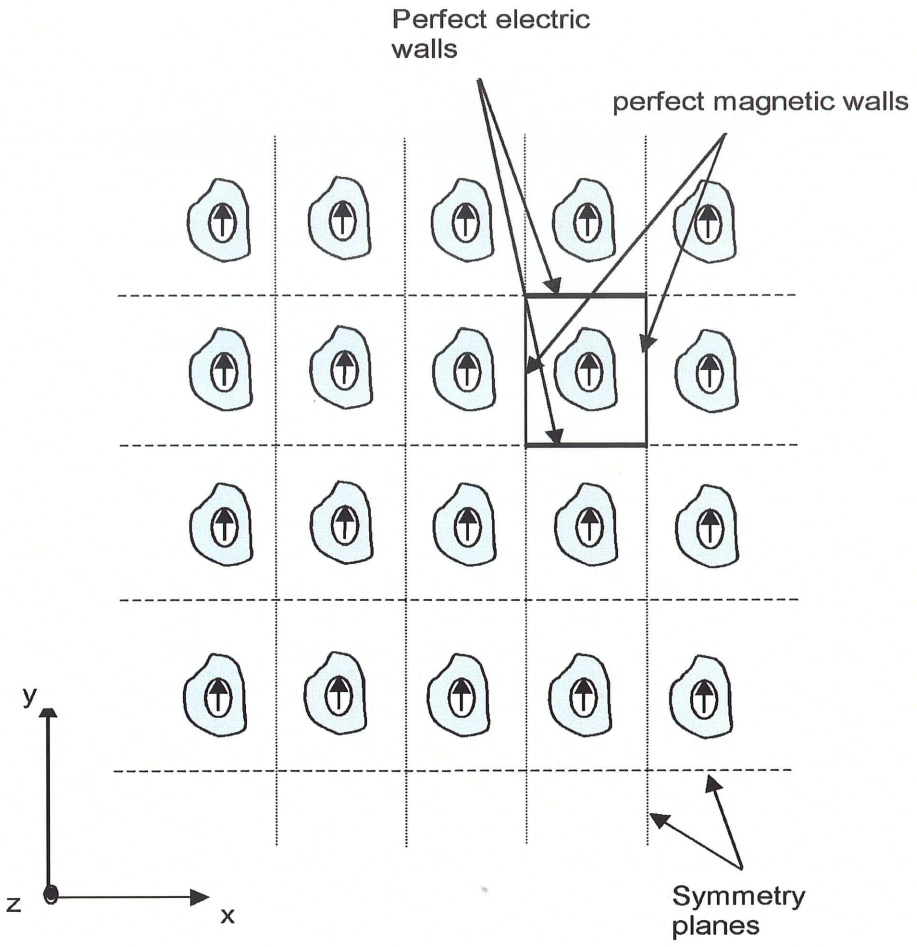

Figure 2-1: Schematic top view of a planar periodic structure with reflection symmetry.

In this analysis the feed function F is represented by $cos^q(\theta)$ function and for the upcoming set of simulations q=12 was set for E and H-planes, respectively. For the pattern function A of single rectangular microstrip patch on the flat plate, a simple model using the dual- slot theory [38] is employed. One argument for the validity of this approach is that the mutual coupling between elements is very small for thin microstrip substrate so the effect of neighboring patches is negligible. In this model the radiation pattern of single element (no mutual coupling effect) with results in close agreement with the infinite array model was considered.

Fig. (2-3) shows the measured and calculated radiation patterns for a reflectarray with variable patches. The design consisted of 31 ×31 patches with constant length=3mm and variable width. The antenna substrate was 0.5 mm thick and ε_r=2.2.

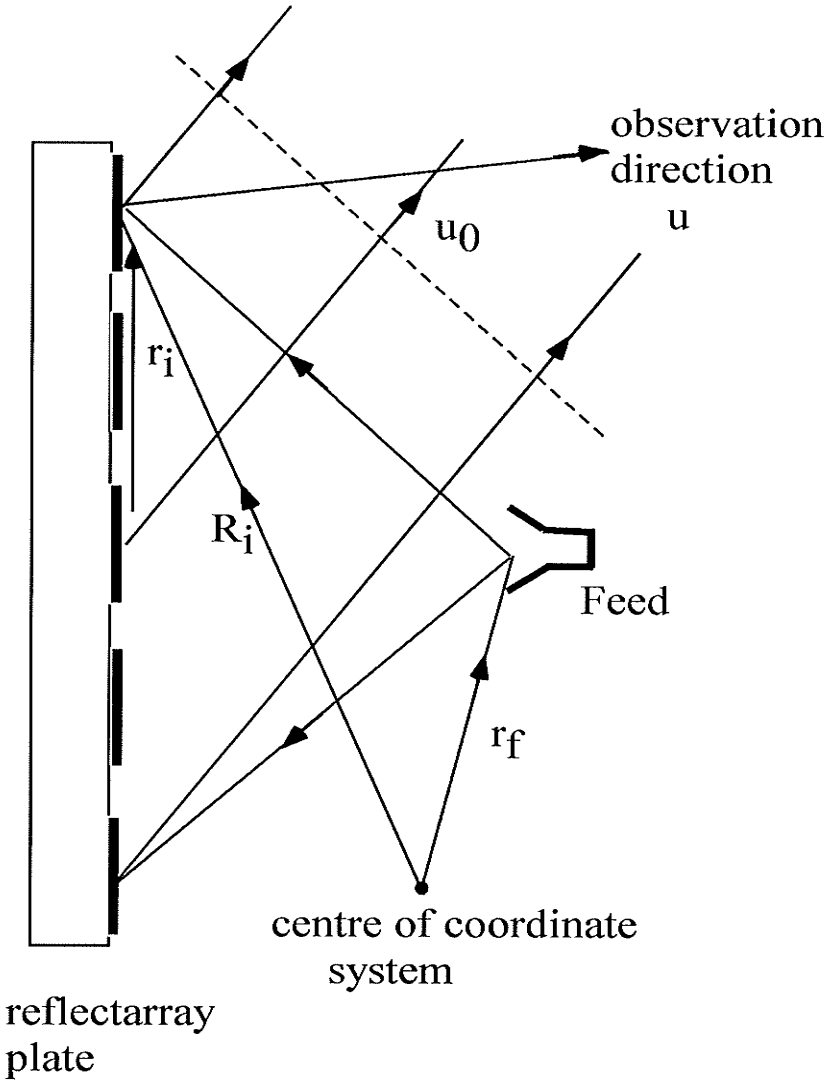

Figure 2-2: Geometry of microstrip reflectarray.

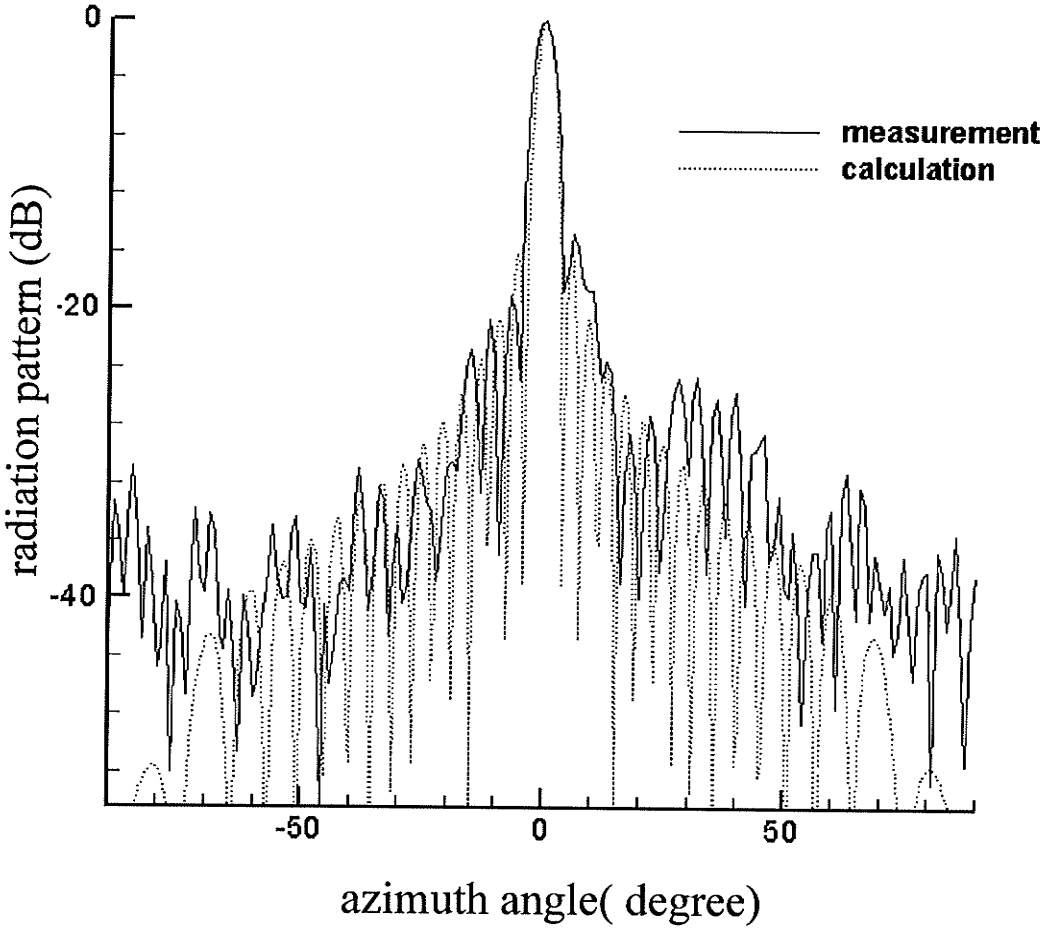

Figure 2-3: Measured and calculated E-plane radiation pattern for a reflectarray with F/D=0.9

2.3 Reflectarray design consideration

Microstrip reflectarray transforms the phase of the field radiated by the feed into a desired phase front or vice versa. This is accomplished by appropriate adjustment of the phase response of individual patches. The required phase shift ϕ_i for element "i" is determined by [39]

$$\phi_i = 2\pi N + k_0(R_i - r_i.r_0) \tag{2-2}$$

where R_i is the distance from the phase center of the feed to *ith* element, r_i is the vector from the center of array to the *ith* element, and r_0 is unit vector along the direction of the main beam. The key feature of microstrip reflectarray implementation is the method that is used to adjust the phase of the wave scattered by each constituent element. Various versions of printed reflectarray have been developed. The techniques for the adjustment of the phase of the radiated field are discussed briefly in the following:

- Variable stub length [40]: This flat reflector antenna is composed of a thin slab of dielectric back by thin ground plane onto which microstrip patches of similar size are etched. Each patch is loaded with an open stub. The phase of the scattered wave can be adjusted by changing the stub length.

- Patches of variable size [41]: This type of reflectarray is consists of a thin-grounded substrate onto which patches of variable length are etched. In this case the phase adjustment can be achieved by changing the patch size.

- Microstrip reflectarray with variable rotation angles [42]: In this method the phase variation can be achieved by rotating the patches on the surface

of reflectarray. This method is solely applicable to CP reflectarray structures fed by a CP feed.

- Aperture coupled reflectarray [43]: In this method the reflectarray is composed of microstrip patches of similar size that are coupled to the strip of variable length through a slot in the ground plane. The phase adjustment can be achieved by changing the strip length.

A class of novel reflectarray antenna topologies is also proposed in this dissertation. The common features of these multilayer printed reflectarray topologies are the presence of microstrip patches of similar size arranged into a regular lattice configuration on the top layer and periodic configuration of slots of variable size on the lower layer that are utilized to adjust the phase shift of the incoming wave. This configuration is discussed in more detail in the next chapter.

2.4 Phase errors

Phase errors incurred in the design process are due to the fact that the entire 360^{o} can not be achieved by the variation of the unit-cell. This extent of phase variation depends on the thickness and permittivity of the substrate. The other source of phase error is random phase errors resulting from fabrication tolerances. These two types of phase errors reduce the gain and the efficiency of reflectarray.

A source of error that occurs in the design process is the application of the infinite periodic structure model to obtain phase variations. However because only small number of cells are on the edge of reflectarray, the error due to infinite periodic structure

assumption can be considered of second order. It is evident that the accuracy of the model is reduced as we approach the periphery of the reflectarray. Also, another departure from the infinite periodic structure model is the unequal size of the reflectarray cell elements. Unfortunately, this error cannot be quantified without simulating the finite reflectarray, which is an impractical endeavor considering the limited memory and CPU time available on most platforms. Finally, normal incidence of the plane wave that is assumed in the design stage is only valid for the central region of the reflectarray and can be a potential source of error. However, the effect of this error can be minimized by partitioning the reflectarray into various regions based on having relatively constant angle of incidence for each region.

2.5 Polarization error

In the process of the simulation of a center fed reflectarray, it is assumed that all the unit cells are illuminated by a plane wave with the same electric field polarization as in the boresight direction of the feed. This assumption is nearly accurate for the unit cells in the central region of the reflectarray, however as we approach the periphery of the reflectarray the polarization of incident field changes compared to the central region of the reflectarray. This polarization-mismatch reduced the efficiency of antenna.

2.6 Conclusion

Microstrip reflectarray antenna is an appealing candidate where high gain antenna is required, avoiding high losses associated with feed network of microstrip phased arrays and bulky structure of reflector antennas. A number of numerical methods for the analysis of periodic structures were reviewed in this chapter. Different versions of printed

reflectarray antennas were described and some of the sources of error in the design and fabrication stages were pointed out. In next chapter a class of novel reflectarray antenna topologies based on slots of varying length size will be presented.

CHAPTER3

REFLECTARRAY ANTENNA WITH SLOTS OF VARYING LENGTH ON THE GROUND PLANE

Introduction

The main objective of the present research is the development of a non-mechanical MMW scanning technique, which employs a light-modulated photoinduced method, based on reflectarray technology. A class of novel reflectarray antenna topologies that are amenable to photoinduced technology are proposed in this chapter [44]. The common features of these multilayer printed reflectarray topologies are the presence of microstrip patches of similar size arranged into a rectangular lattice configuration on the top layer, and a periodic configuration of slots of variable size on the lower layer that are utilized to adjust the phase shift of the incoming wave. Different topologies arise by the addition of a ground plane below the slot layer in order to reduce the back lobe radiation, and the additional dielectric layers between the slots and patches in order to improve the bandwidth performance.

Three novel techniques for the design of this class of reflectarrays are presented in this chapter and an investigation is carried out as to their performance characteristics such bandwidth, gain, and phase sensitivity. A mechanically controlled method for beam

scanning based on slots of varying size is also presented [45]. This chapter is closed by conclusion remarks.

3.1 Reflectarray with slots of variable length in the ground plane

The novel reflectarray that is the subject of this chapter is composed of radiating patch elements of identical size on the top layer and slots of variable length in the ground plane. The required phase shift at each position on the reflectarray surface is obtained by adjusting the slot length on the ground plane. Fig. (3-1) shows a schematic view of this configuration.

The incident wave from the feed excites the dominant resonant mode of the microstrip patches. When there is no slot on the ground plane, each patch radiates the energy at its resonant frequency. The presence of the slots acts as an inductive loading of the patches, which introduces a phase shift in the patch response. The inductance of each slot depends on its length. A circuit model for this configuration has been shown in Fig. (3-2). When there is no slot on the ground plane, the resonance frequency is dictated by the inductance and capacitance generated by patches. However when there are slots on the ground plane the resonance frequency is dictated by the inductance that is generated by the slot. The analysis was carried out using Ansoft HFSS software with periodic boundary conditions. An infinite periodic structure that is illuminated by a plane wave has been considered throughout these simulations as explained in section (2.6).

The required phase shift (ϕ) was realized by adjusting the slot length. A patch-slot reflectarray was designed to operate at 26 GHz. The antenna substrate was 0.020" thick with $\varepsilon_r = 3.0$ (3003 Rogers material). The design consists of 25 × 25 patches with fixed

dimensions of 3.2 mm × 2.3 mm, the unit cell size was set at 6 mm × 6 mm. The slot width was set at approximately $\lambda/20$ to mitigate the leakage into the lower half space and achieve a good phase variation by changing the slot length. The slot width was set at ds=0.2mm for this example and the antenna was designed for F/D = 0.9. To obtain the phase versus slot length variation, infinite periodic structure approximation was used and it was assumed that the structure is illuminated by a plane wave normal to its surface. The simulation result is shown in Fig. (3-3) that shows close to 340^{o} phase swing for the whole range slot length variation.

The reflectarray was centre fed by a pyramidal horn, located, 13.5 cm away from its centre. The feed location was chosen to maximize the illumination efficiency. The far field radiation pattern was measured in a far field anechoic chamber in the frequency band of 24 GHz to 26.5 GHz. The maximum gain of 28.65 was observed at 26 GHz, which is equivalent to 38% radiation efficiency. A typical plot of H-plane radiation pattern for both co-polarization and cross polarization is shown in Fig (3-4). Apart from slightly higher side-lobe level, the radiation pattern in the E-plane resembles the H-plane radiation pattern.

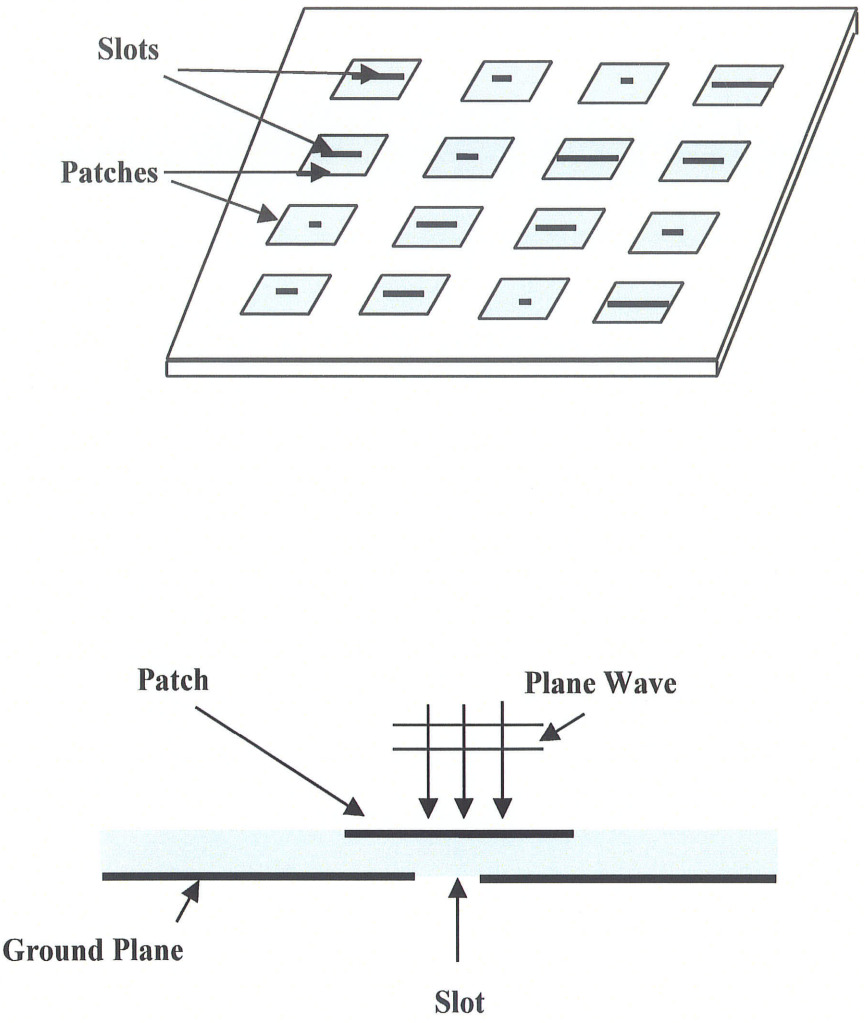

Figure 3-1: Microstrip reflectarray with the variable slot on the ground plane

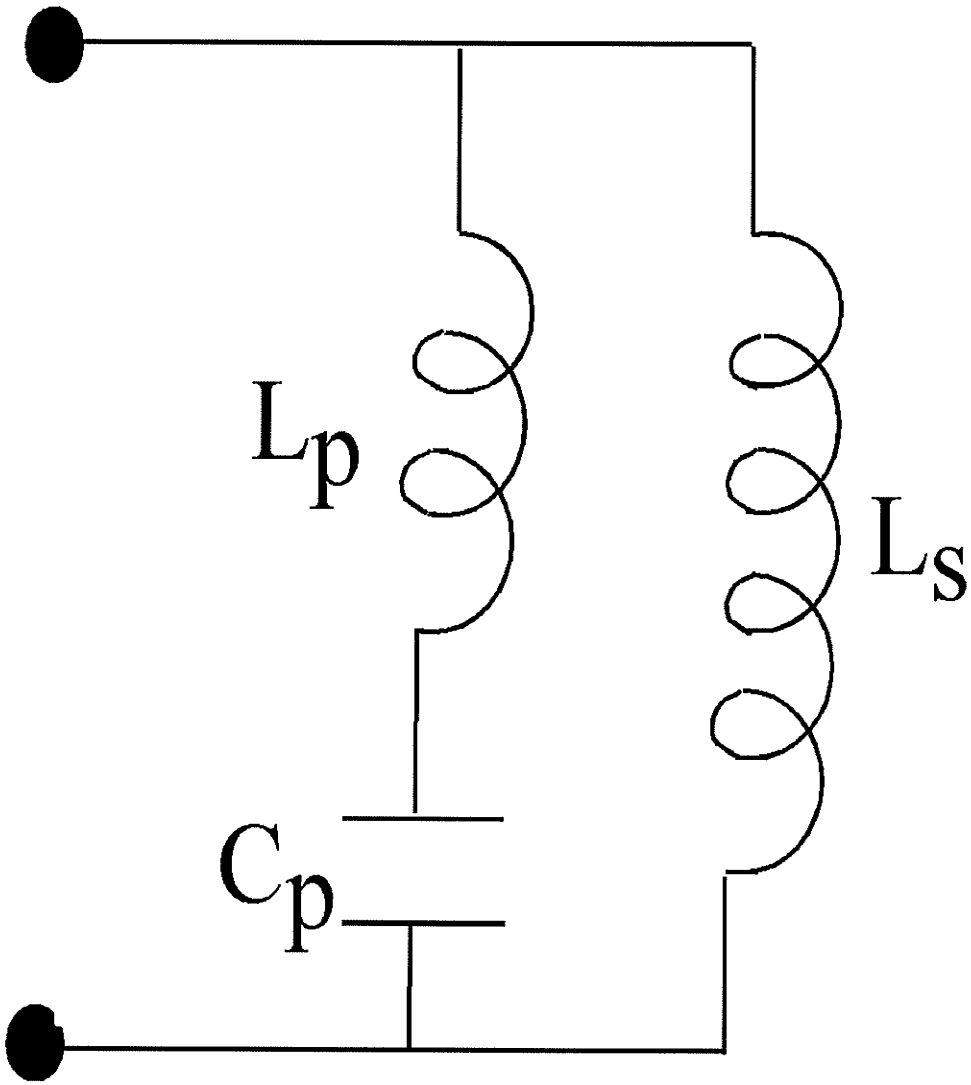

Figure 3-2: A circuit model for the reflectarray with slots of varying length in ground plane

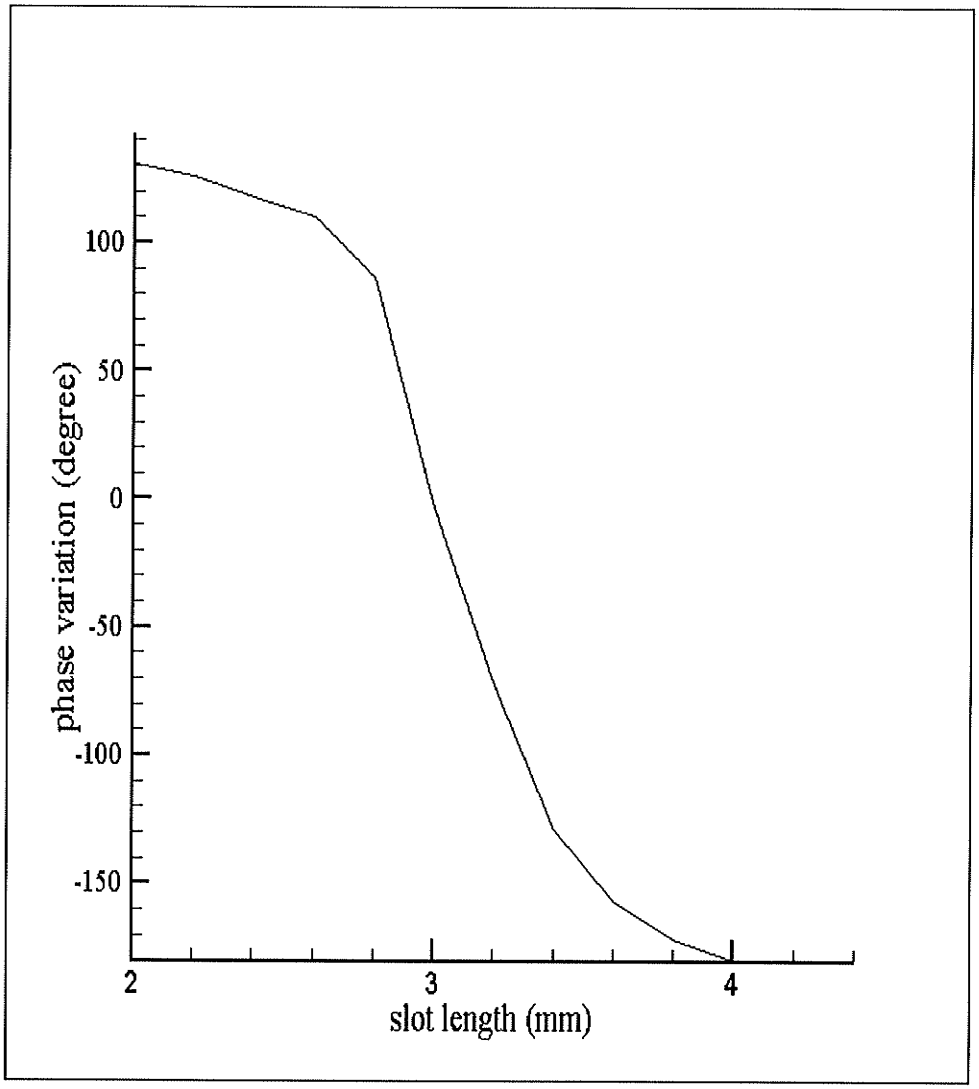

Figure 3-3: Phase shift of the reflected wave versus the slot length

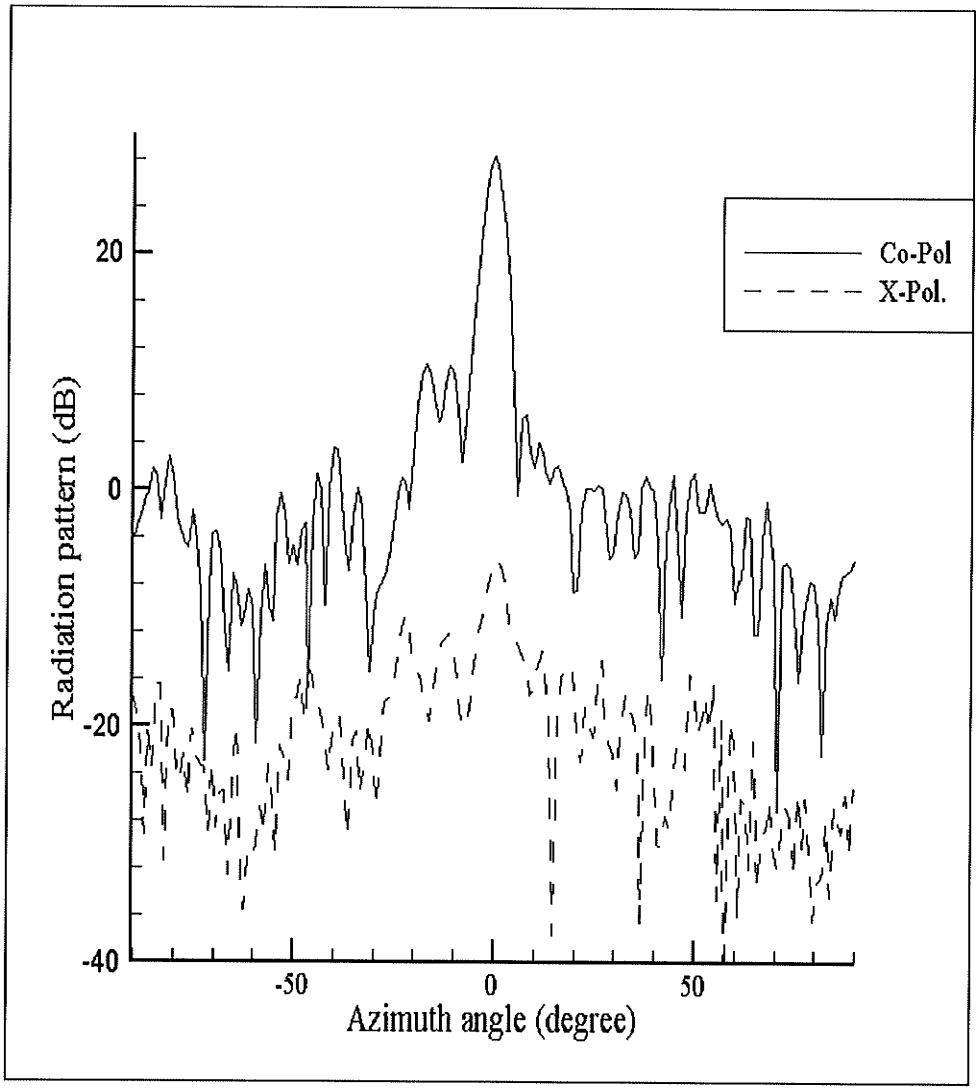

Figure 3-4: Measured Co-Pol. and X-Pol. radiation patterns of the one-layer reflectarray antenna, f=26GHz.

3.2 Reflectarray with two layers and variable slots in the middle plane

The difference between this configuration and the previous case is the presence of a ground plane beneath the slot layer, which prevents the leakage of power into the lower half space and also isolate the upper half space from the lower half space. This isolation is very useful for our application of photonically controlled beam scanning. Fig. (3-5) shows a schematic view of this reflectarray.

HFSS was used in the design of an antenna based on this configuration at 30 GHz. The phase variation (ϕ) is implemented by changing the slot length. The substrate thickness for the upper and lower substrates was set at 0.020" and 0.010", respectively. The design consisted of 31 × 31 patches with the fixed dimensions of 3.2 mm × 2 mm, the unit-cell size was 5 mm × 5 mm, and slot width was d_s = 0.2 mm. The simulated phase variation versus slot size for three different frequencies is shown in Fig. (3-6). It can be seen that a larger phase shift can be realized compared to the configuration described in the previous section, which leads to an improved phase efficiency figure for the reflectarray.

Different argument can be made to demonstrate that surface wave is not supported in the substrate behind the slots in this reflectarray. Some of these arguments are as follow:

1. Simulation of infinite periodic structure in HFSS indicates that the amplitude of the S_{11} for all frequency bands and different slot lengths is 0 dB, which implies that there is no surface wave excitation inside the substrate behind the slots.

2. Transmitted power through slot can be calculated according to the following equation:

$$P_{trans} = \iint_{s} (\vec{E} \times \vec{H}^{*}).\hat{n}ds \tag{3-1}$$

Where s is the surface of the slot, E and H are the electric and magnetic fields on the surface of the slot and n is the unit vector normal to the slot surface.

Table (3-1) shows the calculated transmitted power for single layer and two-layer reflectarrays at three frequencies. The incident power is 1 W. As shown in this figure the transmitted power for two-layer is very low and almost negligible.

Slot length (mm)	Transmit power (W) Single layer f = 30GHz	Transmit power (W) Two-layer f=29GHz	Transmit power (W) Two-layer f=30GHz	Transmit power (W) Two-layer f=31GHz
0.2 ×0.6	6.05×10^{-6}	5.33×10^{-18}	9.39×10^{-18}	1.23×10^{-18}
0.2 ×1.6	4.67×10^{-5}	4.80×10^{-17}	4.15×10^{-17}	3.25×10^{-17}
0.2 ×2.0	3.25×10^{-4}	4.21×10^{-16}	1.96×10^{-16}	4.22×10^{-16}
0.2 ×2.4	9.45×10^{-4}	5.24×10^{-16}	2.06×10^{-16}	4.47×10^{-16}
0.2 ×2.6	1.25×10^{-3}	6.96×10^{-16}	2.80×10^{-16}	6.63×10^{-16}
0.2 ×3.0	5.98×10^{-3}	8.67×10^{-16}	7.28×10^{-16}	9.76×10^{-16}

Table (3-1) Transfer power from the slots for single layer and two-layer reflectarrays

3) The small electrical size of the substrate thickness at the operating wavelength and imparting different phase values by the slots on the incoming wave exclude the possibility of guided wave excitation. Also, low level of antenna radiation in the endfire direction and lack of any grating lobe in radiating zone verify the absence of guided wave.

The radiation pattern was measured in the frequency band of 28 GHz - 31GHz. A maximum gain of 29 dB with an efficiency close to 40% occurred at 30 GHz. A typical plot of the H-plane pattern for both co-polarization and cross-polarization for F/D = 0.9 is shown in Fig. (3-7). The E-plane pattern is similar to the H-plane pattern.

3.3 Reflectarray with three layers and variable slots in the middle plane

The structure presented in this section is the same as the two-layer reflectarray mentioned in previous section, except for the additional layer between the variable slots and upper microstrip patch layer. This additional layer improves the bandwidth and radiation pattern. Fig. (3-8) shows a schematic view of this reflectarray. The antenna was designed based on this configuration to operate at 30 GHz. The phase variation (ϕ) is implemented by changing the slot length. The shape of the curve for phase variation versus the slot length is similar to Fig. (3-6) except that the slope for this configuration is smoother. The substrate thicknesses for the upper, middle and lower substrates were set at 0.020", 0.025" and 0.08", with permittivities of 2.2, 10.2 and 1, respectively. The design consisted of 31 × 31 patches with the fixed dimensions of 3.2 mm × 2.8 mm, the unit - cell size was 5 mm × 5 mm, and slot width was d_s = 0.2 mm. The radiation pattern was measured in the frequency band of 28 GHz -31 GHz. A gain of 30.5 dB was obtained at 30 GHz, which translates into 50% efficiency. A typical plot of the H plane pattern for both co-polarization and cross-polarization for F/D=0.9 is shown in Fig. (3-9).

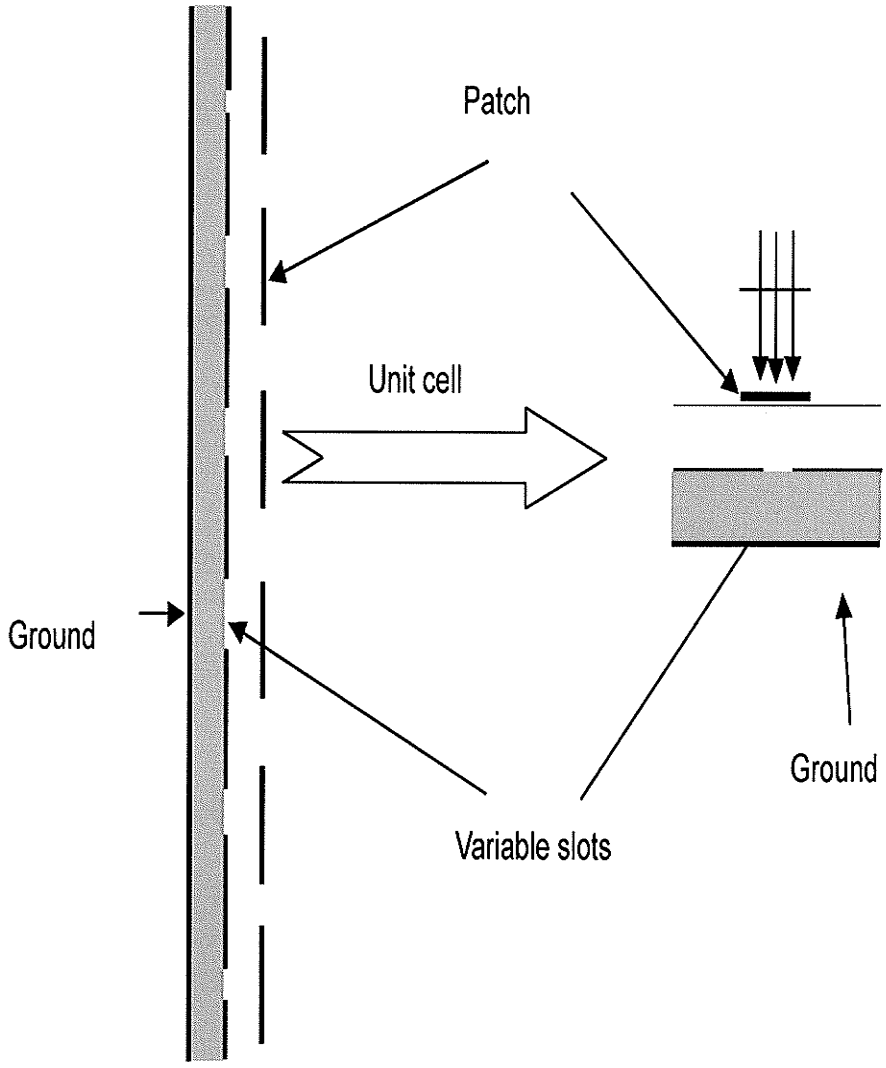

Figure 3-5: The schematic view of a two-layer reflectarray with variable slot.

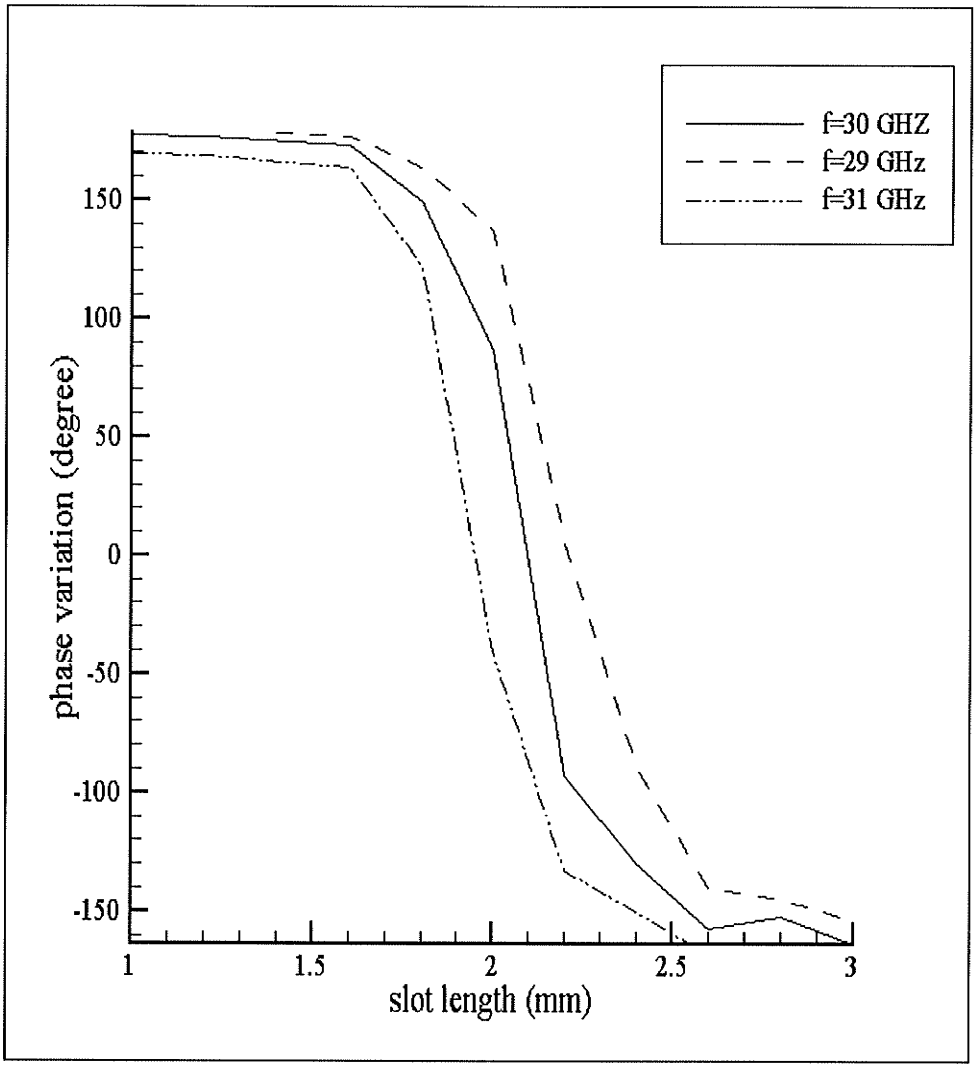

Figure 3-6: Phase shift of the reflected wave versus slot length of two-layer reflectarray with variable slot.

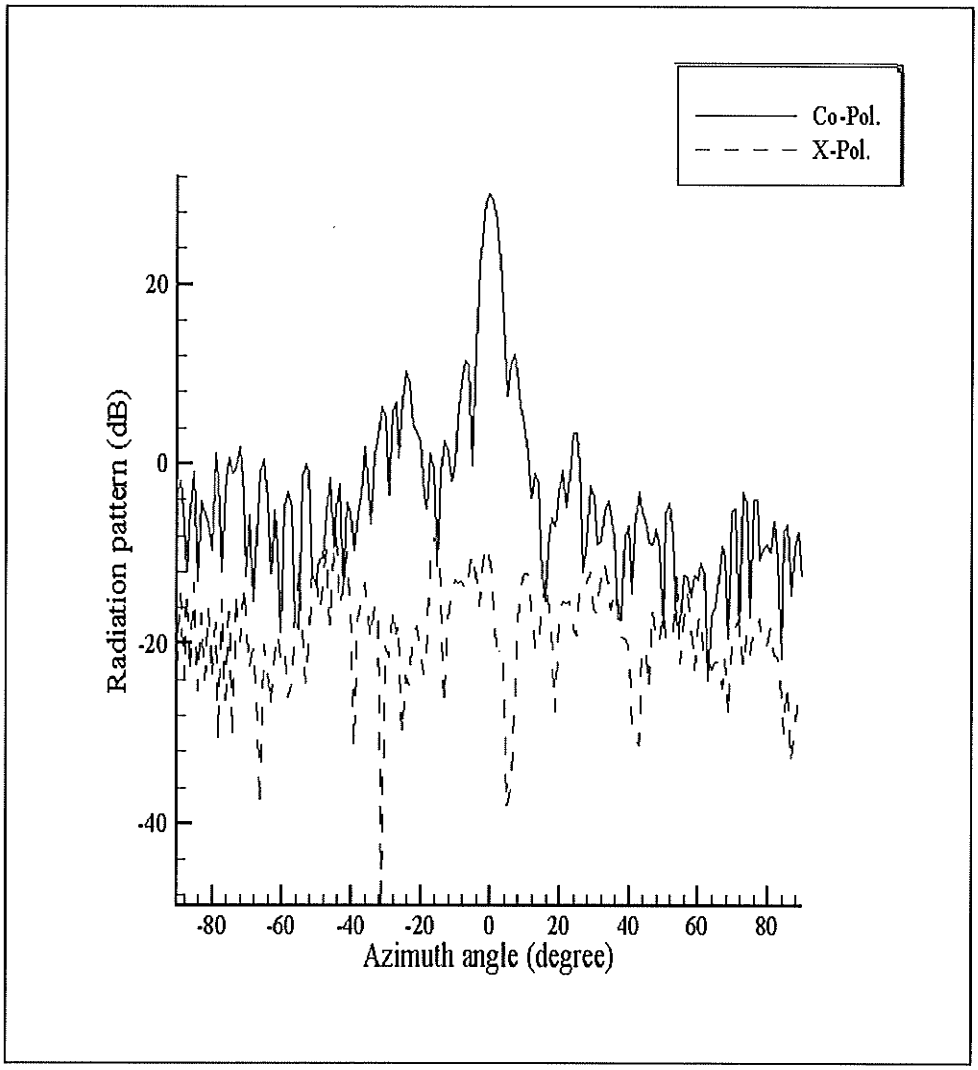

Figure 3-7: Measured Co-Pol. and X-Pol. radiation pattern of the antenna configuration of Fig. (3-5), f=30GHz.

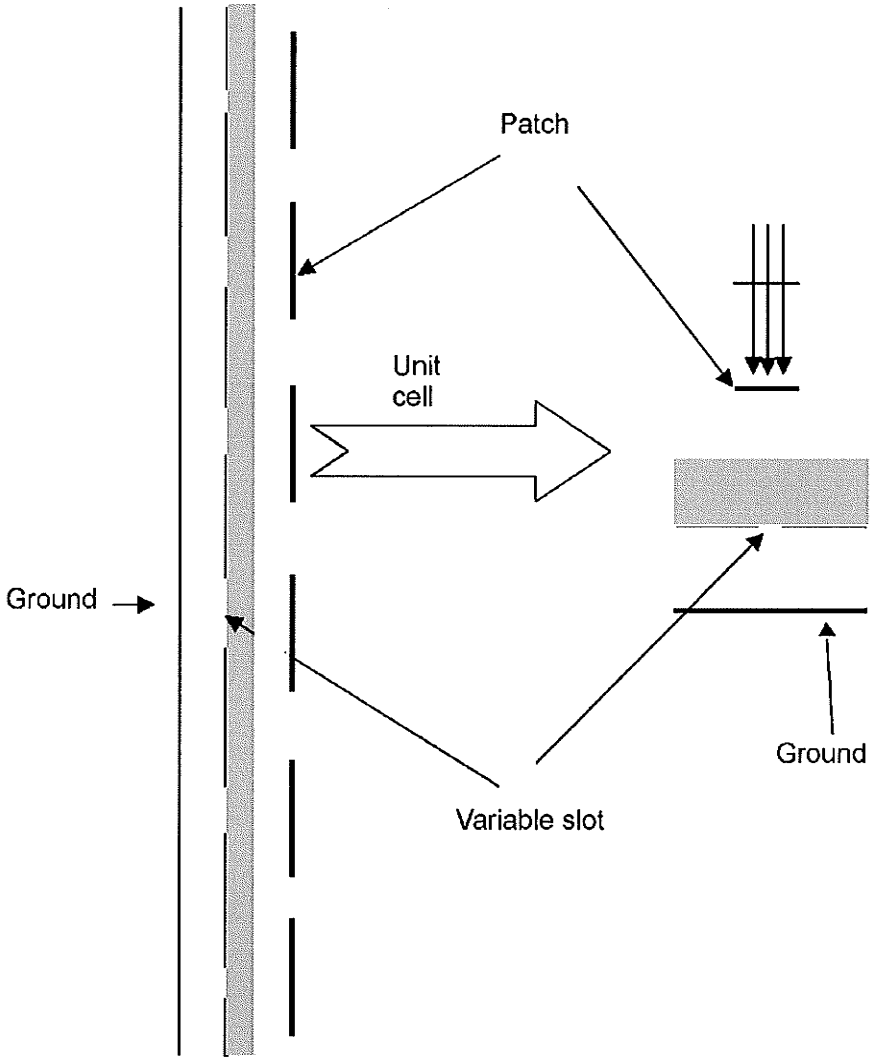

Figure 3-8: The schematic of a three-layers reflectarray with variable slot

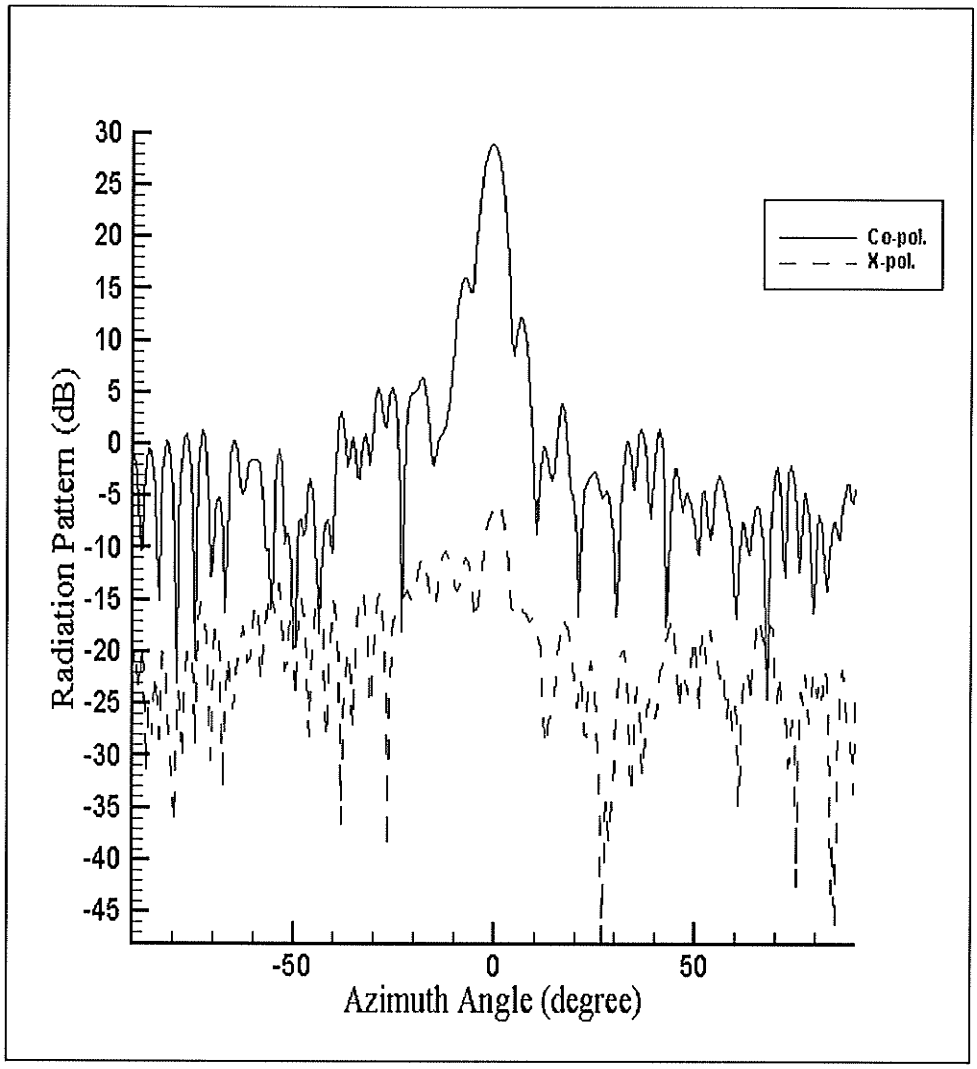

Figure 3-9: Measured Co-Pol. And X-Pol. radiation pattern of the antenna configuration of Fig. (3-8), f=30GHz

3.4 Bandwidth

The bandwidth of a reflectarray is limited primarily by phase errors that tend to increase as the frequency is shifted away from the design frequency and also as a result of a nonlinear dependence of the phase shift on the slot size.

One method to widen the bandwidth in one layer reflectarray with slots of varying length is to increase substrate thickness. Fig. (3-10) shows the phase variation versus the slot length for different thickness values of the substrate layer. As it is exhibited in this Fig., reflectarray with thinner substrate has the largest slope and therefore less bandwidth. As can be seen the dependence of phase on slot length tends to become more gradual as the thickness of the substrate increases and realizable phase range is decreased. A balance between these two conflicting factors would result in optimum performance in terms of gain value and bandwidth.

Another method to increase the bandwidth is to cascade a larger number of substrate layers between the slots and patches. Fig. (3-11) shows the reflectarray gain versus frequency for the one, two and three layers configurations with variable slot size on the ground plane, and also for a single layer reflectarray composed of patches of variable size. As can be seen, the bandwidth for the three-layer reflectarray with variable slot size in the ground plane is wider than the other configurations including reflectarray with variable patches. The bandwidth of double layer reflectarray of variable slots also shows some improvement over its single layer counterpart.

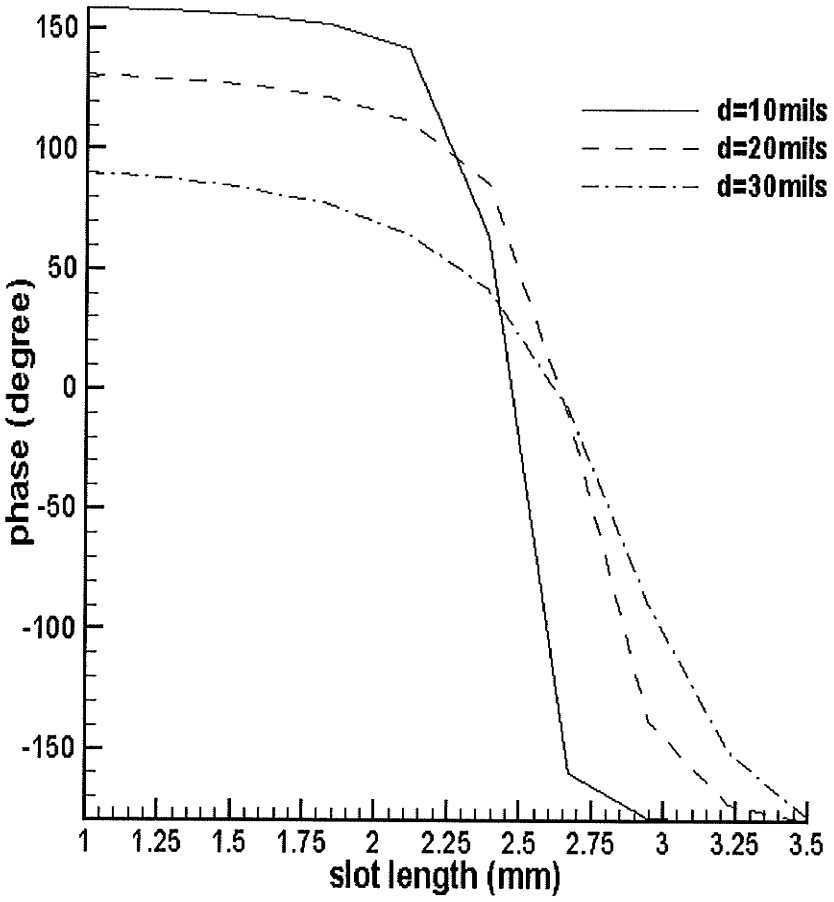

Figure 3-10: Phase versus slot length for different substrate thickness

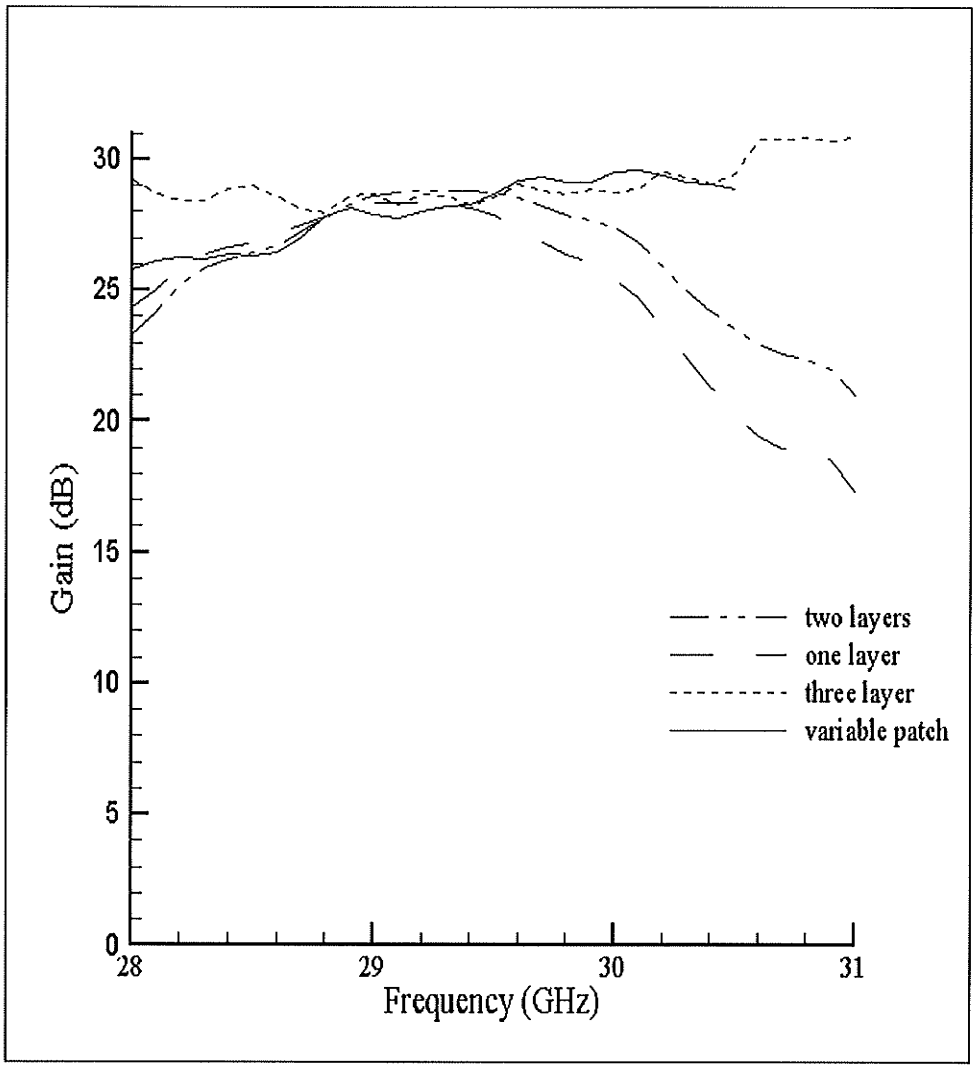

Figure 3-11: Gain versus frequency for the one layer two-layer and three layers reflectarray with variable slot on ground plane, and one layer reflectarray with variable patches

3.5 Phase sensitivity

The phase variation can be achieved by changing the slot length in the ground plane. However, the fabrication and alignment errors can result in a phase error that should be accounted for in the design stage. An accurate estimate of such errors is indispensable to the operation of optically induced reflectarray that is the subject of this thesis. These types of errors are studied in this section for one layer reflectarray with slots of varying length in the ground plane.

3.5.1 Slot position

The slots are to be located right at the centre and beneath the patches. However, because of fabrication errors, the slots may shift in X (left - right) or Y (up -down) direction. The simulation results for phase variation versus slot shift in X and Y directions are shown in Fig. (3-12). It is assumed that the feed is polarized along Y direction. As can be seen from this Fig., the phase perturbation is higher due to the movement of the slots in the Y direction. This implies that the structure is more sensitive to slot shift in feed polarization direction

3.5.2 Slot rotation

Slot rotation is another source of error during the fabrication of antenna. The simulation result for phase variation versus slot rotation is shown in Fig. (3-13). This Fig. shows that even 5^{o} degree slot rotation does not change the phase significantly. Therefore, structure is not very sensitive to slot rotation.

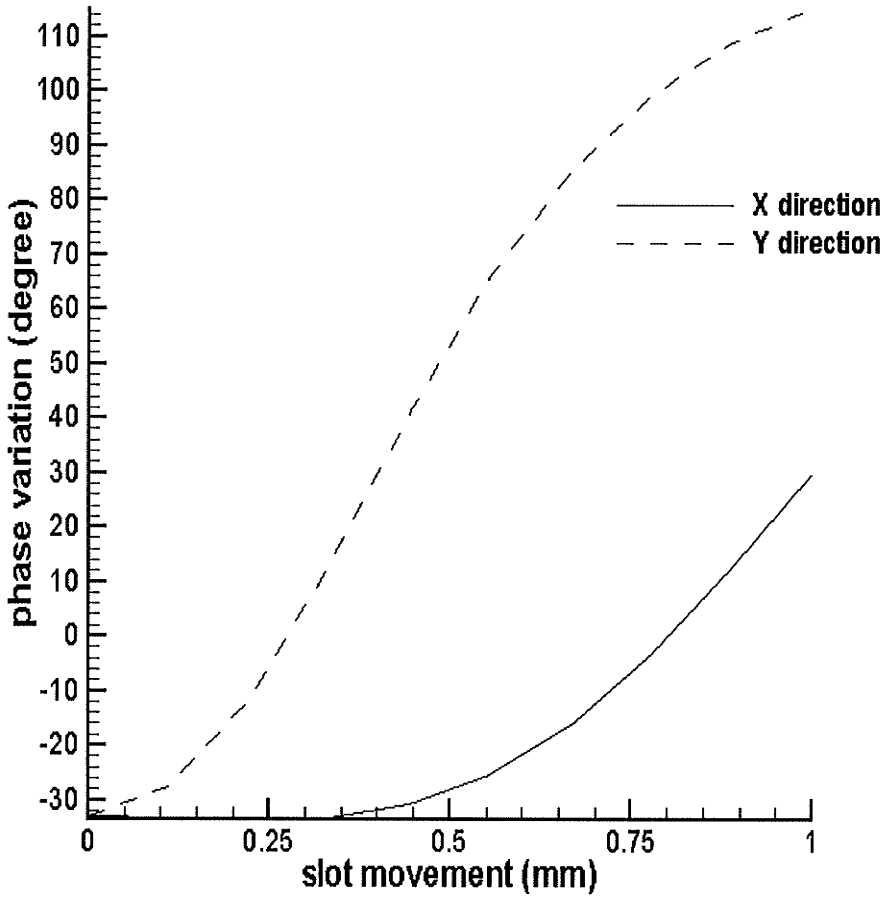

Figure 3-12: Phase variation, versus slot movement at X and Y directions

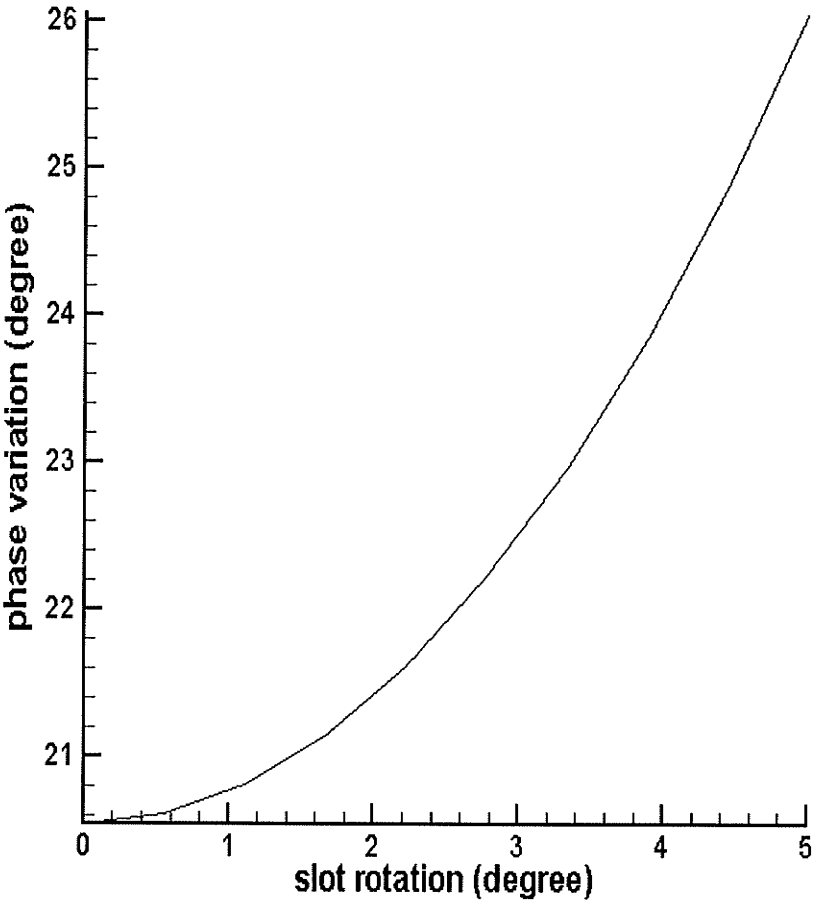

Figure 3-13: Phase variation versus slot rotation

3.6 Novel mechanically controlled reflectarray antenna for beam switching [45]

We have already addressed the problem of a reflectarray with slots of varying size to realize the required phase transformation. A novel mechanically beam scanning method based on this configuration is presented in this section. The proposed reflectarray antenna is comprised of a two-layer reflectarray with identical size patches on the top layer, and slots of identical lengths and slots of dissimilar lengths on the bottom layer as shown in Fig. (3-14). On the middle layer there are two sets of slots ((1) and (2)). The first set of slots (1) are slots with identical sizes and the second set of slots are several groups of slots of dissimilar lengths. There is no air gap between these two sets of slots and each group of slots of varying lengths corresponds to one and only one beam. The slots with identical length size act as a window through which only one set of variable slots are being seen by patches. Fig. (3-14) shows three sets of slots in each unit cell on layer 2 for collimating the beam at -30^{o}, 0^{o} and $+30^{o}$ depending on the alignment of the respective slots set with the centre of the uniform slots. It should be noted that only the slots that are aligned with the uniform slots are seen by the incoming wave and the slots that belong to the other sets are covered by the ground plane. The separation between the slots in the same unit cell is 1 mm. Therefore upward or downward displacement of the second layer with respect to the first layer is ±1 mm which results in three different beams pointing to -30^{o}, 0^{o} and $+30^{o}$. The width of the slots on layer 1, (1), is 0.2mm and the width of slots on layer 2, (2), is a little bit larger in order to avoid the alignment error due to the inaccurate mechanical movement of the slot layers with respect to each other.

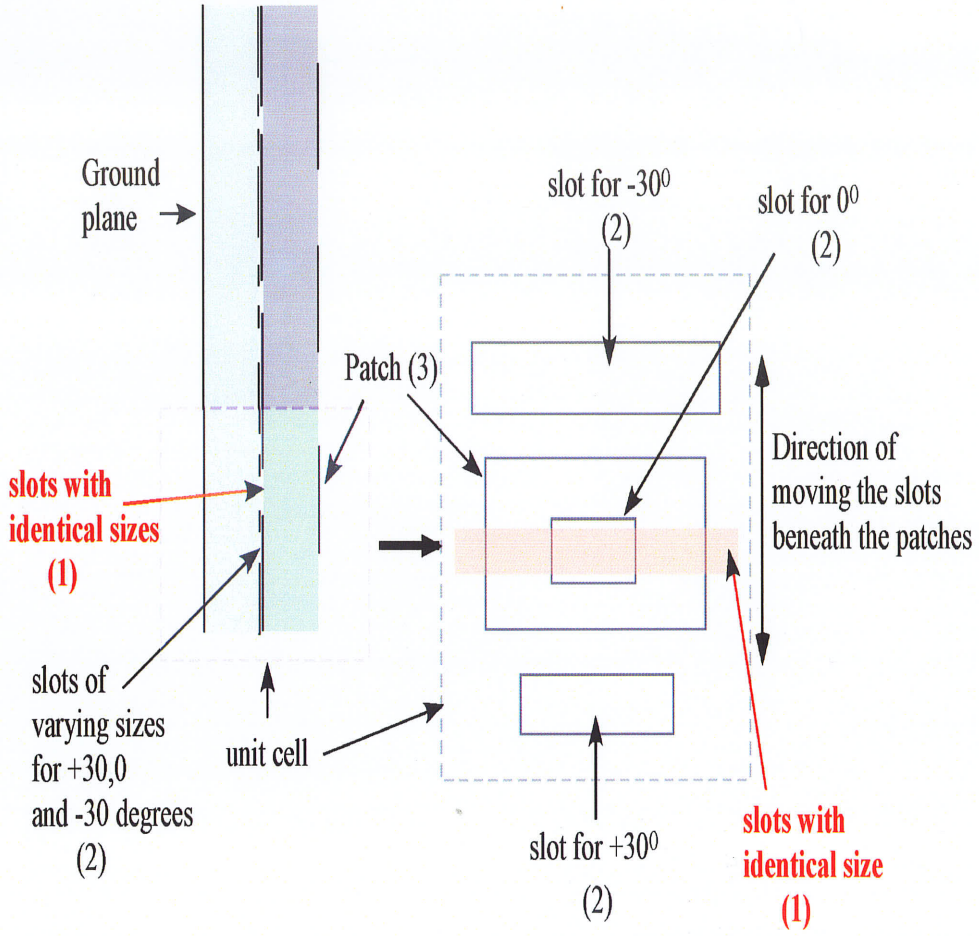

Figure 3- 14: A schematic view of the reflectarray antenna with its unit-cell

A prototype was made based on the above principle and 0.020" dielectric substrates of ε_r=3.0 were used for layers one and two. The patch size was 1.8mm × 3.2 mm. The size of identical slots was set at 0.2 mm × 3.4 mm. The width of slots on the second layer was set at 0.5 mm. Fig. (3-15) shows a reflectarray antenna based on this concept. As it is shown in this Fig., a digital caliper has been used to move the variable slots up and down to switch the beam.

Fig. (3-16) shows the normalized radiation pattern for this antenna at 30 GHz. As shown in this Fig., the beam can be switched between $+30^{o}$,0^{o} and -30^{o} by the movment of the second layer. The maximum gain that has been achieved with this antenna is 28 dB which is equivalent to 34 % radiation efficiency which is close to the gain of a single beam reflectarray.

The mechanically controlled method presented in this section shows that the idea of beam scanning with changing the slot length size is work properly. In chapter 6 other technique based on changing the slot length size with generating photoinduced plasma inside the substrate is presented.

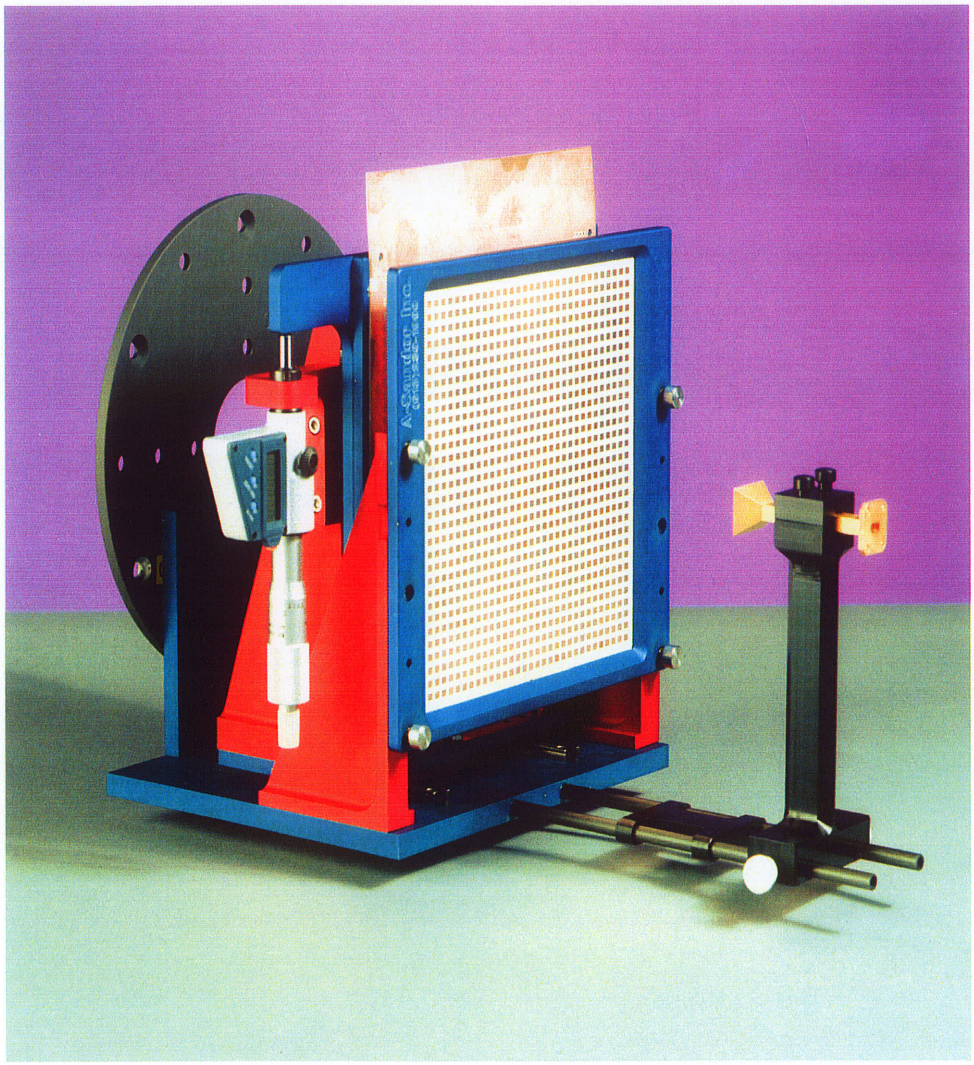

Figure 3-15: A view of the designed reflectarray antenna

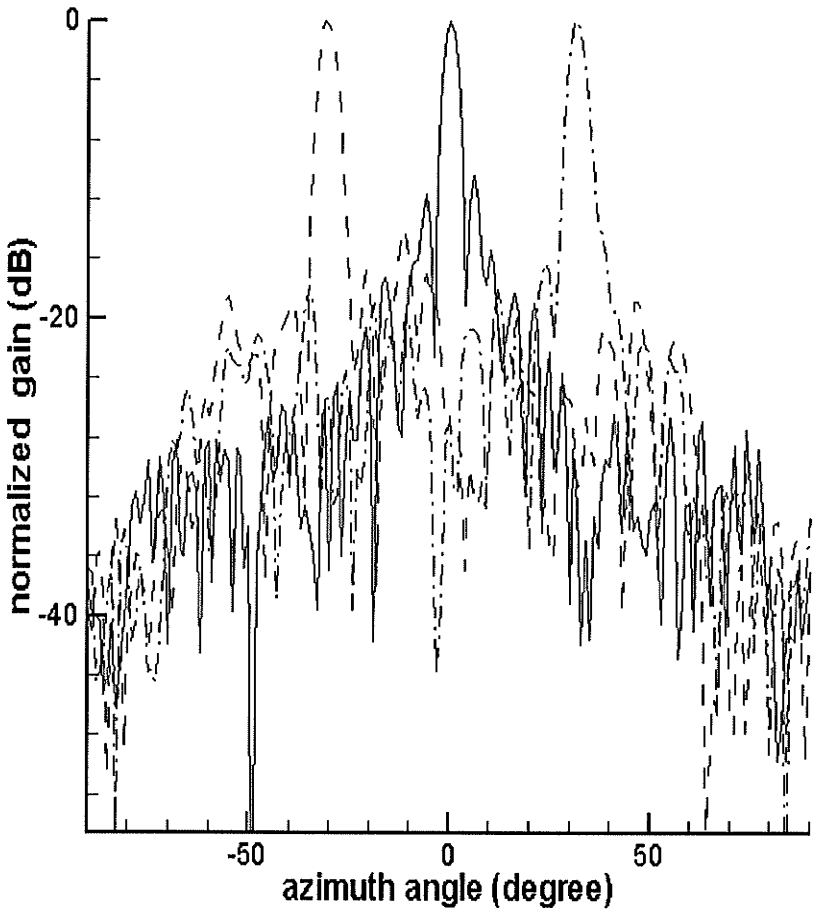

Figure 3-16: Radiation pattern of the reflectarray for different scanned beam at $\pm 30^0$ and 0^0

3.7 Conclusion

The design procedures for microstrip reflectarrays with variable slots on the ground plane based on three novel structures were presented. Results of the numerical simulations and measurements were presented to demonstrate the validity of the design procedure. These configurations offer improved bandwidth performance when compared to a conventional reflectarray design that employs the variable patches as the cell element. A novel mechanical method was suggested to switch the beam of a reflectarray antenna based on the slots of varying size in the ground plane.

CHAPTER 4

PHOTOINDUCED PLASMA PROFILE IN HIGH RESISTIVITY SILICON

Introduction

In this research, optical control of antennas based on photoconductivity in semiconductor is investigated for beam-forming in the millimeter wave antennas. Considering that the incident photons have energies greater than the semiconductor band-gap energy, the photons are absorbed by the semiconductor material. This leads to the creation of electron-hole pairs and thereby generating a plasma profile inside the semiconductor. The electrical conductivity of the material increases in proportion to the photon flux.

Numerous methods have been introduced in the literature for the calculation of the profile of plasma in a semiconductor that is exposed to optical illumination [46]. One method, based on the solution of a differential equation subject to certain boundary conditions is explained briefly in this chapter. An equivalent uniform profile for plasma is derived and the parameters of this model such as effective conductivity and effective thickness have been evaluated. Since the carrier lifetime of a semiconductor is an important parameter in this calculation, a non-destructive method for the measurement of the carrier recombination lifetime in silicon based on a waveguide technology is introduced and the measurement results are presented in this chapter.

4.1 Analyzing the profile of photoinduced plasma in a semiconductor

4.1.1 Excess carrier density in semiconductor

Optical excitation of semiconductors is used in a variety of lifetime or diffusion measurement techniques. There are two basic methods for the measurement of recombination properties:

1) The excitation source is abruptly terminated, and the excess carrier decay rate is measured. An example of this method is the photoconductance decay where the conductivity of the sample is monitored as a function of time.

2) The steady state excess carrier density due to continuous optical excitation.

To evaluate the number of excess carriers in the plasma and the profile of carrier diffusion in the wafer, a semiconductor sample with area A on S_1 and S_2 and thickness d is considered (see Fig. (4-1)). The current density leaving the volume J (x+d) can be larger or smaller than the current density entering, J(x), depending on the generation and recombination of carriers that takes place within the volume.[47]

The following equation can be used in a medium in which the photoinduced carrier overwhelms the thermal carrier generation:[48]

$$D\frac{d^2\Delta n(x,t)}{dx^2} - \frac{\Delta n(x,t)}{\tau} + G(x,t) = \frac{\partial \Delta n(x,t)}{\partial t} \qquad (4\text{-}1)$$

where $G(x,t)$ is the carrier generation function. τ is the carrier lifetime, D is the carrier diffusion coefficient and $\Delta n(x,t)$ is excess carrier density.

For steady-state excess carrier density which is the case in this dissertation, $\frac{\partial \Delta n(x,t)}{\partial t} = 0$ and $G(x,t)$ is independent of t . In this case,

$$G(x) = \Phi(\lambda).\alpha(\lambda).(1-R(\lambda)) \tag{4-2}$$

$\alpha(\lambda)$ is absorption coefficient which is a function of wavelength (λ) [49]

$R(\lambda)$ is reflection coefficient from the surface of wafer

$\Phi(\lambda)$ is photon flux density of monochromatic light and is equal to:

$$\Phi(\lambda) = \frac{P\lambda S(\lambda)}{hc_0 A} \tag{4-3}$$

h is Plank's constant, P is the incident optical power, A is the illuminated area and $S(\lambda)$ is the relative spectral response at the optical power [49].

Equation (4-1) is subject to the following two boundary conditions:

$$\frac{d\Delta n(x)}{dx}\Big|_{x=0} = s_1 \frac{\Delta n(0)}{D} \tag{4-4a}$$

$$\frac{d\Delta n(x)}{dx}\Big|_{x=d} = -s_2 \frac{\Delta n(d)}{D} \tag{4-4b}$$

where s_1 and s_2 are surface recombination velocities at S_1 and S_2, respectively. This differential equation has been solved analytically [50].

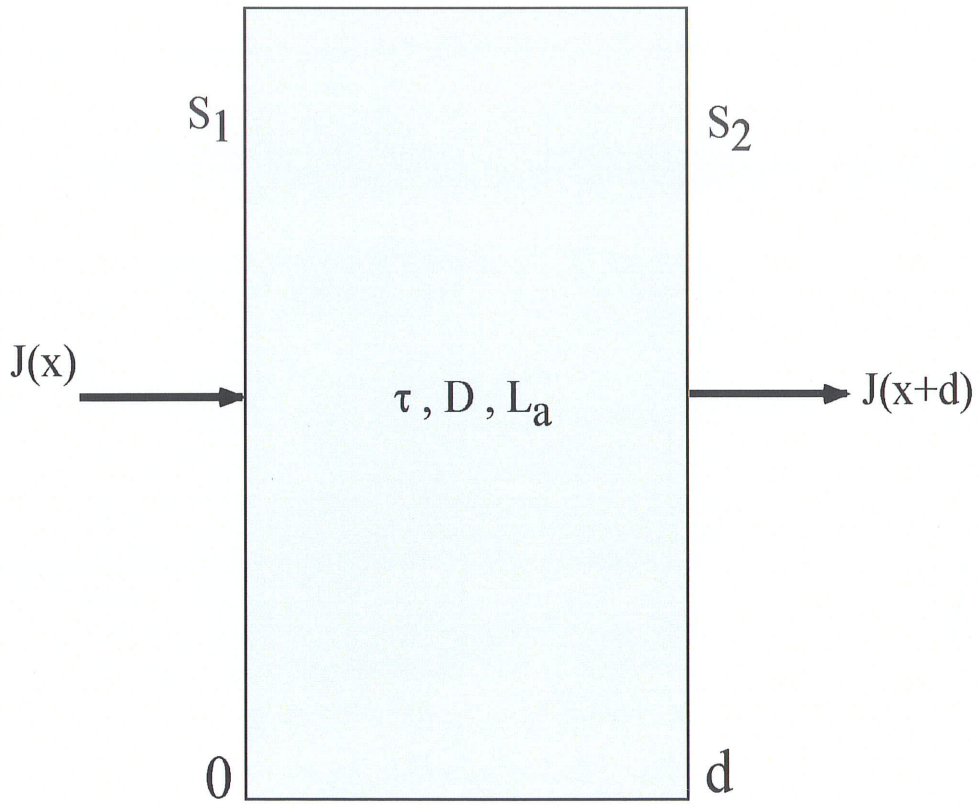

Figure 4-1: Current entering and leaving a semiconductor sample

$$\Delta n(x) = \frac{(1-R)\Phi\alpha\tau}{(\alpha^2 L_a^2 - 1)}\left[\frac{A_1 + e^{-\alpha d} B_1}{D_1} - e^{-\alpha x}\right] \tag{4-5}$$

where

$$A_1 = \left(\frac{s_1 s_2 L_a}{D} + s_2 \alpha L_a\right) sinh(\frac{d-x}{L_a}) + (s_1 + \alpha D) cosh(\frac{d-x}{L_a}) \tag{4-6a}$$

$$B_1 = \left(\frac{s_1 s_2 L_a}{D} - s_2 \alpha L_a\right) sinh(\frac{x}{L_a}) + (s_2 - \alpha D) cosh(\frac{x}{L_a}) \tag{4-6b}$$

$$D_1 = \left(\frac{s_1 s_2 L_a}{D} + \frac{D}{L_a}\right) sinh(\frac{d}{L_a}) + (s_1 + s_2) cosh(\frac{d}{L_a}) \tag{4-6c}$$

L_a is the carrier diffusion length and α is the absorption coefficient.

Based on the Einstein equation $D/\mu = KT/q$ and because $D=L_a^2/2\tau$, it can be shown that

$$L_a = [(2\mu_n \mu_p \tau K_B T/q)(\mu_n+\mu_p)]^{1/2} \tag{4-7}$$

where μ_n and μ_p are the hole and electron mobility, respectively, K_B is Boltzman's constant [J/K] and T is the temperature.

The conductivity of photoinduced plasma can be calculated according to the following equation:

$$\Delta\sigma = \Delta n(\mu_n + \mu_p)q \tag{4-8}$$

4.1.2 Simulation Results

The simulation results reported here are obtained for a silicon wafer with the following characteristics:

ε_r =11.8, $s_1 = s_2$ = 1000 cm/s , λ= 940 nm , μ_n= 1500 $cm^2/V.s$, μ_p=600 $cm^2/V.s$, $\Phi(\lambda)$= P/A= 400 mw/cm^2 ,$S(\lambda)$ = 0.7 , α=6400 cm^{-1}.

Fig. (4-2) shows the $\Delta n(x)$ as a function of diffusion length in wafer for four different values of carrier lifetime. As shown, Δn increases inside the plasma as the carrier lifetime is increased.

4.2 Effective plasma depth at quasi-CW optical excitation

Suppose a semiconductor wafer with an optical mask on its upper face is illuminated by a CW-optical source as shown in Fig. (4-3). The general distribution of carrier density $\Delta n\ (x)$ as explained before is similar to Fig. (4-4a). As shown in this Fig., the profile of plasma is not uniform throughout the excitation region. However, the theoretical formulation is significantly simplified for a uniform structure that is shown in Fig. (4-4b). The maximum photoconductivity $\Delta\sigma_m$ can be calculated from equation (4-8). The result is shown in equation (4-9). The effective plasma depth d_e can be expressed by equation (4-10) which results from the equal area condition A_1=A_2, which $A_2 = \int_0^\infty \Delta\sigma dx$ from equation (4-8) to establish equivalence between non-uniform and uniform profiles. [50].

$$\Delta\sigma_m = \frac{\Delta\sigma_0}{(1+\alpha\ L_a)}\left\{\frac{1}{\alpha\ L_a}\left(\frac{\alpha\ L_a^{\,2}+s\tau}{L_a+s\tau}\right)\right\}^{-\alpha\ L_a/(1-\alpha\ L_a)} \tag{4-9}$$

$$d_e = \frac{1}{\alpha}\left\{\frac{L_a(1+\alpha\ L_a)+s\tau}{L_a+s\tau}\right\}\left\{\frac{1}{\alpha\ L_a}\left(\frac{\alpha\ L_a^{\,2}+s\tau}{L_a+s\tau}\right)\right\}^{\alpha\ L_a/(1-\alpha\ L_a)} \tag{4-10}$$

where $\Delta\sigma_0$ is the conductivity on the surface of the semiconductor.

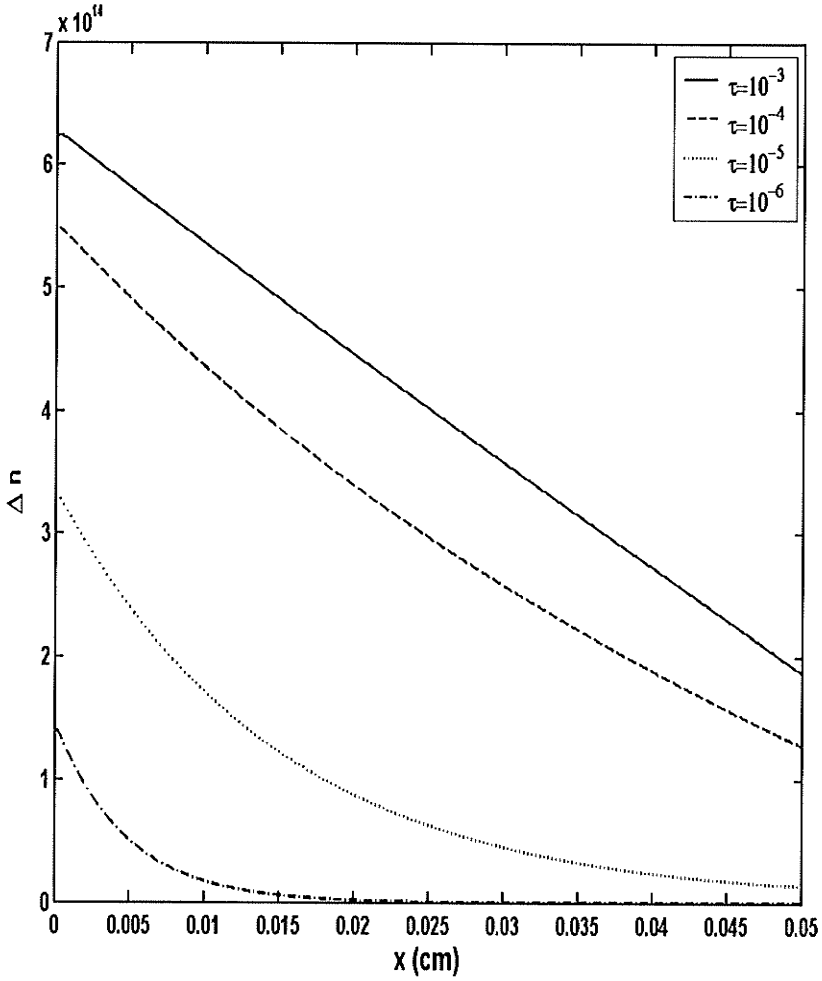

Figure 4-2: $\Delta n(x)$ as a function of diffusion length in wafer for four different carrier lifetimes

In most situations, diffusion does not occur only in the Y direction. In this case the diffusion in the X direction can be also calculated according to the proper boundary condition. The following equation shows the conductivity of plasma, which takes into account the lateral diffusion in 'X' direction. (4-11)

$$\Delta\sigma(x) = \Delta\sigma_m \exp(-x/L_a)\sinh(w/2L_a) \qquad \begin{matrix} -\infty \le x \le -w/2 \\ w/2 \le x \le +\infty \end{matrix} \tag{4-12}$$

To incorporate this effect into the lumped element it is quite useful to introduce an effective (uniform) photoconductivity $\Delta\sigma_e$ based on diffusion in X and Y directions.

$$\Delta\sigma_e = \Delta\sigma_m (w/4L_a)(1-\xi^2)^{1/2}\{Arctanh[(1-\xi)/(1+\xi)]^{1/2}\}^{-1} \tag{4-13}$$

$$\zeta = W/2L_a \tag{4-14}$$

Fig. (4-5) shows the normalized effective photoconductivity $\Delta\sigma_e/\Delta\sigma_m$ as a function of normalized gap width W/L_a. As seen for $W/L_a >> 1$, $\Delta\sigma_e/\Delta\sigma_m \approx 1$ which implies higher diffusion in the X direction as a result of decreasing gap width.

The above calculations are carried out based on the assumption of infinite wafer thickness, which is not the case in practice. Equation (4-5) can be used to consider the effect of the wafer thickness. Fig. (4-6) shows the effective thickness versus the wafer thickness. It can be observe that the effective thickness of the plasma for the substrate of finite thickness approaches the effective thickness of the substrate of infinite thickness as the thickness is increased.

The effective thickness is an important parameter in our simulations. The importance of plasma thickness will be verified through the simulations as an application of photoinduced plasma in changing the slot length in reflectarray antenna will be introduced later on.

The effective thickness is the function of semiconductor thickness, carrier recombination lifetime and surface recombination velocity. As it can be observed in Fig. (4-6) when semiconductor thickness is much thicker that carrier diffusion length the effective thickness is independent of the semiconductor thickness. Fig. (4-7) shows the effective thickness versus the carrier recombination lifetime. The surface recombination velocity for both side is 2000 cm/s and absorption coefficient is 6400 cm^{-1}. It is evident from this Fig. that higher effective thickness can be expected by increasing the carrier lifetime.

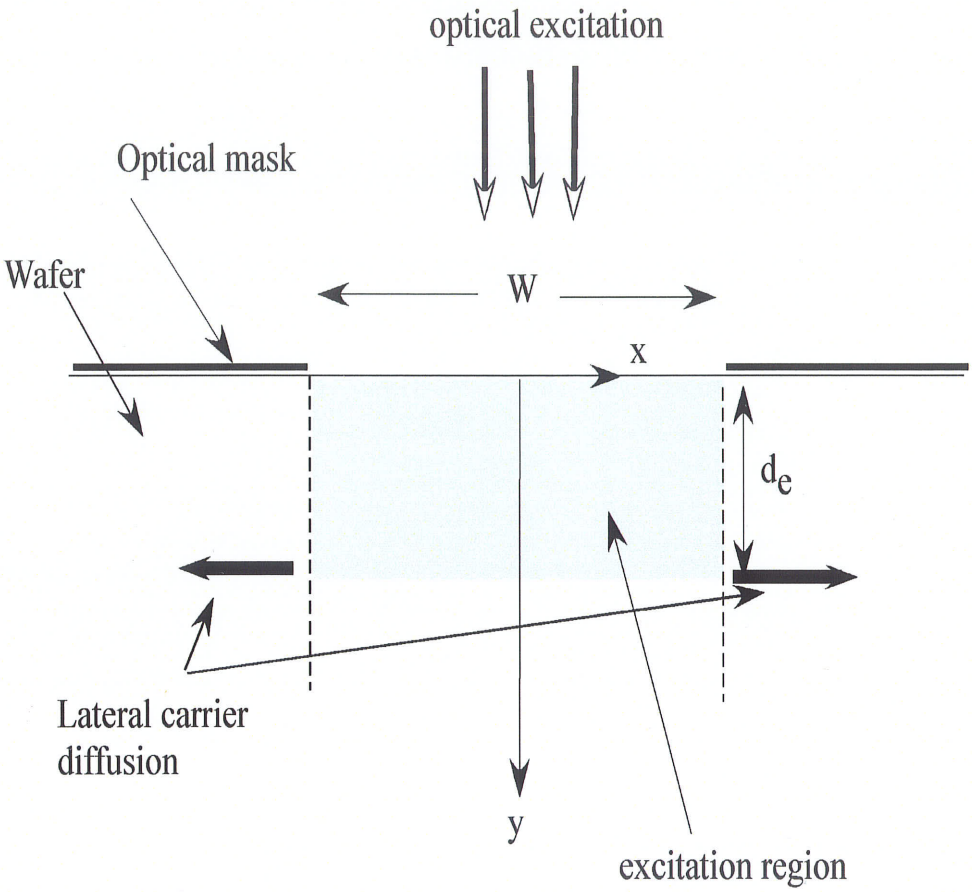

Figure 4-3: Microstrip gap structure

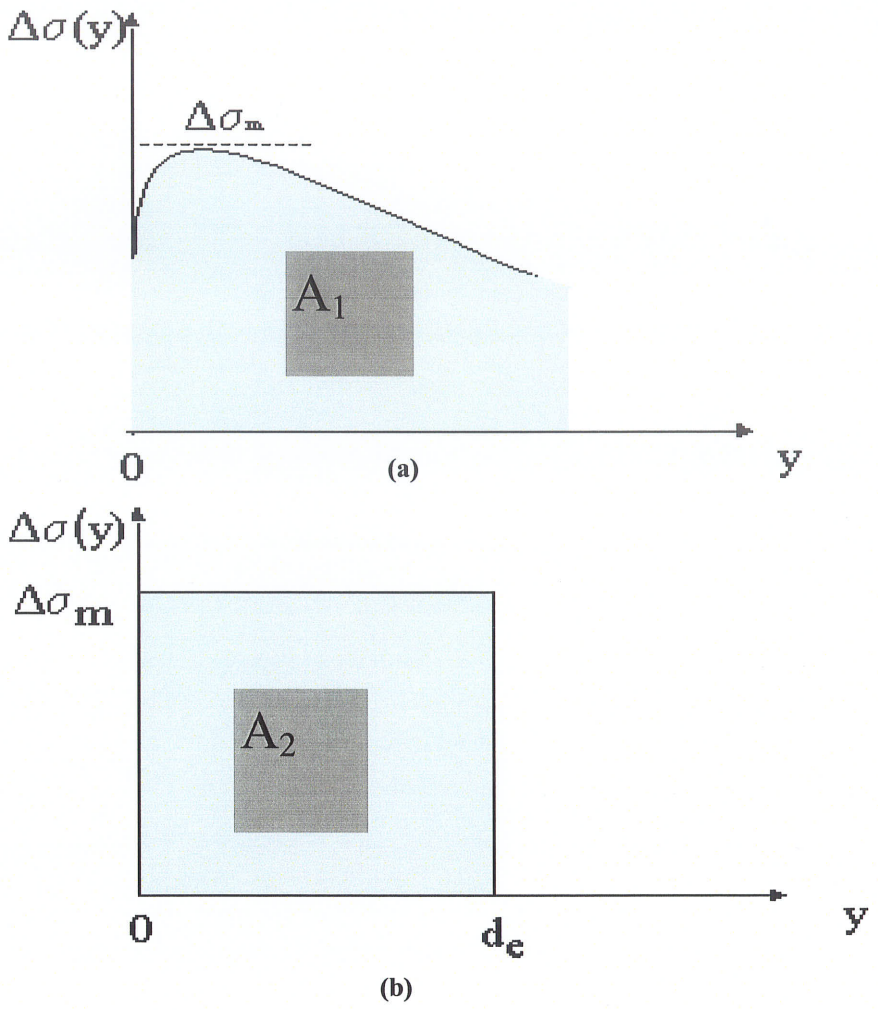

Figure 4-4: Profile of photoconductivity Δσ(y) at quasi-CW laser excitation (a) Real (b) Equivalent

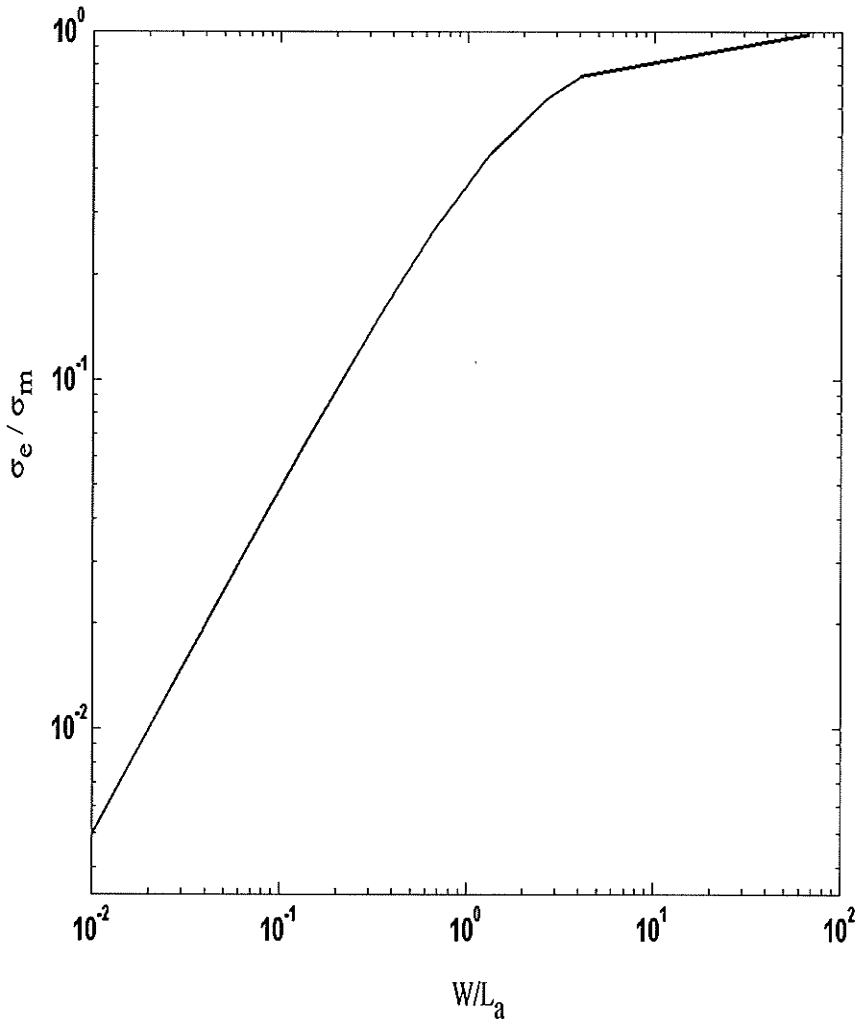

Figure 4-5: Normalized effective photoconductivity $\Delta\sigma_e/\Delta\sigma_m$ as a function of normalized gap width W/L

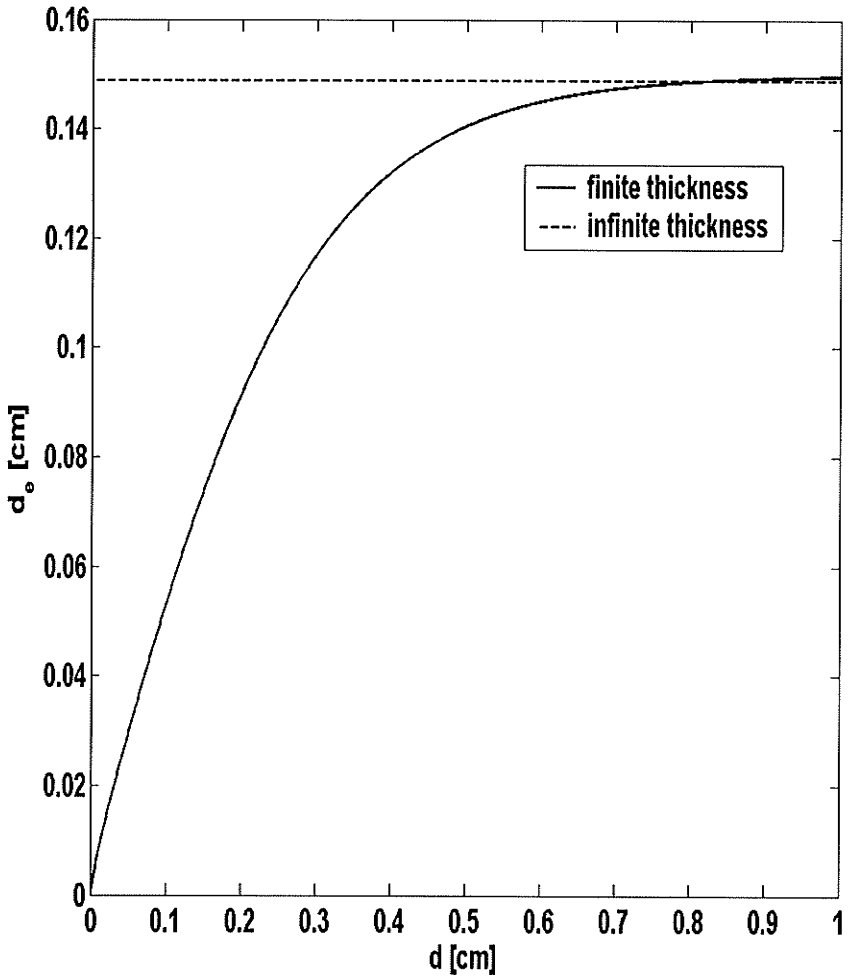

Figure 4-6: Effective length as a function of wafer thickness

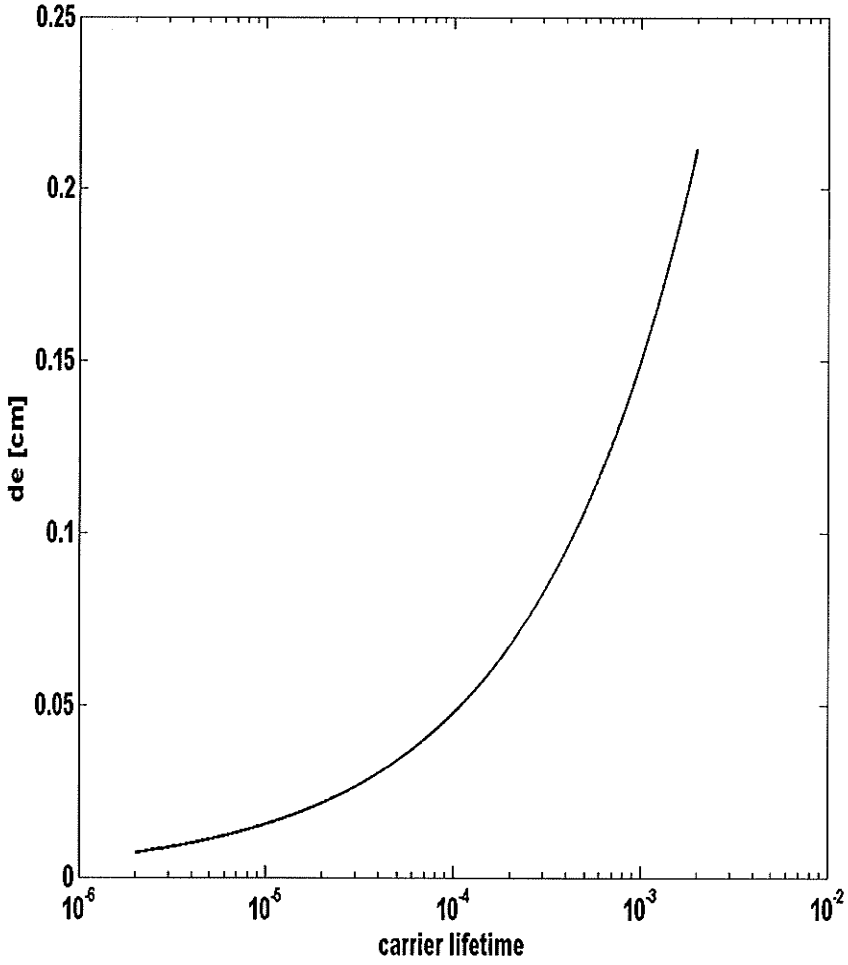

Figure 4-7: Effective length as a function of carrier lifetime

4.3 Complex permittivity in the plasma region

So far the number of excess carrier density and conductivity in the semiconductor illuminated by the CW optical excitation are considered. However, sometimes the profile of permittivity in plasma is needed. Noting the presence of bound and free charges in plasma, the polarization vector can be described as:

$$\vec{P} = \varepsilon_0(\chi_b + \chi_f)\vec{E} \tag{4-15}$$

where b and f subscript in (4-15) refer to bound and free charges, respectively.

$$\varepsilon_r = 1+\chi_b+\chi_f \tag{4-16}$$

$$P_f = \varepsilon_0 \chi_f E \tag{4-17}$$

The equation of motion of carriers in a semiconductor excited by electric field E given by [52]:

$$m^*\left(\frac{d^2}{dt^2}+\frac{1}{\tau}\frac{d}{dt}\right)\delta\vec{r} = -e\vec{E} \tag{4-18}$$

where τ is the collision time and $\tau = \mu m^*/e$, δr is the spatial displacement, m^* is the effective mass of charge carrier and μ is electron mobility. Also the polarization due to free charge is:

$$P_f = -Ne\delta r$$

Considering (4-15), (4-17), and (4-18), the following relation is obtained.

$$\vec{P}_f = \frac{Ne^2}{m^*}\frac{1}{(-\omega^2 + j\frac{\omega}{\tau})}\vec{E} = \varepsilon_0\chi_f\vec{E} \tag{4-19}$$

where N is the density of the plasma. By introducing the plasma frequency ω_p as $\omega_p^2 = Ne^2/\varepsilon_0 m^*$ and $\nu = 1/\tau$, and substituting (4-19) into (4-17),

$$\varepsilon_r = \varepsilon_L - \frac{\omega_p^{\,2}}{\omega^2 + \upsilon^2} - j\frac{\upsilon}{\omega}\frac{\omega_p^{\,2}}{\omega^2 + \upsilon^2} \tag{4-20}$$

The refractive index can be calculated according to the following relation:

$$n = \sqrt{\varepsilon_r} = \eta - j \tag{4-21}$$

We have to note that:

$$N = n_{p0} + n_{n0} + n_p + n_e \tag{4-22}$$

where n_{p0} and n_{n0} are the density of intrinsic holes and electrons due to doping and n_p and n_e are the density of photoinduced holes and electron, respectively.

Fig. (4-8) shows the real part (ε_r) and imaginary part (ε_i) of the photoinduced plasma permittivity, versus the frequency for different carrier densities. It is interesting to note that the negative values of the real part of permittivity for carrier densities above 10^{17}.

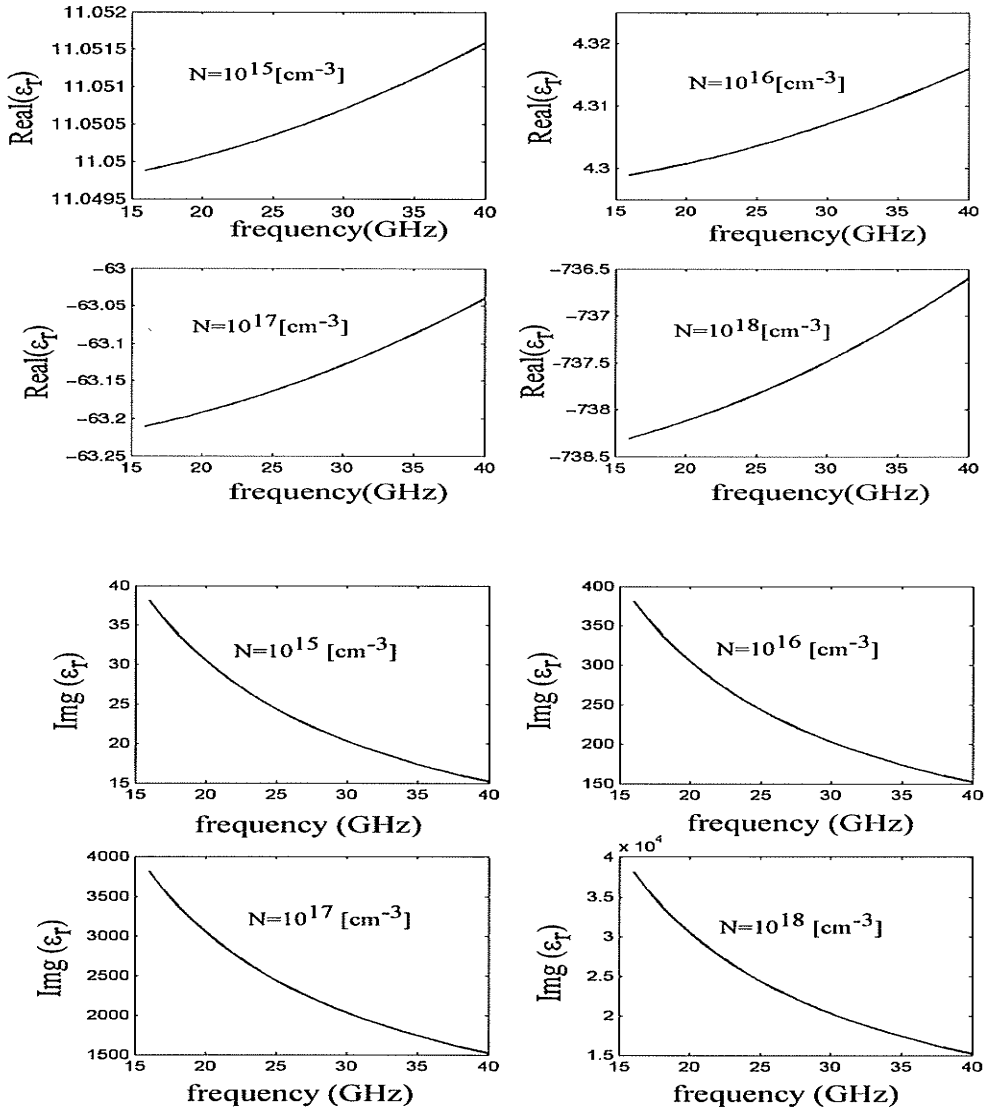

Figure 4-8: Real and imaginary parts of permittivity of plasma with different number of carrier densities

4.4 Calculation of the carrier lifetime for silicon

Carrier recombination lifetime that is defined to be the time span, before carriers in conducting band descend to valence band, is an important parameter in the calculation of photoinduced carrier density and profile of plasma inside the semiconductor. This parameter is a function of doping and number of carriers inside semiconductor [53]. A non-destructive measurement technique is used in this dissertation to characterize carrier lifetime of a silicon wafer based on reflection from a waveguide aperture loaded by the silicon sample that is exposed to an optical source.

4.4.1 Measurement setup

A block diagram of the measurement setup is shown in Fig. (4-9). In this Fig., the silicon is placed onto the aperture of a WR28 waveguide. The optical excitation source is a high power strobe Xenon lamp as depicted in Fig. (4-10) (CAIRN, 3 inch collimated output flash photolysis system). The lamp generates optical pulse with different energy levels and pulse durations. Decay of photoconductivity following the generation of excess carriers as a result of the optical pulse is determined by monitoring the reflection of the millimeter waveform on the waveguide aperture. The MMW, generated by VNA is directed through a WR28 waveguide onto the wafer and the reflection is redirected via a directional coupler toward the detector. The time dependence of this quantity is recorded by a digital storage oscilloscope.

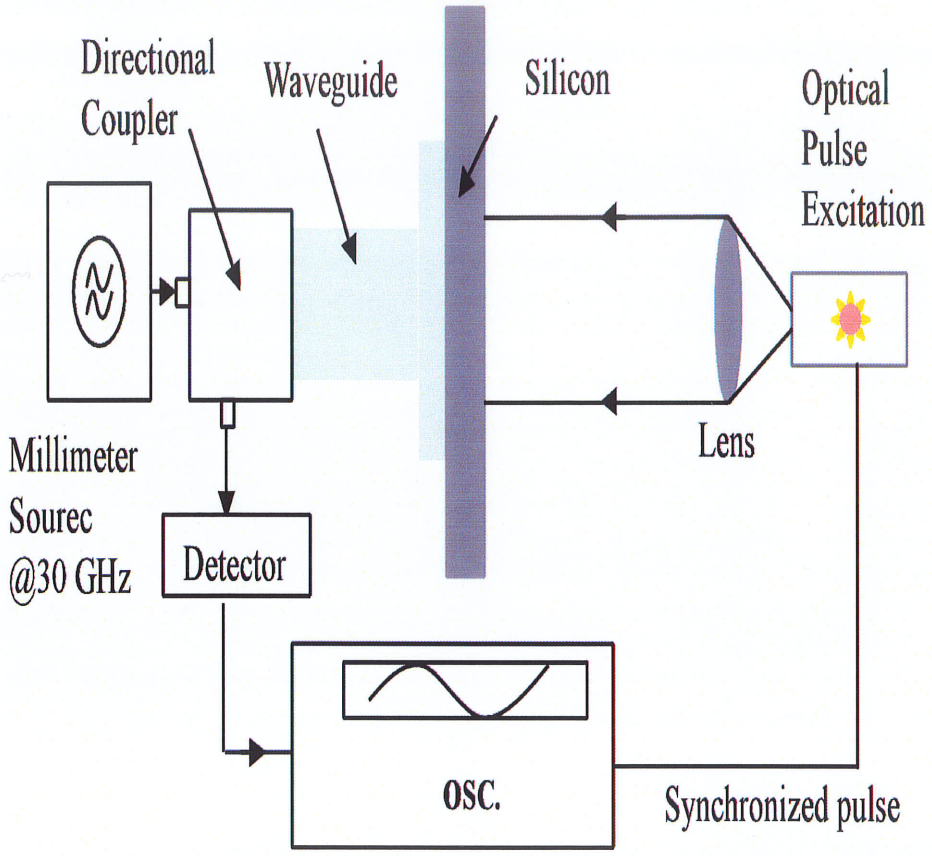

Figure 4-9: A schematic view of the setup for the carrier life time measurement

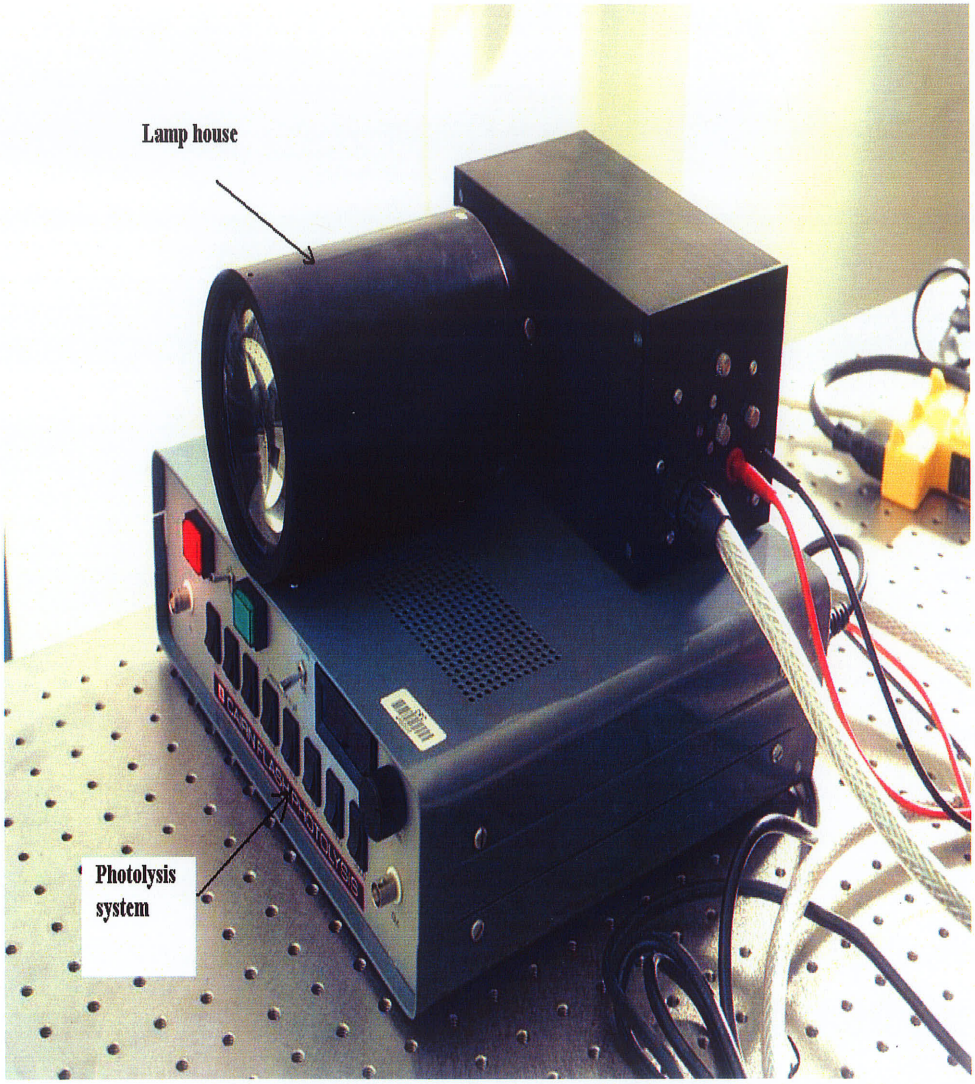

Figure 4-10: Optical source with photolysis system

The relationship between the reflection coefficient Γ_s at the sample and the reflection coefficient Γ_D at the detector is approximated as follow:

The microwave system between the detector and surface of the sample can be considered as a linear reciprocal two-port network described by scattering parameters S_{11}, S_{12} and S_{22}. The relationship between Γ_D and Γ_s is given by:

$$\Gamma_D = S_{11} + \frac{S_{12}^{\ 2}\Gamma_s}{(1+S_{22})} \tag{4-23}$$

Using only the first term (other terms are small) of the Taylor series expansion of the above equation the following equation results

$$\Delta\Gamma_D = \frac{S_{12}^{\ 2}\Delta\Gamma_s}{(1+S_{22})^2} \tag{4-24}$$

that shows the variation of the reflection coefficient at the detector is directly proportional to the variation of the reflection coefficient at the sample. The conductivity, σ, is proportional to the excess carriers (see equation 4-8). When the optical excitation is switched off, the conductivity decays with the time constant, τ as expressed in the following equation.

$$\sigma(t) = \sigma(0)e^{-\frac{2t}{\tau}} \tag{4-25}$$

The time constant, τ, is defined to be the carrier lifetime. The factor 2 in the exponent is due to the square-law nature of the detector.

4.4.2 Results and discussion

For the first set of measurements taken with the setup that was described in the previous section, a 3" silicon of 1.2 mm thickness was used. The excitation pulse width is 100

μsec and can be changed by adjusting the capacitors in the photolysis system of the lamp. The reflected millimeter wave is detected with a RF crystal detector. The detector is a HP R422 which is a crystal detector in the frequency range of 26 GHz – 40 GHz and maximum sensitivity of 0.3 mv/μw. The output of the detector is connected to 50 Ω input of a digital oscilloscope and the signal is monitored by this digital oscilloscope. The TTL pulse that is generated by the optical system is used to trigger the digital oscilloscope.

Fig. (4-11) shows the detected voltage decay as a function of time when the sample is illuminated by the optical pulse of the Xenon flash lamp. The optical pulse was also detected by a photodetector. The time constant τ_D of the decay as obtained from the Fig. is 500μs and knowing that the recombination life time τ_e is twice τ_D the recombination lifetime for this wafer is estimated as 1 msec. Table (4-1) shows the measured carrier recombination lifetime for three different wafers.

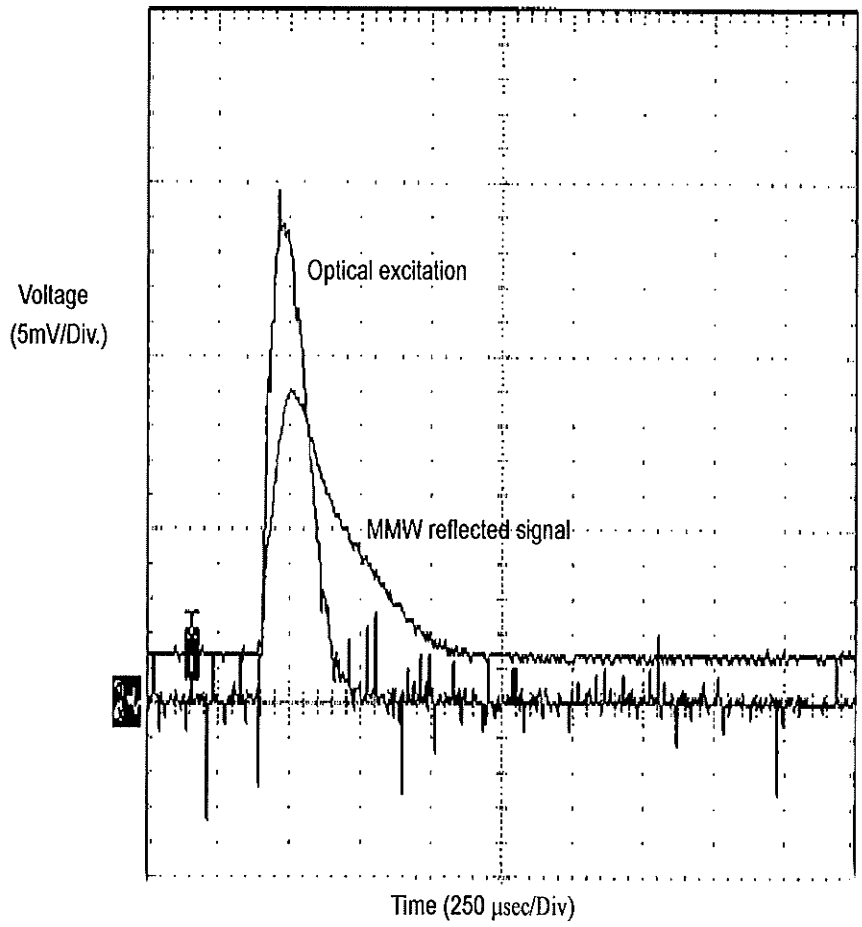

Figure 4-11: Optical excitation and reflection from silicon

Silicon wafer	Diameter	Thickness	Carrier lifetime
1	3"	1.2 mm	1 msec
2	3"	0.42 mm	0.6 msec
3	6"	0.5 mm	1.2 msec

Table 4-1: Carrier lifetime for 3 silicon wafers with different thicknesses.

4.5 Conclusion

In this chapter, we demonstrated that the effect of carrier diffusion and the number of carriers inside the semiconductor excited by a continuous wave optical excitation can be calculated using a two-dimensional differential equation. The plasma profile inside the semiconductor that is exposed to optical illumination was considered and a model based on uniform plasma profile beneath the gap was introduced. The model for the plasma profile can be very useful for analyzing the photonically controlled slot length, which will be explained in next chapter. A method for measuring the carrier recombination lifetime in silicon was also presented.

CHAPTER5

THE REFLECTION COEFFICIENT OF 2-D AND 3-D PHOTOINDUCED PLASMA STRUCTURES: SIMULATION AND MEASUREMENT

Introduction

When a semiconductor is illuminated by an optical excitation, free carriers will be generated inside the semiconductor. The profile of photoinduced plasma depends on the profile of optical excitation and also the characteristics of semiconductor such as carrier lifetime and semiconductor thickness. A model for plasma profile was introduced in the previous chapter.

Two techniques for the calculation of the reflection coefficient of an incident plane wave on a photoinduced plasma structure are presented in this chapter [54]. The first method is a measurement technique based on waveguide technology. The profile of the photoinduced plasma inside the semiconductor can be determined using this method. The measurement results will be compared with simulations from Ansoft HFSS. The plasma characteristics as presented in the previous chapter are used throughout these simulations. The same measurement setup has been utilized to analyze the reflection coefficient of a waveguide terminated in an optically controllable slot.

Surface impedance based on a transmission line method is the second technique that is presented in this chapter to analyze photoinduced plasma in a grating structure. In this technique, method of moment has been used for the calculation of the Floquet's mode coefficients. The simulation results based on this method will be compared with simulation results from HFSS.

5.1 Reflection coefficient measurement of an optically controllable slot based on waveguide technology

5.1.1 Waveguide setup

In order to understand the behavior of semiconductor material under an optical illumination, a measurement method based on waveguide technology is presented in this chapter. This method is based on the reflection coefficient measurement of a waveguide terminated by a slot etched on a high resistivity silicon wafer. The measured result is compared with HFSS simulations and a parameter study is carried out in order to estimate the profile of plasma and carrier density.

The measurement setup is shown in Fig. (5-1). The setup consists of a WR28 waveguide, a Vector Network Analyzer (VNA) to measure the amplitude and phase of the reflection coefficient, a piece of high resistivity (typically > 4 kΩ/cm) silicon wafer of 1.2 mm thickness, and a CW halogen lamp as the optical source. To illuminate the silicon uniformly, a beam collimator was designed using an ellipsoid mirror and a lens. The optical source setup is shown in Fig. (5-2). The halogen point source is placed at one of the ellipsoid focal points and the focal point of the lens is located at the other ellipsoid focal point. Since the halogen lamp is not a point source, the optical illumination is not

uniform. However, the illumination is assumed to be uniform on the slot due to its small area.

Waveguide calibration was used to calibrate the VNA. The waveguide is terminated by a metal plate with the thickness of 10 mils and a slot of the size of 1mm × 7.112 mm in the middle. The metal plate is placed in front of a 1.2 mm high resistivity silicon wafer. In the absence of the optical excitation, the high resistivity silicon behaves as a dielectric slab of $\varepsilon_r = 11.8$ onto which a slot is etched. A circuit model for this configuration is shown in Fig. (5-3).

Illumination of the silicon by the CW optical excitation leads to the generation of photoinduced plasma inside the silicon, which increases the conductivity of the silicon and the reflection coefficient of the waveguide. Increasing the power of optical excitation gives rise to higher carrier density inside the silicon and higher S_{11}.

Fig. (5-4) shows the measured S_{11} versus frequency for different levels of optical power. The carrier lifetime for this silicon is 1msec as measured in previous chapter. It is important to note that the halogen lamp generates a white light with a wide frequency bandwidth. However, the maximum silicon photosensitivity occurs around 900nm [55] as shown in Fig. (5-5). Therefore, a 900nm filter was located between the source and the optical power meter (Coherent model # 33-0290) to measure the optical energy in the frequency band for which the silicon is highly sensitive. A thermal sensor has been used for measuring the optical power in power meter. The power levels used in Fig. (5-4) are the readings after 900nm filter.

The optical source power was changed by changing the voltage of power supply. Increasing the optical power causes the S_{11} to approach unity, which demonstrates the metal like behavior of the wafer for the high optical power. However, due to the lossy nature of plasma, its reflection coefficient remains below the reflection coefficient of perfect metal. For instance, the reflection coefficient is –3dB for the maximum optical power, which implies 3dB loss inside the plasma.

5.1.2 Simulation results

To analyze the profile of plasma inside the silicon the structure shown in Fig. (5-1) was simulated using Ansoft HFSS. It was assumed that the conductivity of the plasma profile is constant throughout the thickness d_e of the silicon wafer and is equal to maximum conductivity σ_m as described in chapter 4. The permittivity of the photoinduced plasma generated by the optical excitation inside the silicon can be calculated using equation (4-20).

The real (ε_r) and imaginary parts (ε_i) of the permittivity of photoinduced plasma was plotted versus frequency in Fig. (4-8) for different carrier densities. Equation (4-9) was used to set the equivalent thickness of plasma to 0.2mm. The slot dimensions of the measurement setup (1 mm × 7.112mm) were used in the simulations.

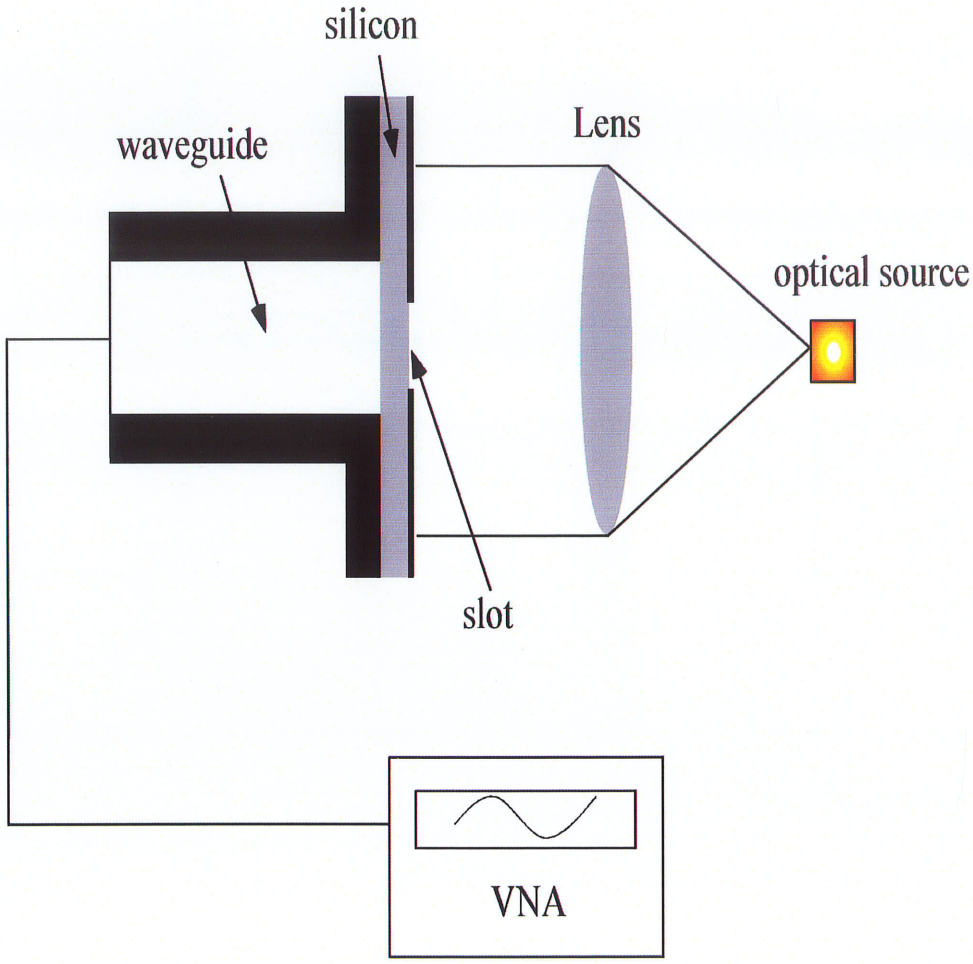

Figure 5-1: Waveguide setup to measure the profile of plasma

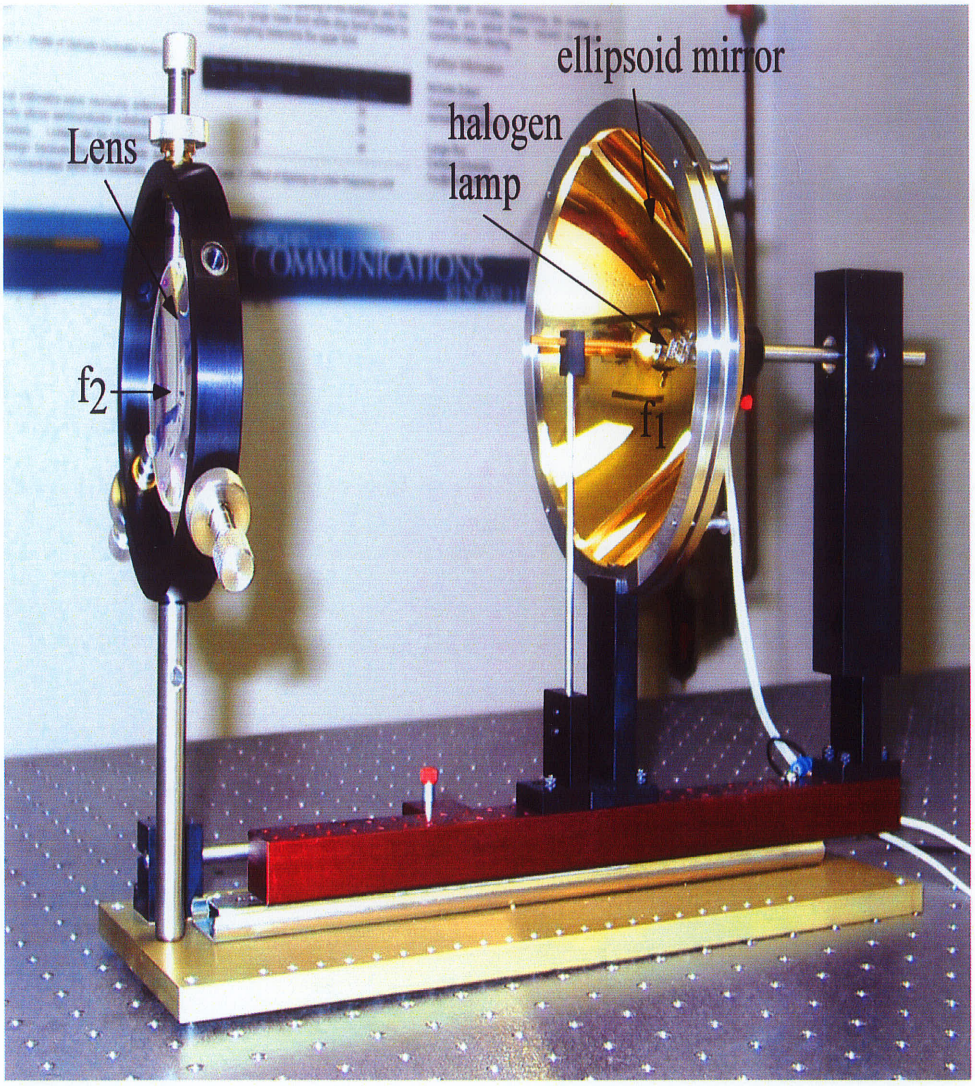

Figure 5-2: Halogen lamp setup, f1 and f2 are the two focal points of the ellipsoid mirror

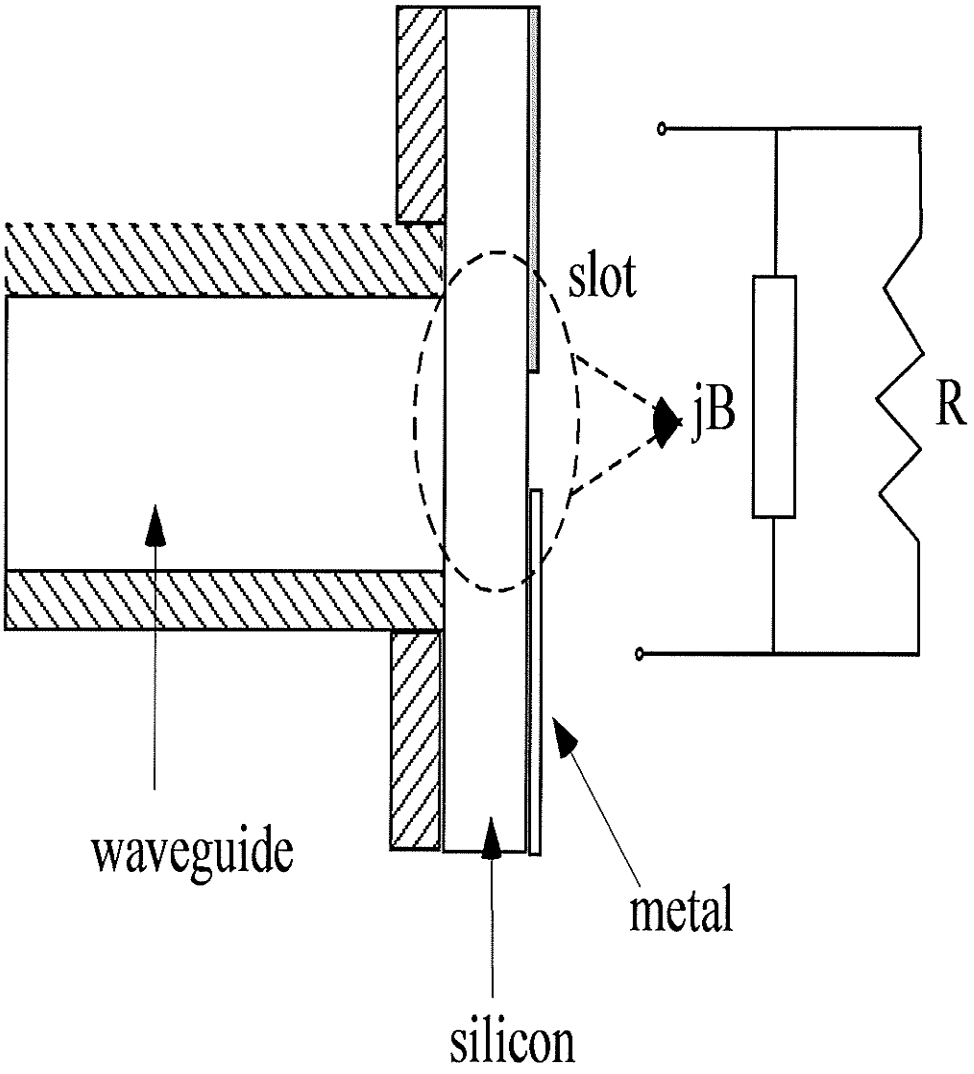

Figure 5-3: Equivalent circuit model for the slot as a load in the waveguide

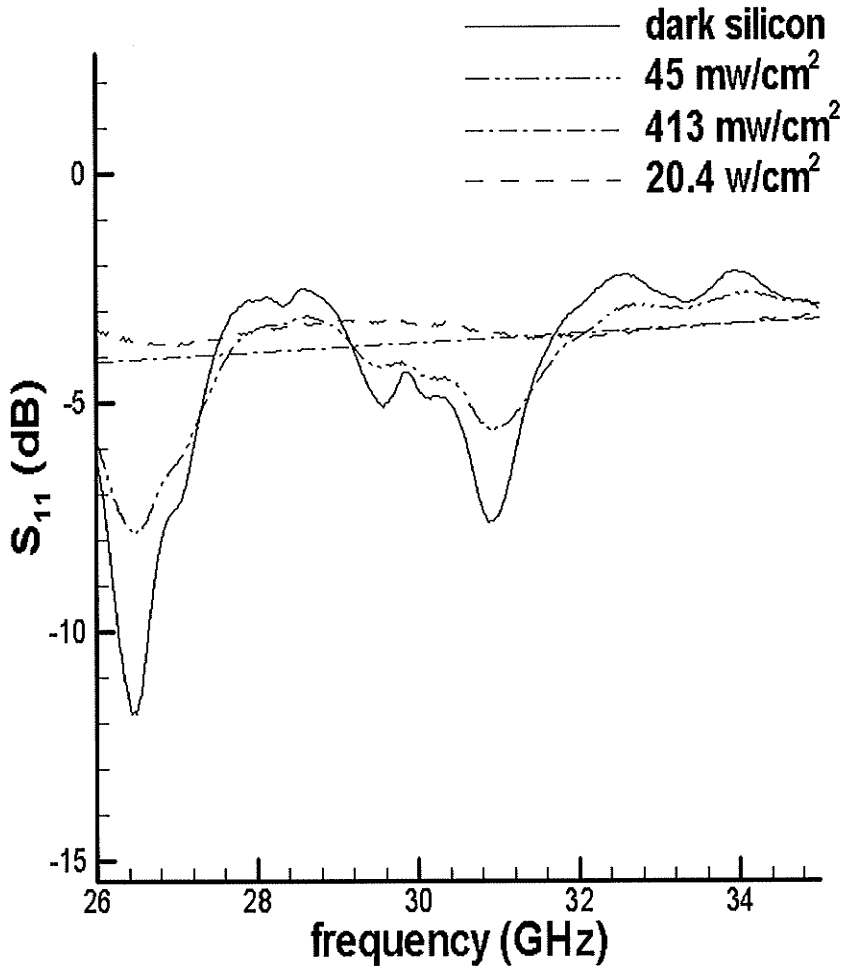

Figure 5-4: Measured S_{11} versus the frequency for different optical excitation powers

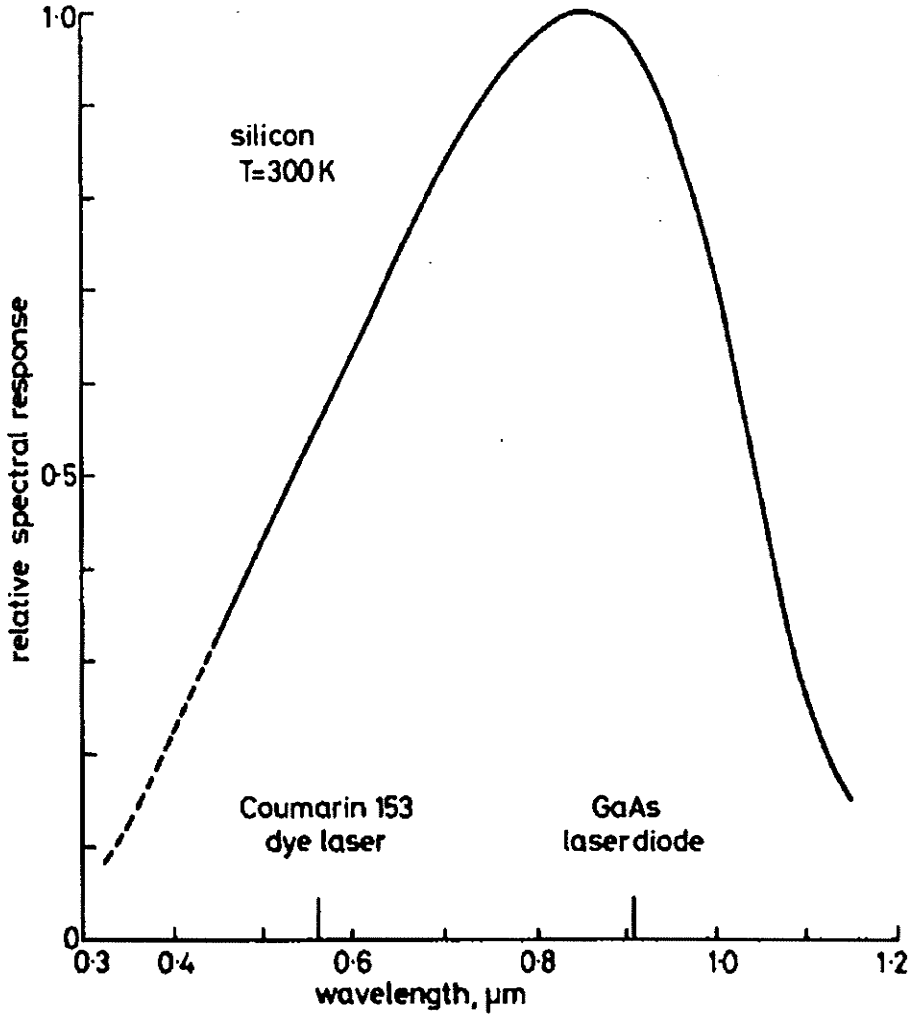

Figure 5-5: Spectral response of bulk silicon material

Fig. (5-6) shows the simulated S_{11} , versus frequency for different carrier densities. It was assumed that a plasma layer of 0.2mm thickness is induced inside the silicon and thickness does not change as the carrier density varies. The value of carrier density in the plasma region was varied in the simulations to get the best agreement between the measured and simulated resonant frequency.

Simulations were carried out for three carrier densities $N=10^{14}$ [cm^{-3}] $N=10^{15}$ [cm^{-3}] and $N=10^{17}$[cm^{-3}]. Fig. (5-7) shows the simulation and measurement results for different carrier densities and optical illumination, respectively. It is seen that the salient features of the measurement results such as resonances for $N=10^{14}$, and the flat nature of frequency response for $N=10^{15}$,and 10^{17} has been captured by the simulations. This implies the validity of the application of equivalent plasma thickness and conductivity as given in equations (4-9 and 4-10). This Fig. also shows the relationship between generated carrier density inside the silicon and optical illumination. Fig. (5-7) shows that the carrier density approaches 10^{17} as the optical power from the halogen lamp is maximized. Table (5-1) established correspondence between carrier density and plasma permittivity and the level of the optical power. The three different carrier densities, correspond to the optical excitation powers and plasma permittivity based on the measurement and simulation results for a cube plasma of the size of 1 mm × 7.112 mm × 0.2 mm.

Optical excitation power [mw/cm^2]	Carrier density [cm^{-3}]	Plasma permittivity
0	0	11.8
45	10^{14}	11.73 – j 2.03
413	10^{15}	11.05 – j 20.29
20400	10^{17}	- 63.13 – j 2024

Table 5-1: Carrier densities, correspond to the optical excitation powers

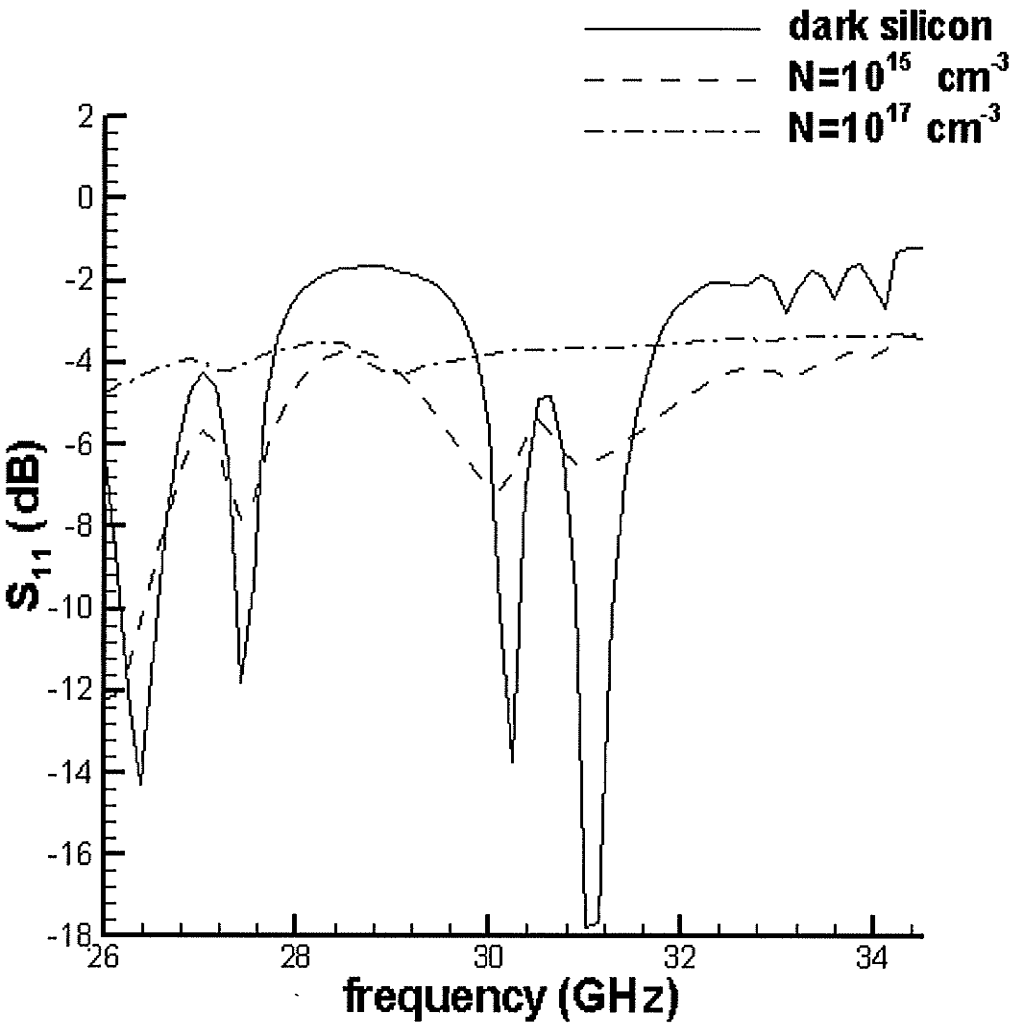

Figure 5-6: Simulated results of S_{11} versus frequency for different carrier densities

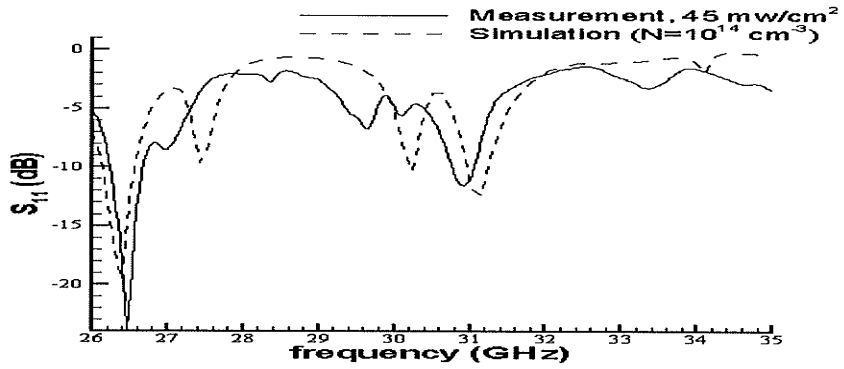

(a)

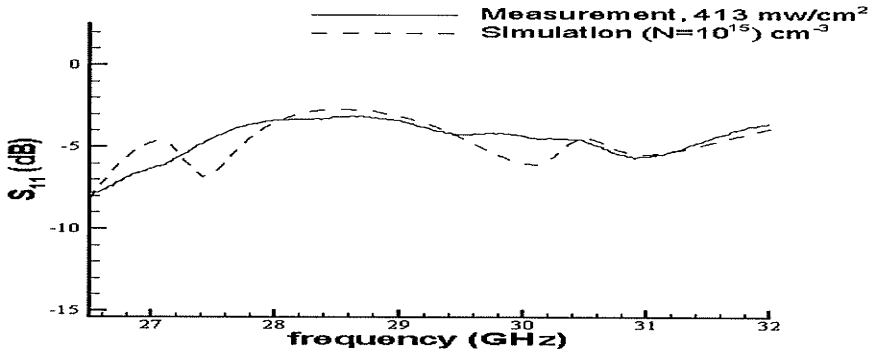

(b)

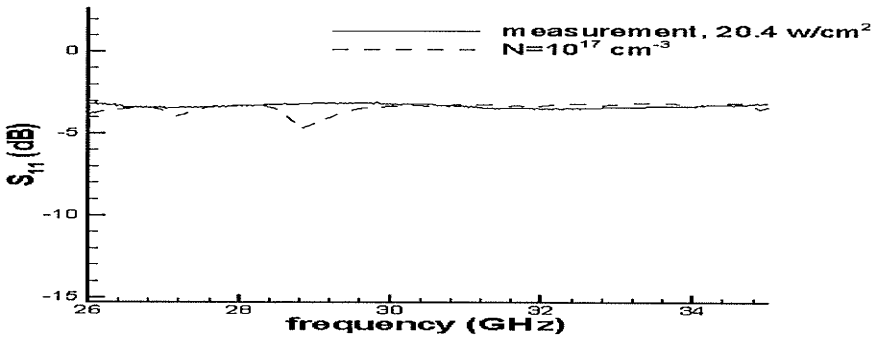

(c)

Figure 5-7: Measured and simulated results of S_{11} versus frequency for the carrier densities (a) $N=10^{14}$ cm^{-3} (b) $N=10^{15}$ cm^{-3} (c) $N=10^{17}$ cm^{-3}

5.1.3 Phase and amplitude of the reflection from a waveguide loaded with photonically controllable slot

The relationship between the photoinduced plasma characteristics and the optical power excitation has been presented thus far. The calculation of the reflection coefficient of a waveguide terminated in an optically controlled slot is studied in this section. The importance of this topic stems from the verification of the accuracy of HFSS simulations, which plays a pivotal role in the design of an optically controlled reflectarray as will be outlined in the next chapter.

The setup for the measurement of the phase and amplitude of the reflected wave is as same as Fig. (5-1), except in this setup a mask is located between the optical source and silicon to change the slot size photonically (see Fig. (5-8)). The slot length is controlled by generating the photoinduced plasma inside the silicon based on the mask pattern.

In this measurement since the optical source is not exactly plane wave, the optical rays diverge after passing through optical mask and the photoinduced plasma generated in the silicon is not as the same size as it is expected. To decrease this effect and generate almost the same mask pattern on the silicon the mask should be very close to the silicon. However a small distance between mask and the slot is required to avoid the loading of the waveguide setup by the mask.

Fig. (5-9) shows the measured and simulated results for the amplitude and phase of S_{11} for a slot of 1.0 mm length. The lamp was operating at its maximum power during this measurement. HFSS has been used to simulate this structure. The plasma thickness of 0.2 mm and plasma carrier density of 10^{17} were assumed throughout the simulations.

Fairly good agreement within 2% is observed between the measured and simulated resonant frequency. The agreement is sensitive to the slot length used in the simulation models. The discrepancies are mostly due to the uncertainty of the parameters values used in the simulation. However, the results demonstrate the validity of the simple model used in the simulation. The sources of disagreement between simulation and measurement are as follow:

1. Since the optical wave is not plane wave the size of plasma generated inside the silicon is not the same as the size of the transparent region in the mask. Therefore, the simulated resonant frequency was shifted in the simulation in comparison to the measurement. Figure (5-10) shows the simulation results for reflected wave when the length of plasma region changed around the length of openings in mask. It can be seen that the calculated resonant frequency approached measured resonance frequency when the extent of plasma is slightly larger than the mask opening.

2. The carrier density is assumed to be 10^{17}. As mentioned in the previous section an error was made in selection of the carrier density generated inside the silicon and what was chosen for the simulation. The loading effect of optical mask was not considered in the simulation either.

More simulation results will be presented in the next chapter when the topic of optically controlled reflectarray will be addressed.

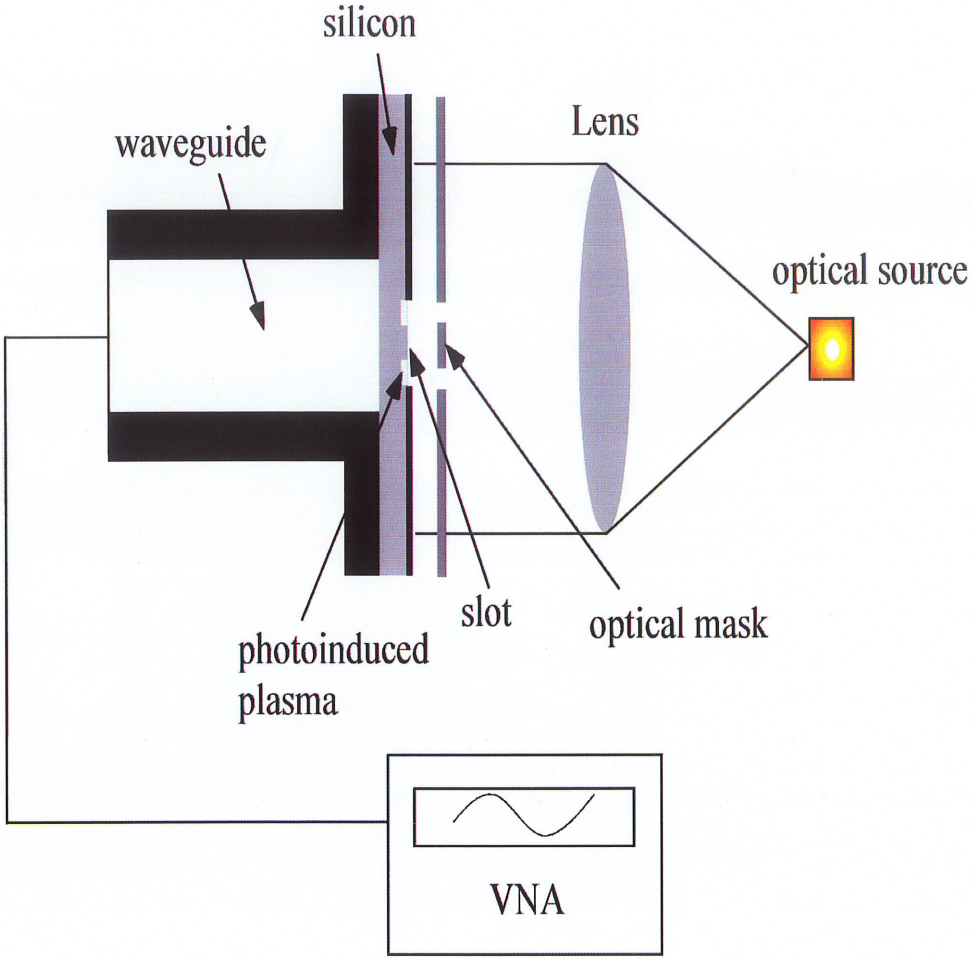

Figure 5-8: Waveguide setup for the measurement of the phase and amplitude of the reflected wave

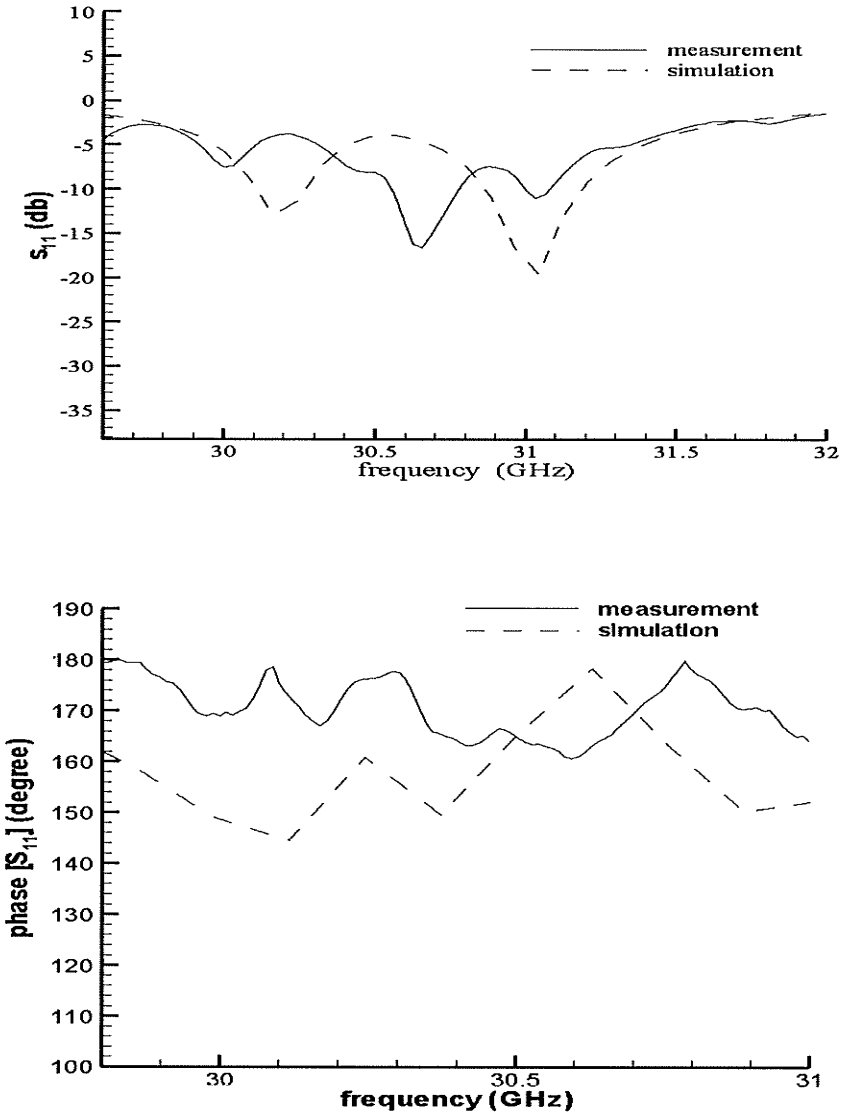

Figure 5-9: The measured and simulation results of the amplitude and phase of S_{11} for a waveguide setup with 1mm slot generated on the silicon

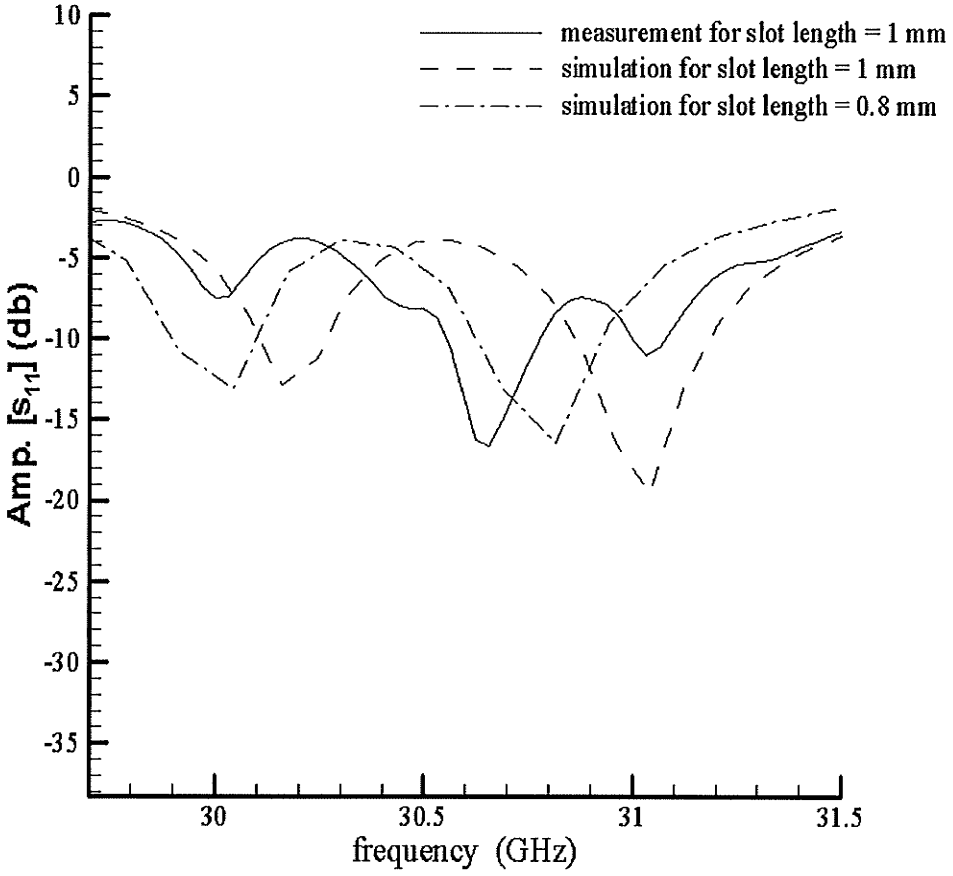

Figure 5-10: The measured and simulated results of the amplitude of S_{11} for two simulated different slot lengths

5.2 Calculation of the reflection coefficient of a 2-D photoinduced plasma grating structure

The first method that outlined in the chapter for the characterization of the photoinduced plasma in high resistivity silicon was based on the measurement of the reflection from a waveguide terminated in an optically controlled slot. The accuracy of this method is sufficient for the analysis of a 3-D plasma structure. However, noting that HFSS is based on finite element, the drawbacks of using this software for the simulations are its intensive memory and computational requirements.

To analyze 2-D photoinduced plasma structures a second technique has been presented in this chapter that is less intensive in terms of memory and computational requirements. In this method the induced plasma elements are replaced by equivalent surface impedance and the Floquet modes analysis based on MOM is applied to analyze the periodic structure. This method appeared to be much faster than the earlier method but it is not as accurate.

The array consists in thin metallic regions within a semiconductor slab. This is achieved by the illumination of the slab with a particular light source in conjunction with an optical mask placed between the source and the slab as shown in Fig. (5-11). Therefore, only the regions that are not covered by the mask will be exposed to the optical illumination, which leads to the creation of photoinduced plasma in these regions.

Changes in the dielectric material properties can be achieved by means of an optical source of variable intensity. To generate the photoinduced plasma grating lines as depicted in Fig. (5-11) a high power optical source is required. Since this optical source

was not available, in this dissertation only the simulation results based on the equivalent surface impedance method are presented and compare with the simulation results in HFSS.

5.3 Theoretical analysis using surface impedance

Following the geometry shown in Fig. (5-11), the array is represented by the photoinduced plasma elements with thickness S_p and permittivity ε_r^{si}. It is assumed throughout this analysis that the plasma thickness remains constant (d_e) as was discussed in chapter (4) while the plasma density is varied by changing the optical power. The induced plasma is thinner than the semiconductor substrate thickness. Noting the low lateral (x-direction) carrier diffusion, the width of plasma strips can be assumed to be the same as the width of openings in the mask (W).

The semiconductor relative permittivity is given in equation (4-20). As noted in chapter 4, ε_r^{si} is a function of microwave frequency and the plasma density N. Assuming a periodic structure of infinite extent Floquet method was used to represent tangential electric and magnetic fields. The field in the dark region can be written as follow:

$$E(r.,z) = \sum_{mpq} (T_{mpq} e^{-j\beta_{pq} z} + R_{mpq} e^{j\beta_{pq} z}) \Psi_{mpq}(r) \tag{5-1}$$

$$H(r.,z) = \sum_{mpq} \eta_{mpq} (T_{mpq} e^{-j\beta_{pq} z} - R_{mpq} e^{j\beta_{pq} z}) \Psi_{mpq}(r) \tag{5-2}$$

where T_{mpq} and R_{mpq} are the modal transmission and reflection coefficient respectively. η_{mpq} is the modal admittance, pq are the modal indices and m=1,2 stands for TM and TE modes respectively [56].

The propagation constant is $$\beta_{pq} = \sqrt{k_0^{\,2}\varepsilon_r - k_{tx}^{\,2} - k_{ty}^{\,2}} \tag{5-3}$$

where k_{tx} and k_{ty} are the tangential wave vector components and k_0 is the free space wave-number. Enforcing the condition of the total (scattering and incident) electric field $E^{tot} = Z_{sp}J$, where Z_{sp} is the surface impedance.

It is assumed that there are no transverse currents flowing through the plasma elements. The surface impedance in z = $-S_p$ can be calculated according to a transmission line method, as follow:

$$Z_{sp} = Z_a \frac{Z_l \cosh(\gamma) + Z_a \sinh(\gamma)}{Z_l \sinh(\gamma) + Z_a \cosh(\gamma)} \tag{5-5}$$

According to Fig. (5-12) and based on equation (5-5) when $Z_l = Z_0$, $Z_a = Z_0 / n_r$ *and* $\gamma = jk_0 n_r s_p$

$$Z_{sp} = \frac{Z_0}{n_r} \frac{Z_0 \cosh(jk_0 n_r s_p) + \dfrac{Z_0}{n_r}\sinh(jk_0 n_r s_p)}{Z_0 \sinh(jk_0 n_r s_p) + \dfrac{Z_0}{n_r}\cosh(jk_0 n_r s_p)} \tag{5-6}$$

$$Z_{sp} = \frac{Z_0}{n_r}\left[\frac{n_r \cosh(jk_0 n_r s_p) + \sinh(jk_0 n_r s_p)}{n_r \sinh(jk_0 n_r s_p) + \cosh(jk_0 n_r s_p)}\right] \tag{5-7}$$

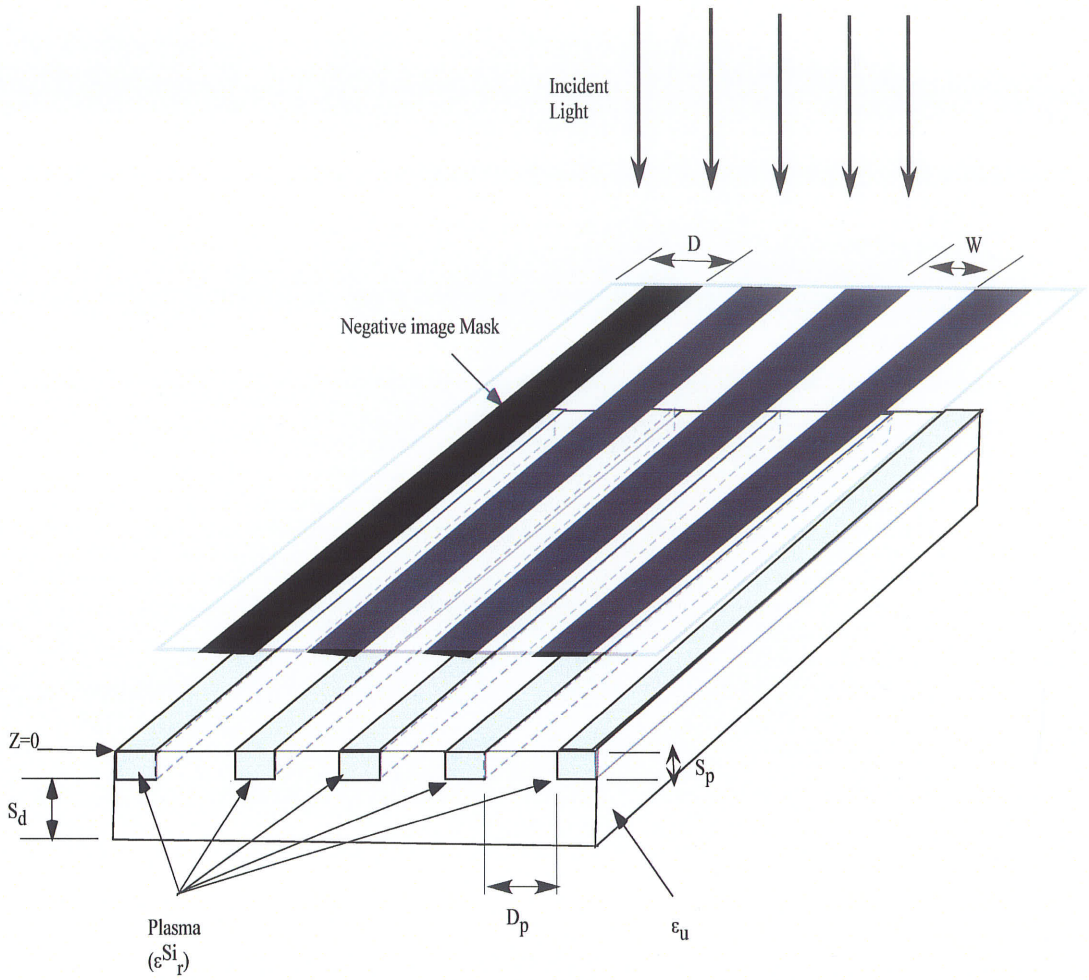

Figure 5-11: Schematic view of a photoinduced plasma grating structure

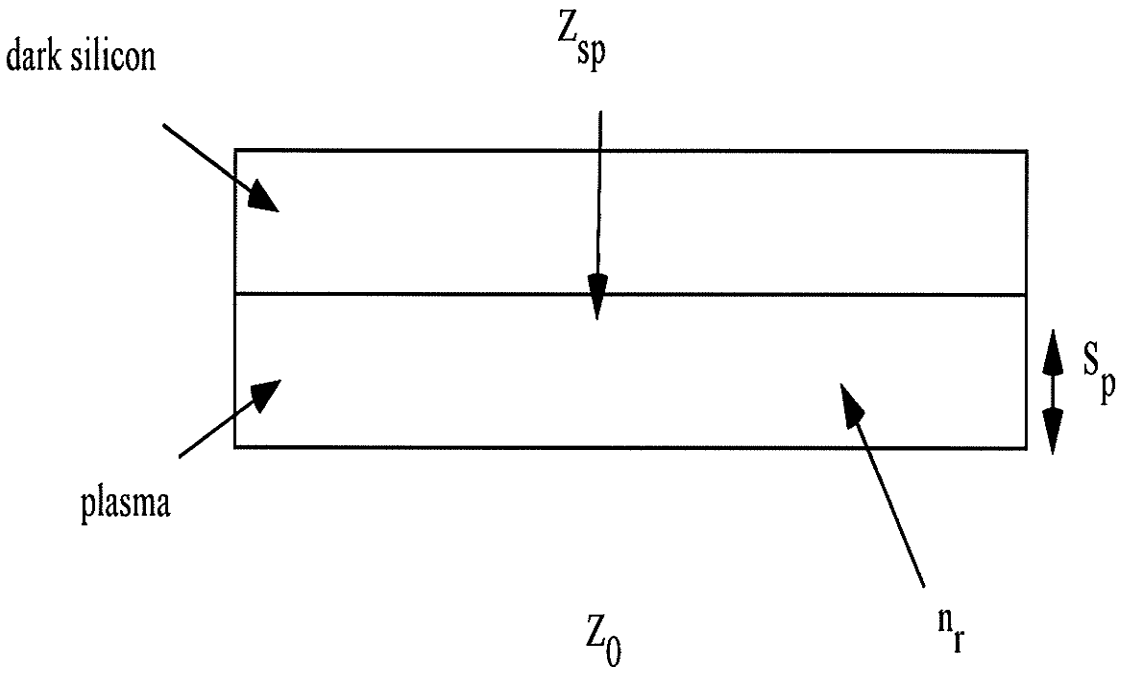

Figure 5-12: A transmission model for calculating surface impedance of plasma generated inside a silicon wafer

The surface impedance is a function of the carrier density inside the plasma. Fig. (5-13) shows the impedance for different plasma concentration. At low concentration the imaginary and real parts of Z_s are both high. The magnitude of imaginary part increases but real part decreases as the plasma thickness increases. At the intersection point of the real and imaginary parts of the refractive index, real and imaginary parts of the impedance coincide as well.

In this simulation EMPiCASSO™ [56], which is a commercial software based on MOM is utilized for analyzing the structure. In this software instead of defining the 3-D plasma profile as depicted in Fig. (5-11) a 2-D microstrip line grating structure as shown in Fig.

(5-14) has been defined. The properties of these microstrip lines are defined in such a way that the same surface impedance as calculated in equation (5-7) will be assigned to these lines. The permittivity of substrate (ε_{si}) is 11.8, which is equal to the permittivity of dark silicon. A cell element was defined as shown in (5-14) periodic boundary conditions were used to simulate the whole periodic structure.

Fig. (5-15) shows the simulation results of the amplitude of the transmitted wave for different carrier densities based on this method and also the simulation results for the same structure using HFSS. To analyze this structure in HFSS, a 3-D plasma profile, which is shown in Fig. (5-10) has been defined and waveguide simulator method as explained in chapter 2 is utilized for this simulation. Fig. (5-15) shows a good agreement between both simulations in HFSS and PiCASSO.

In the 2-D method presented in this section the transmission line method has been used for the calculation of the surface impedance and also it was assumed that there in no vertical current in the z direction. Therefore, this method is not suitable for analyzing 3-D waveguide structure with finite plasma profile inside the silicon. However, finite element is capable of handling such problems with high accuracy.

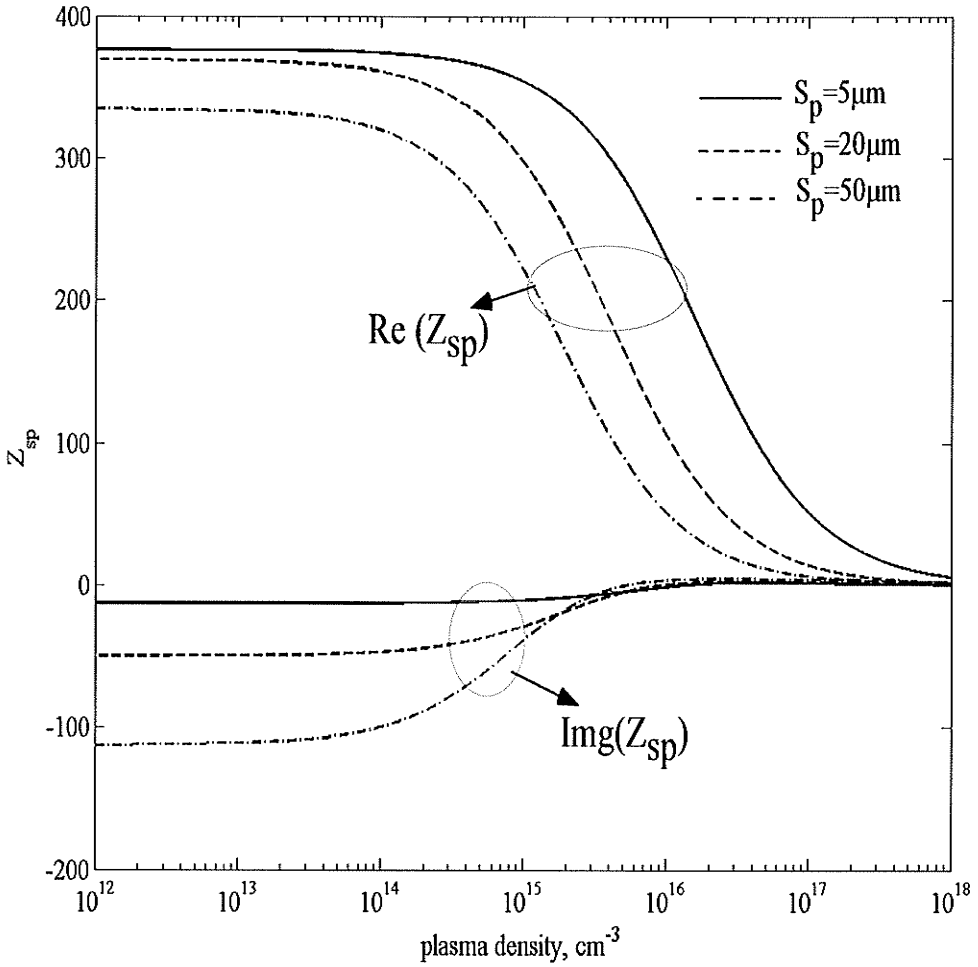

Figure 5-13: Surface impedance as a function of plasma carrier density for different plasma thickness

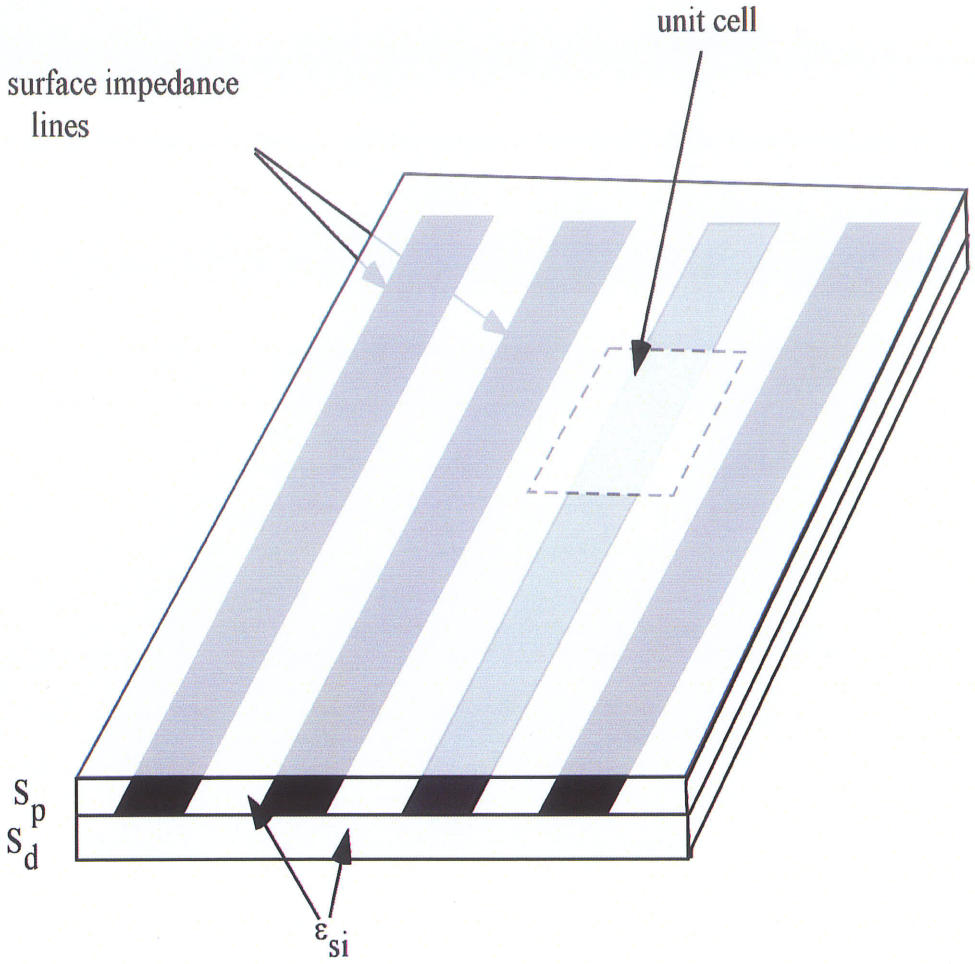

Figure 5-14: Schematic view of the photoinduced grating structure applied in PiASSO

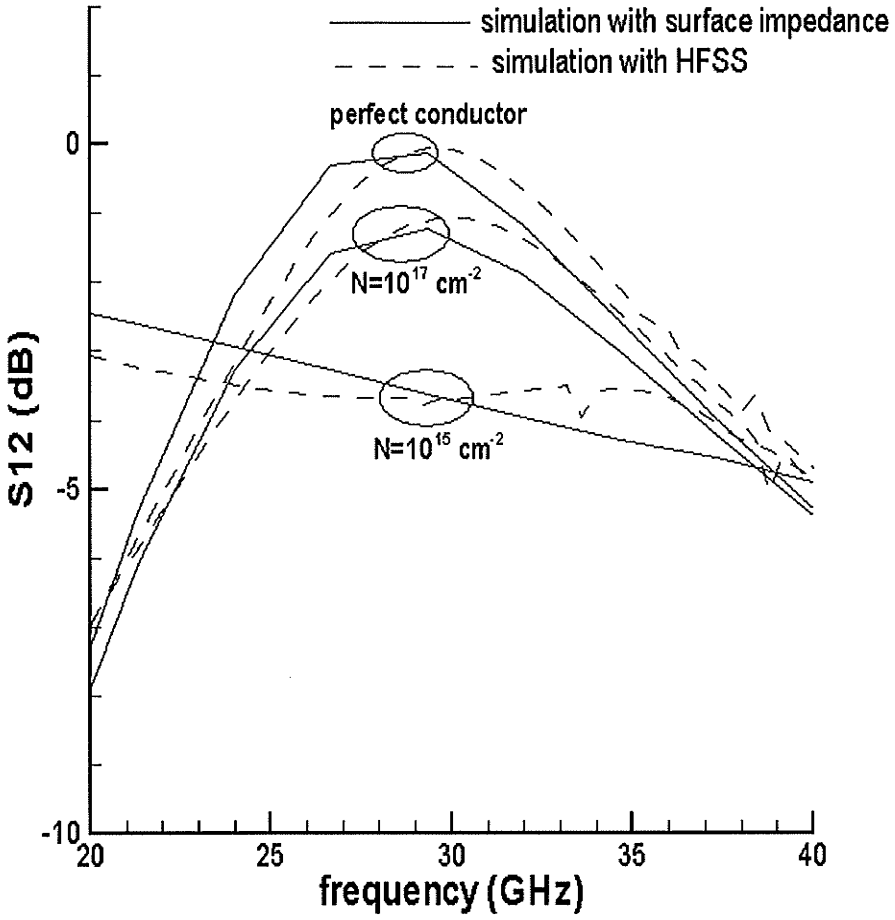

Figure 5-15: Transmission coefficient versus frequency in PiCASSO and HFSS

5.4 Conclusion

A measurement method based on reflection coefficient of a rectangular waveguide loaded with a silicon wafer is considered. This method was used for the measurement of the plasma profile inside the silicon. Two methods for the simulation of photoinduced plasma structures were presented. These methods are utilized for 2-D and 3-D structures. In 3-D method, HFSS was utilized and the plasma profile and plasma permittivity, introduced in chapter 4 was used for this simulation. The waveguide structure presented in measurement setup was simulated with this method. The simulation results were compared to the measurement results in the waveguide setup to find a relationship between carrier densities employed in the simulation and the optical power in the measurement.

The 2-D method presented in this chapter was utilized for analyzing the 2-D grating structure. This method is much faster than 3-D method however it is not as accurate for analyzing the 3-D structures with limited size plasma.

CHAPTER 6

PHOTONICALLY CONTROLLED REFLECTARRAY ANTENNAS

Introduction

A novel photonically controlled method to adjust the aperture phase distribution of a reflectarray antenna was briefly described in chapter 3 of this thesis. The method is based on varying the slot length by the generation of photoinduced plasma inside the silicon. The present chapter is devoted to a detailed exposition of the method and its implementation.

The reflectarray is simulated by HFSS software and the approximation to the plasma profile that was discussed in chapter 4, is utilized to analyze the photoinduced plasma regions of the reflectarray. Two configurations based on single layer and multi layers reflectarrays are presented and advantages and disadvantages of each structure are discussed in this chapter. A prototype is fabricated and its radiation pattern is measured. An optical pulse source is used to illuminate of the prototype and the effect of optical illumination density on the radiation pattern and efficiency of the antenna is evaluated. The fabrication process of the multilayer reflectarray is presented and the potential sources of loss and phase error are studied. This chapter will be closed by concluding remarks.

6.1 Single layer reflectarray with slots of varying size

The novel single layer printed reflectarray that consists of microstrip patches of similar size arranged into regular lattice configuration on the top layer and periodic configuration

of slots of varying size on the bottom layer was presented in chapter 3. In this section an optically controlled method is introduced for the variation of the slot length.

A schematic view of this reflectarray is shown in Fig. (6-1). The antenna comprises a silicon wafer as the substrate layer. The radiating patch elements of identical size are etched on the top surface of silicon. The bottom surface is an array of slots of identical size that are centered beneath the patches. The reflectarray is fed by a pyramidal horn operating at 30 GHz from the patch side and an optical source that illuminates the reflectarray from the slot side. An optical mask is located between the optical source and reflectarray. The pumping light illuminates the reflectarray through the optical-mask, creating a plasma pattern of the same shape as the pattern on the mask. The plasma profile changes the slot length printed on the silicon and the slot variation changes the phase distribution on the reflectarray surface. The phase distribution on the reflectarray surface is controllable by using different mask patterns.

Fig. (6-2) shows the phase and amplitude of reflected wave versus slot length when the slot length is changed by photoinduced plasma. The structure was simulated using waveguide simulator feature of HFSS as described in section (2.1.4). The plasma depth for all the cases was constant and set to 0.2mm. Equation (4-10) was used to calculate the depth of plasma for a silicon of 1 msec carrier lifetime and 1.2 mm thickness. The patches on the top layer are 3.2 mm × 2.0mm each. The calculations were done for plasma carrier densities of 10^{17} cm^{-3} and 10^{18} cm^{-3}. The structure was also simulated as a perfect conductor instead of photoinduced plasma to investigate the effect of plasma loss.

The phase variation for all the cases (carrier densities 10^{17} cm^{-3} and 10^{18} cm^{-3} and perfect conductor) are almost the same and about 310° phase variation can be achieved by changing the slot length. However, the amplitude of the reflection changes as a result of varying the plasma density. As expected, decreasing the carrier density of the photoinduced plasma gives rise to a higher loss inside the plasma. The level of carrier density is a measure of how well the photoinduced plasma regions can emulate the perfect conductor behavior. For the carrier density of 10^{17} cm^{-3} the amplitude of S_{11} plunges to –12 dB for the slot length of 2 mm. This shows most of the MMW energy is absorbed by the photoinduced plasma or radiated from the slot. The behavior of photoinduced plasma is very close to perfect conductor for the carrier densities above 10^{18} cm^{-3}.

The slope of the linear region in Fig. (6-2b) is about 17°/mils, and for a fabrication tolerance of 1mil, the random fabrication error can contribute as much as 17° of phase error. Since the slot length is changed by generating the photoinduced plasma inside the silicon and the plasma profile is controlled by the pattern of optical mask, the mask should be located as close as possible to the slot to avoid the phase error because the optical ray divergence. For single layer reflectarray, placing the optical mask very close to reflectarray will load the slots and changes the phase variation. The mask has to be located at least 2λ far from the reflectarray to suppress the coupling.

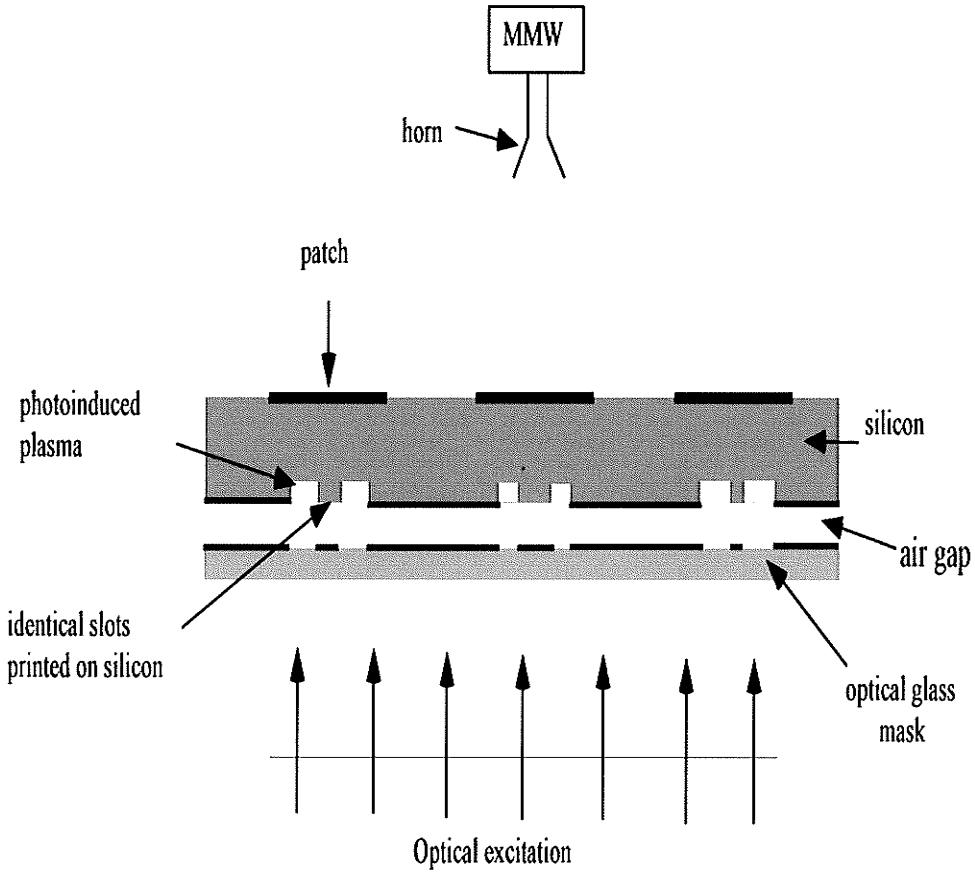

Figure 6-1: Schematic view of a single layer reflectarray with optically controlled slots on the ground plane

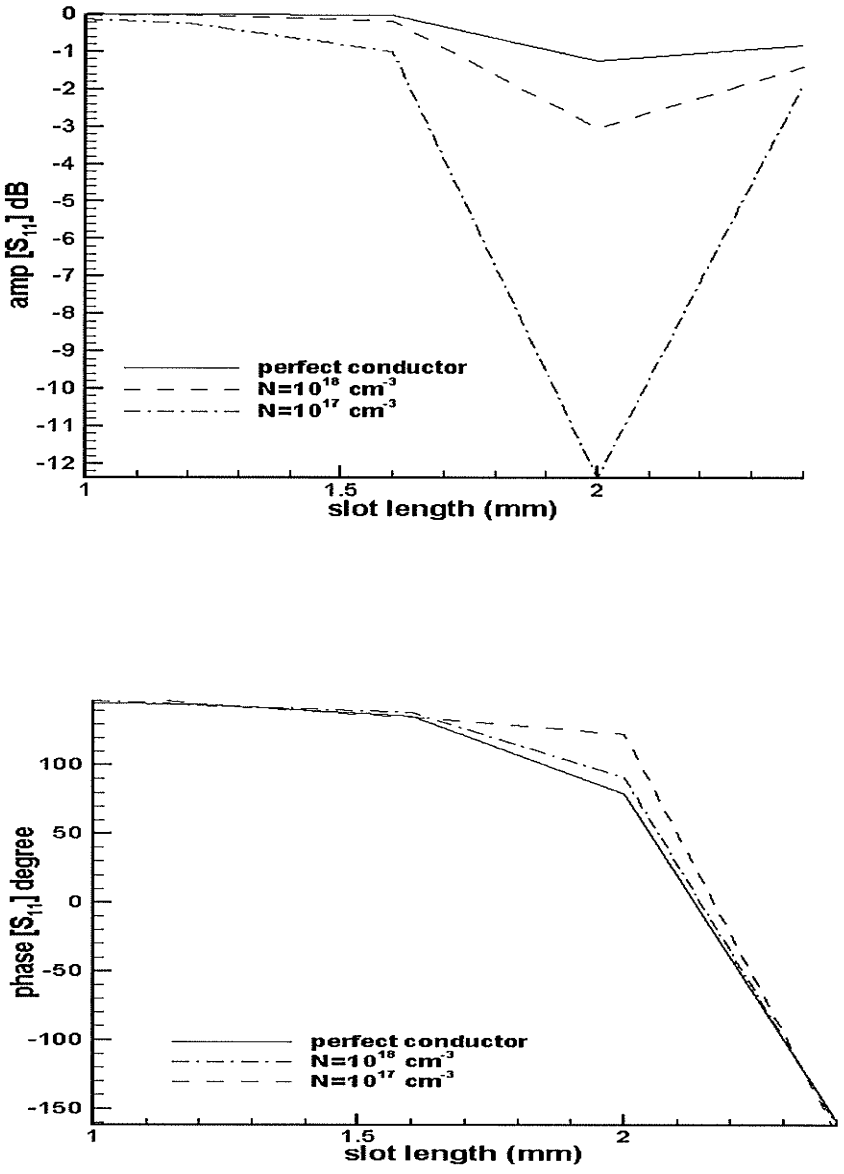

Figure 6-2: Amplitude and phase of S_{11} versus slot length of the single layer reflectarray for the different carrier densities of plasma

To overcome the drawbacks of a single layer prototype another reflectarray based on multilayer configuration is presented in next section.

6.2 Three- layer reflectarray with slots of varying size

The reflectarray antenna presented in this section consists of three layers. A schematic view of this structure is depicted in Fig. (6-3). This antenna consists of a dielectric substrate layer onto which an array of microstrip patches of identical size are etched, the second layer is a silicon wafer with the slots of identical size that are etched on its lower surface, an optically transparent substrate layer (glass) that is located beneath the silicon, a small airgap between this glass plate and the silicon wafer as shown in Fig (6-3), and an Indium Tin-Oxide (ITO) sheet is interposed on top of glass between the silicon wafer and glass layer. The ITO sheet is optically transparent and reflective at the wavelength of the RF signal. The characteristics of the ITO material will be explained later. The optical mask is attached to the glass. An optical source illuminates the reflectarray from the glass side and the array of microstrip patches are excited by a pyramidal horn designed to operate at a frequency of 30 GHz.

The silicon substrate layer provides variable inductive slots acting on the microstrip patches through photoinduced plasma effect in order to impart a predetermined phase shift onto the reflected electromagnetic signal. The optical mask consists of an array of apertures being disposed opposite to the slot such that the two apertures that fall below each slot expose a predetermined region to optical signal to generate plasma and change the effective length of that particular slot. The ITO layer acts as a ground plane in this structure and brings about a good isolation between optical source and MMW signal.

Because of this isolation, the optical mask can be attached to antenna right after ITO layer.

6.3 Reflectarray design methodology

The following section outlines the design steps required to build the photonically controlled reflectarray. The described antenna is a three-layer reflectarray with the slots of varying length size on the ground plane. A schematic view of this antenna is shown in Fig. (6-3). The antenna is designed to operate at 30 GHz. The first layer is a dielectric material with permittivity of 3 and thickness of 0.5mm (Rogers3003). Middle layer is a high resistivity silicon wafer with diameter of 3" and thickness of 1.2mm. The permittivity of this silicon in the absence of optical excitation is 11.8. There is an airgap of 0.5 mm between the silicon wafer and ground plane. A layer of ITO is coated on a thin layer of glass substrate. The ITO acts as a ground plane for this reflectarray. The resistivity of the ITO is 20 ohm/cm^2 and its transmission is close to 80% at 900 nm.

Fig. (6-4) shows the phase and amplitude of the reflected wave versus the slot length when the slot length is changed by photoinduced plasma. The structure was simulated using HFSS. The carrier density of plasma is set 10^{17} cm^{-3}, 10^{18} cm^{-3} and infinite (perfect conductor).

Similar to the single layer reflectarray, as the carrier density of plasma is decreased the plasma becomes more lossy which affects the reflection coefficient of the structure to such an extent that the amplitude of S_{11} is decreased by decreasing the carrier density however in this configuration the presence of a ground plane beneath the slot layer, prevents the leakage of power into the lower half space and this decrease the loss of S_{11}

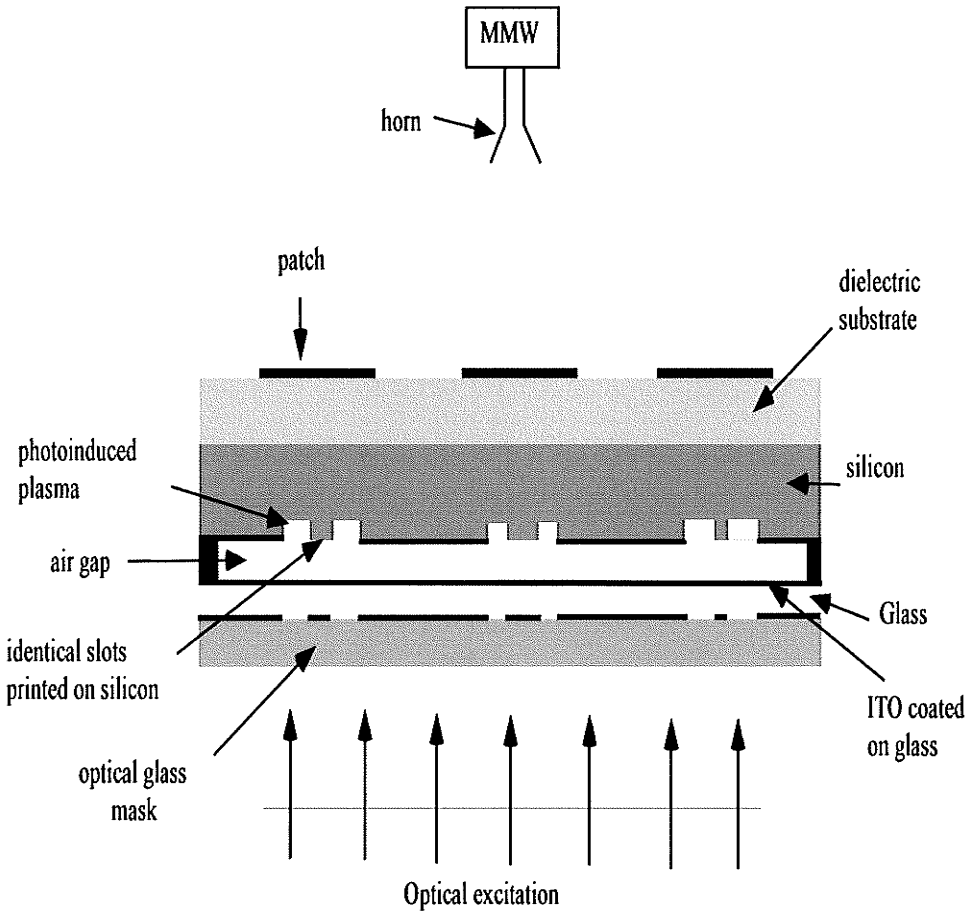

Figure 6-3: Schematic view of a multy-layer reflectarray with optically controlled slots on the ground plane

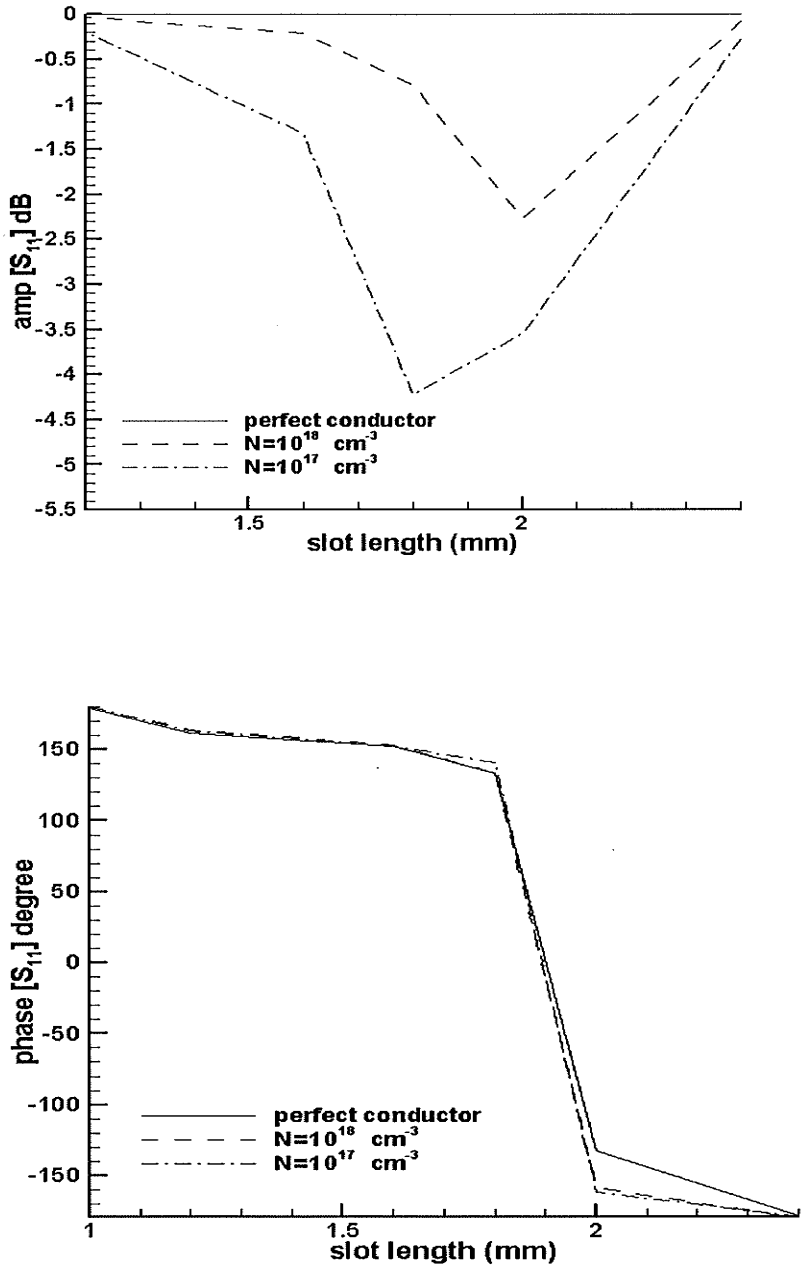

Figure 6-4: Amplitude and phase of S_{11} versus the slot length of three-layer reflectarray for the different carrier densities of plasma

in compare to single layer configuration. The phase variation of S_{11} versus frequency is the same for all the cases.

6.4 Measurement setup

A transmitter- receiver setup as depicted in Fig (6-5) was used for the measurement of the radiation pattern of the reflectarray. The reflectarray under the test is located at the transmit side and it is fed by a pyramidal horn. The signal is received by a pyramidal horn, located at the far field of transmitter. The optical source is a Xenon flash lamp. This high power Xenon lamp comprises of two components; namely an appropriate photolysis system and a lamp house. A flash photolysis system consists of a bank of storage capacitors plus a power supply to charge the capacitors up to 400 V. The storage capacitors are connected across the electrodes of a Xenon lamp [58]. The lamp is normally in high-resistance state, but the application of a brief high-voltage trigger pulse causes a spark to jump between the electrodes. This provides a conduction pathway for very rapid (typically less than 1msec) discharge of the storage capacitors, resulting in an intense light flash. The capacitors are then recharge from the power supply in preparation for the next flash. The pulse duration, intensity and recharge rate of the flashes can be controlled by selecting the capacitors and DC voltage. The flash energy can be calculated according to following equation:

$$E = \frac{1}{2} C V^2 \tag{6-1}$$

where C is the capacitance of a variable charge capacitor and V is the variable charge DC voltage. The flashes generated by Xenon lamp are collimated in lamp house, using a combination of mirrors and lenses. In this system a 3" collimated beam can be generate within the lamp house. A view of this optical source setup was shown in Fig. (4-10).

The reflectarray is illuminated by this optical source and as mentioned before the consequence of this illumination is generation of photoinduced plasma inside the silicon and the variation of slot length printed on the silicon. The variation of slot length adjusts the phase of incoming wave to collimate the beam in the desired direction. Therefore, the reflectarray can collimate the beam only during the ON state of the optical pulse.

The 30 GHz output power from the RF source was set at 0 dBm. The output power is split into two branches by a directional coupler. One branch is routed to the reflectarray feed through an amplifier. To detect the signal during the optical excitation a double balanced diode mixer was utilized on the receiver side. The signal on the second branch of the directional coupler is amplified and then fed to the LO Port of the mixer. The receiver signal is fed onto the RF Port. The IF signal is monitored by a 500MHz digital oscilloscope. The calculation of this signal is described below.

The MMW source generates a sinusoidal signal $x_1(t)$

$$x_1(t) = A_1 \sin(\omega t) \tag{6-2}$$

When there is no optical excitation the signals in LO, RF and IF ports are as follow:

$$x_{RF}(t) = A_1 \sin(\omega t + \phi_1) + FSL. + G_t + G_r = A_2 \sin(\omega t + \phi_1) \tag{6-3}$$

$$x_{LO}(t) = A_3 \sin(\omega t + \phi_2) \tag{6-4}$$

$$x_{IF}(t) = \frac{1}{2} A_2 A_3 \cos(\phi_1 - \phi_2) \tag{6-5}$$

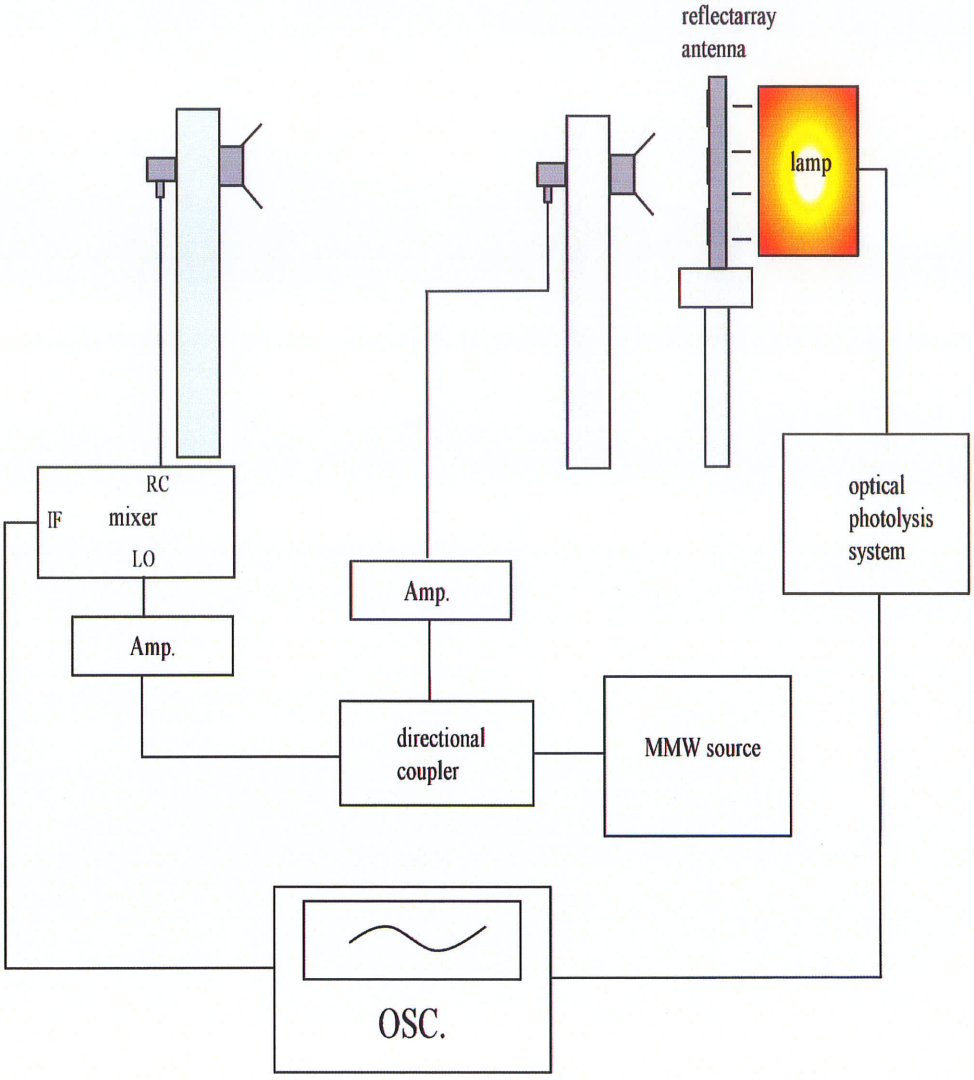

Figure 6-5: Schematic view of the measurement setup

where G_t and G_r are the gains of transmitter and receiver antennas respectively. *FSL* represents the free space loss. Considering the above relations a DC signal is monitored at the output of the mixer.

The reflectarray collimates the beam at along the boresight during the ON state of the optical pulse. The antenna gain depends on the optical excitation (g(t)) as this determines the excess carrier density. In fact the reflectarray acts like a mixer and multiplies the

envelope of the optical illumination and MMW signal generated by RF source. In this situation the signal received at RF port of the mixer is

$$x_{RF}(t) = A_4 g(t) \sin(\omega t + \phi_1) \tag{6-6}$$

And the detected signal monitored by oscilloscope in IF port is:

$$x_{IF}(t) = \frac{1}{2} A_4 A_3 \cos(\phi_1 - \phi_2) g(t) \tag{6-7}$$

As it is shown in equation (6-7) the variation of signal in IF port is similar to the envelope of the optical signal *g(t)*. For this measurement setup as shown in Fig. (6-6), the receiver antenna is installed on a movable arm to adjust the azimuth angle of this antenna between $\pm 30^{o}$. Since the *FSL* is very high at 30 GHz (62 dB for 1m) The amplifier #1 is located before the transmitter to increase the dynamic range. The other amplifier in this setup increases the signal level to 14 dBm at the LO port of the mixer to bias the mixer at its linear area. A TTL pulse, generated by the optical system is used to trigger the digital scope. This trigger pulse is up when the optical signal is on. When the optical source is switched on the photoinduced plasma will be induced inside the silicon. The pattern of this photoinduced plasma is the negative of the mask pattern. A negative glass mask with the thickness of 0.5 mm has been utilized for the mask. The mask pattern is designed to

collimate the beam at boresight. Fig. (6-7) shows the monitored signal by the oscilloscope for different level of the optical illumination. The received signal is increased by increasing the optical energy of the flash lamp. However, beyond a certain level of the optical energy the amplitude of the received signal stays constant due to the highly conductive nature of the induced plasma.

Fig. (6-8) shows the measured radiation pattern of this antenna. In this measurement the receiver is moved in azimuth direction between $\pm 20^{o}$ in 1^{o} steps. The amplitude of IF pulse is observed on oscilloscope at each step. The power is normalized by the measured power at 0^{o}. When the reflectarray is illuminated by an optical excitation the beam is collimated at 0^{o}. The sidelobe level is high as a result of large blockage of feed horn.

Fig. (6-9) shows the normalized power received by the receiver at $\theta = 0^{o}$ for different frequencies. The power is maximum for designed frequency (30 GHz) but is dropped dramatically by changing the frequency. The bandwidth of this antenna is very narrow as a result of the phase error and loss in photoinduced plasma.

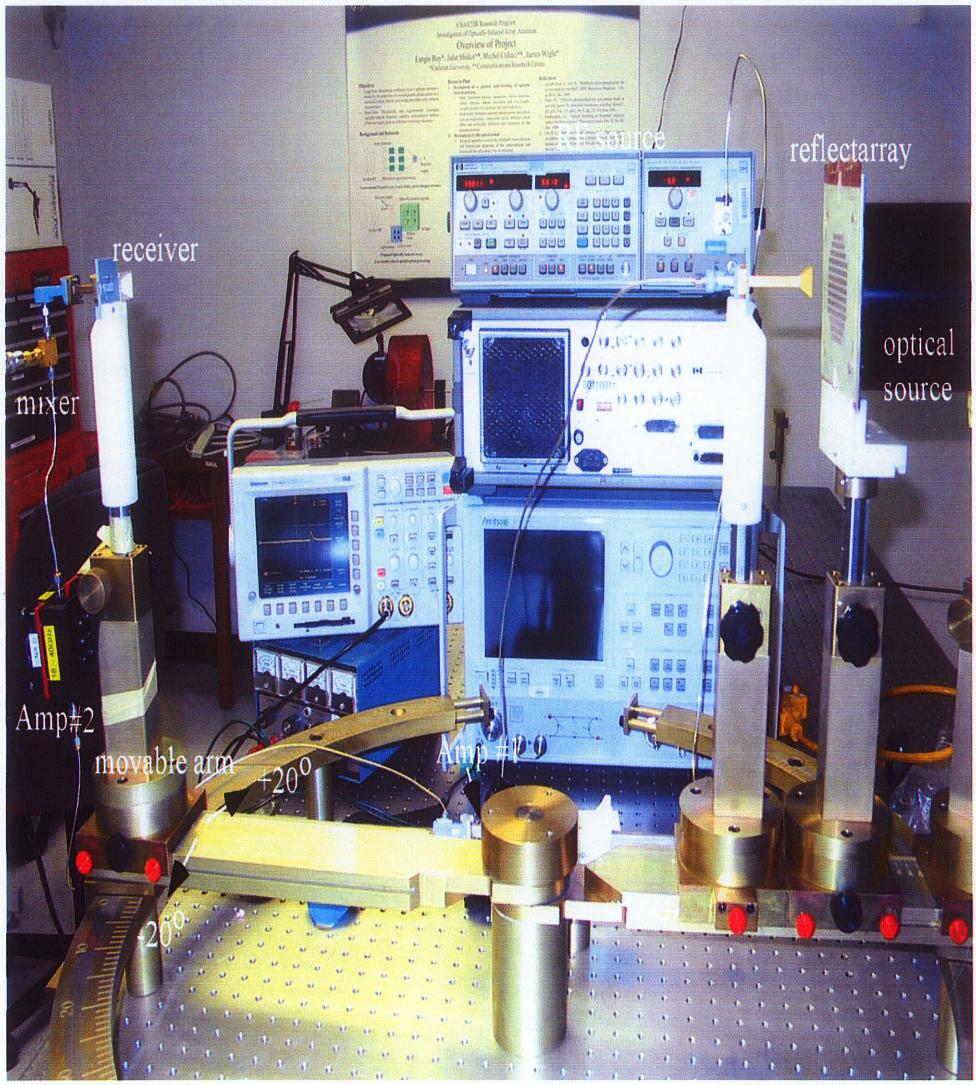

Figure 6-6: A view of the measurement setup

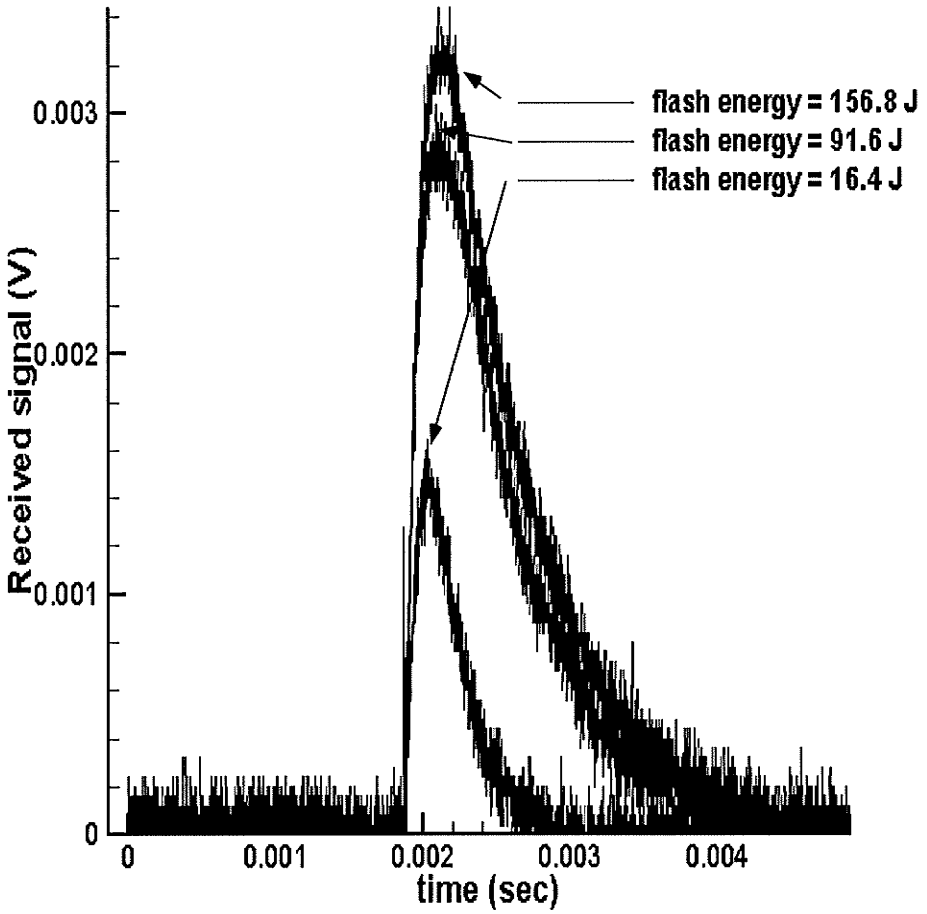

Figure 6-7: Monitored signals in oscilloscope for different optical illumination energies

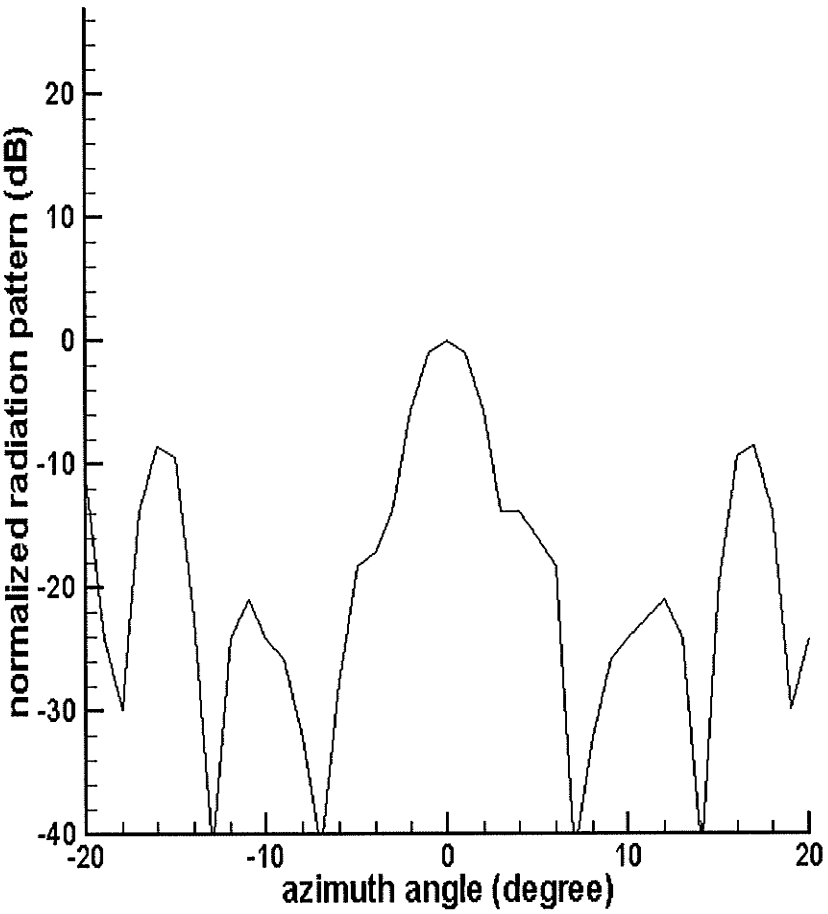

Figure 6-8: Normalized radiation pattern of the reflectarray

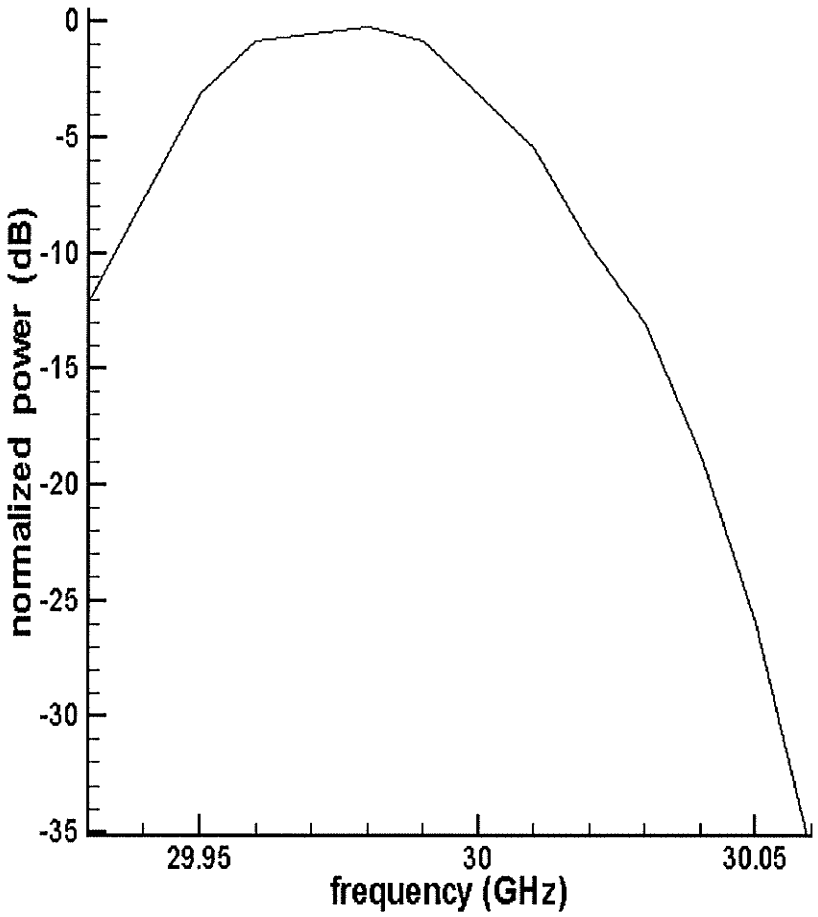

Figure 6-9: Normalized power at $\theta = 0^{o}$ versus frequency

6.5 Efficiency of the reflectarray

The photoinduced plasma is a lossy medium and the loss is an important factor in the design and operation of optically steerable semiconductor-based antenna. However, since only a small part of the slots are covered by the photoinduced plasma in the reflectarray that is introduced in this chapter, the loss is much less than conventional methods for which the whole radiating elements are generated by the photoinduced plasma. The presence of the ground plane in the three-layer reflectarray even decrease the loss further in compare to the single layer configuration.

Fig. (6-4) shows the loss inside the photoinduced plasma. As can be seen from this figure, when the length of the slots is changed by generating the photoinduced plasma inside the silicon the amplitude of S_{11} is decreased. The loss is related to the carrier density of the plasma in the sense that by increasing the carrier density, the plasma becomes more conductive and less lossy. Increasing the power of optical illumination is one way of increasing the carrier density. However, high optical power is required for antennas of large size. The other methods for increasing the carrier density are the improvement of silicon characteristics or choosing different materials instead of silicon. For instance the carrier density can be increased by increasing the carrier recombination lifetime of the silicon. Focusing on the material properties to find candidates with increased carrier density can be done as a future continuation of this thesis.

Phase errors incurred in the design process and random phase errors resulting from fabrication are other sources of reduction in the gain and efficiency of the reflectarray.
The sources of phase error in reflectarray antenna were introduced in chapter 2. Another source of phase error, namely the phase error as a result of non-uniform profile of plasma

was introduced in this chapter. The simulation shows that when the carrier density is higher than 10^{17} the phase variation is almost independent of carrier density and is very close to the case of perfect conductor.

6.6 Fabrication summery

Since random phase error as a result of fabrication tolerance is one of the main sources of error in this reflectarray, a summery of the fabrication process that was used in the construction of the reflectarray prototype is outlined in this section. This fabrication process consists of etching the patches on a RT/duroid substrate and the slots on the silicon and alignment of the reflectarray layers and mask.

6.6.1 Etching the slot on the silicon

As it was mentioned before, the slots of identical size are etched on the silicon wafer. These slots act as phase shifters to change the phase distribution on the surface of the reflectarray. Since the phase variation is very sensitive to the shape of slots, any kind of distortion in the slot configuration can cause a large phase error in the reflectarray. To etch the slots on the silicon, the surface of silicon is coated first by a thin layer of good conductor material (in this reflectarray gold). The thickness of this metal layer is 2-3 times thicker than skin depth (the skin depth of gold at 30 GHz is 0.45 μm). Then, the pattern of slots is etched on the silicon [59].

Fig. (6-10) shows the printed slots on a 3" silicon wafer. The slot length is 3.5 mm. As can be seen in this figure there are some distortions on the edge of the slots as a result of

the fabrication error. Since these distortions are less than 10 micron, they will not generate considerable phase error.

6.6.2 Alignment

The optically controlled reflectarray presented in this chapter has three layers. For this antenna the slots has to be etched on the ground plane right beneath the patches. The effect of slot deviation in X and Y direction and also slot rotation were considered in chapter 3. During the fabrication of the reflectarray the alignment of the slots and patches are very crucial. Besides, since the slot length on the silicon is changed by the generation of the photoinduced plasma in the silicon and the pattern on this plasma profile is matched by the pattern on the photo-mask behind the reflectarray, it is very crucial to have a good alignment between the mask and reflectarray.

Two methods for the alignment of the reflectarray layers and also the mask with the reflectarray are presented in this research. In first method, 6 holes were drilled inside the all layers and the layers were aligned by passing the pins through these holes. An ultrasonic drill setup was utilized for drilling the holes inside the silicon. This machine is not accurate for drilling the fragile material like silicon and it entails an error of ±30 micron in drilling the hole inside the silicon wafer. This error causes a misalignment in the reflectarray layers. In the second method a few alignment markers as depicted in Fig (6-11) were etched on all the layers and then the layers were aligned by these alignment

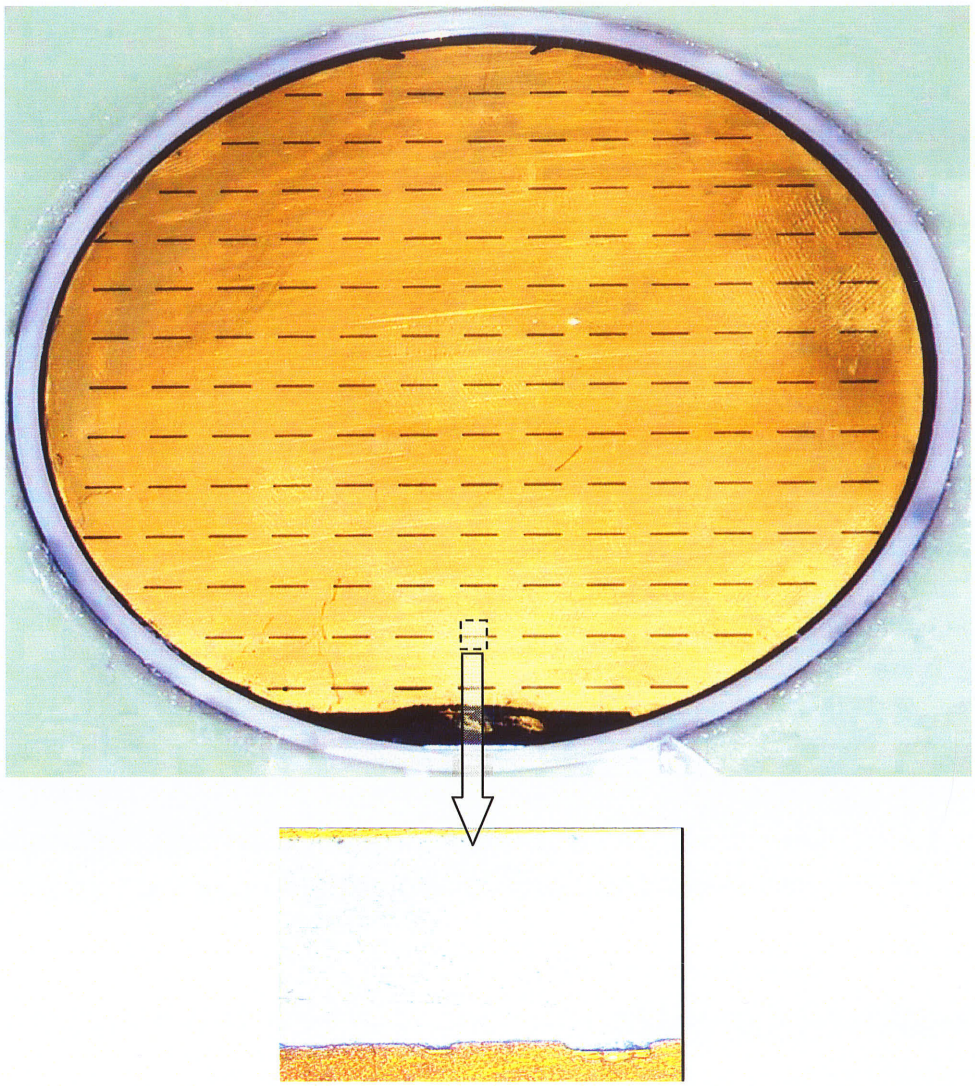

Figure 6-10: A view of the slots, etched on a 3" silicon wafer

Figure 6-11: A view of the alignment markers on the silicon

markers. A microscope was utilized to align the layers accurately. Same radiation patterns were achieved for the reflectarray antennas, fabricated with both alignment methods.

6.6.3 Indium Tin-Oxide (ITO) material

Indium doped with tin oxide (ITO) is used to make transparent conductive coatings [60], [60]. This material is used in applications, which require an electrically conductive coating that is highly transparent in the optical band. A thin layer of ITO is coated on glass substrates. Because of the low electrical resistance, the coating can be used to shield electromagnetic fields while transmitting the light. The optical and electronic properties of ITO films are highly dependent on the deposition parameters and the starting composition of evaporation material used. The deposited film layer must contain a high density of charge carriers in order to be conductive. High conductivity is balanced against high transmission in the visible and infrared region. Sheet resistance can be less than 10 Ohms/sq with a visible transmission power of >80%.

A layer of ITO was utilized as ground plane in the reflectarray antenna and the performance of the structure was compared to a similar reflectarray with PEC ground plane in order to characterize the ITO effect. The ITO was coated on a piece of glass with thickness of 0.5 mm. The thickness of ITO was 1 μm with the resistivity of 20 Ω/cm^2 in RF band and transmission of 80% at 900 nm. To consider the capability of this antenna a three-layer reflectarray with slot of varying length (c.f. Fig. (6-12)) was designed. The radiation pattern of this antenna was measured for two different cases. In first step a metal sheet was utilized as the ground and in the second trial the metal sheet

was removed and an ITO layer was used as the ground plane. The measured radiation patterns of both cases are shown in Fig. (6-13), which demonstrates 0.5 dB loss when ITO was used as the ground plane.

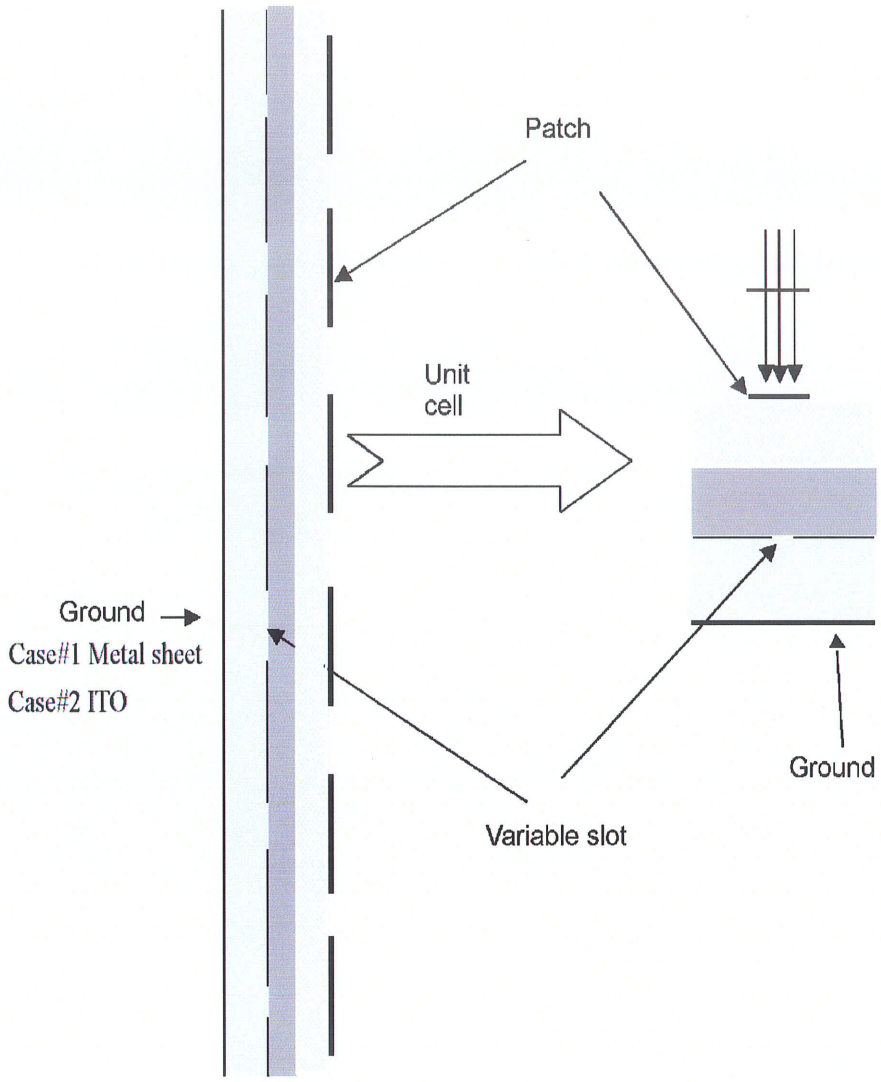

Figure 6-12: A three-layer reflectarray with slots of varying length size in middle layer. Case#1 metal plate for the ground plane, case #2: ITO for the ground plane

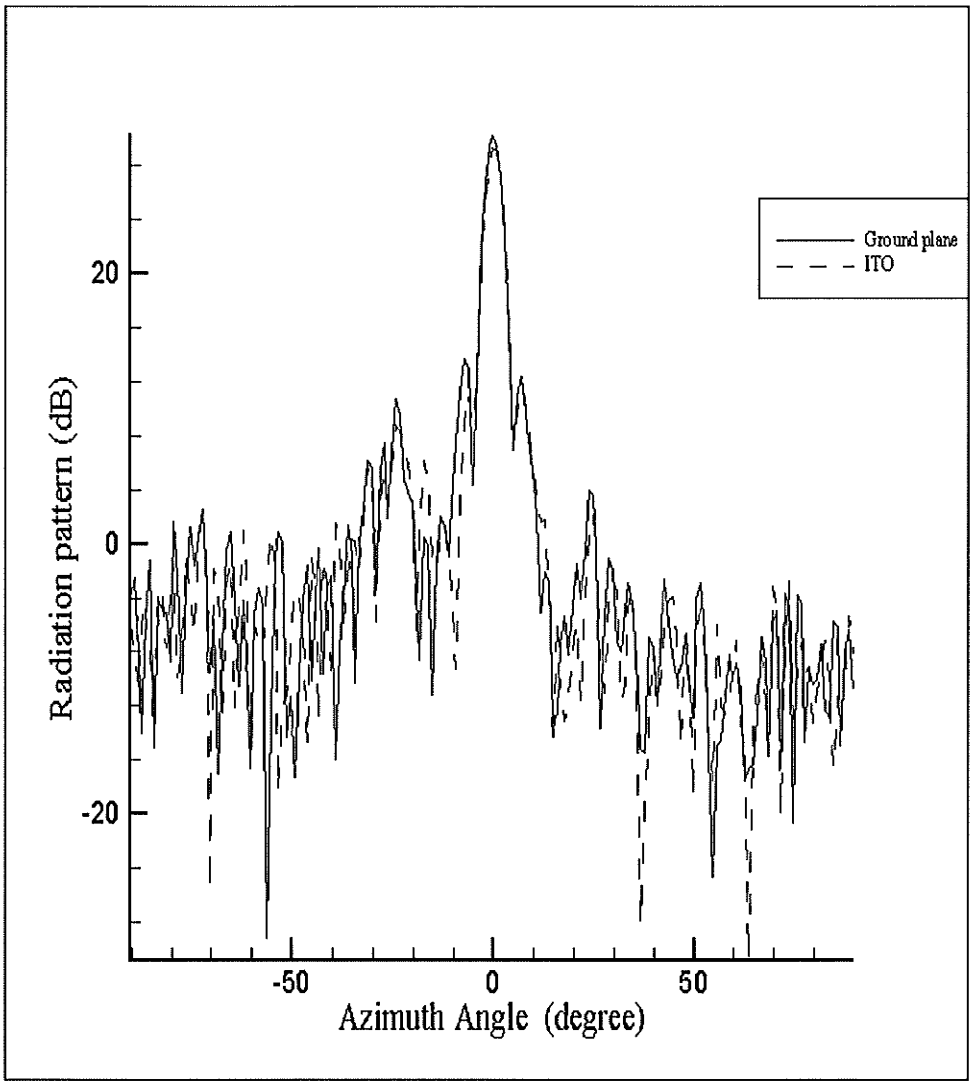

Figure 6-13: Radiation pattern of the reflectarray with metal plate and ITO as the ground plane

6.7 Conclusion

A novel photonically controlled reflectarray antenna was presented in this chapter. This technique is based on the variation of slot length beneath a regular lattice of identical patches by generating the photoinduced plasma inside the silicon. Two configurations based on single layer and multilayer structures were introduced.

An optically controlled three-layer reflectarray was fabricated. A measurement setup for the characterization of the radiation pattern of this antenna was described. This measurement setup has the capability to measure the radiation pattern of the reflectarray antenna when it is illuminated by an optical pulse excitation. The fabrication process of this antenna was presented and sources of phase error and loss were described and evaluated. The measured results show that the antenna can collimate the beam. However, more works is required to improve the efficiency and bandwidth of the antenna.

CHAPTER 7

CONCLUSION

7.1 Thesis summary

A novel photonically controlled method for beam scanning and beam shaping in reflectarray antenna based on slots of optically varying length size in ground plane was introduced. The slot length is controlled by generating the photoinduced plasma inside the silicon wafer. Some of the advantages of this method as compared to conventional methods such as photoinduced plasma grating (PIPG) methods [10]-[12] are as follow:

1) In PIPG methods the whole radiating grating structure is created by shining laser onto the semiconductor and due to the lossy nature of the photoinduced plasma the efficiency is degraded significantly. However, for the method presented in this thesis, the reflectarray partially exists, and the optical illumination of each cell is used to perturb or modify an existing conductive pattern. Therefore, the smaller area of the photoinduced plasma as compared to PIPG method is conducive to lower loss and higher efficiency. Also, smaller area of the photoinduced plasma implies lower optical power requirements.

2) The PIPG method is restricted to beam steering in one or two dimensions, whereas the proposed method is a viable candidate for beam shaping applications. The desired radiation pattern can be generated by modifying the slot lengths and changing the phase distribution on the surface of reflectarray.

3) The proposed configuration ensures isolation between optics and MMW by using the ITO as the ground plane of the reflectarray.

The optical-MMW interaction in high resistivity semiconductor substrate illuminated by an optical source was studied and presented in this thesis. This study was accomplished in two steps. First, the effect of the optical irradiation on such electrical properties as conductivity and permeability of the semiconductor wafer was investigated. A two-dimensional differential equation was utilized for the calculation of the carrier density of photoinduced plasma excited by the continuous wave optical illumination. The plasma profile inside the semiconductor that is exposed to optical illumination was considered and a model based on the uniform plasma profile was introduced for analyzing the photoinduced plasma structure. Two methods for the simulation of the photoinduced plasma structures were introduced in the second stage. These methods were utilized to analyze 2-D and 3-D photoinduced plasma structures. Ansoft HFSS was utilized for the simulation of 3-D structures, to obtain the plasma profile and plasma permittivity that were discussed in the first step. Second method is based on the application of the method of moment to the analysis of 2-D structures. The execution time of the 2-D software is much shorter as compared to the 3-D code but the 3-D calculations are more accurate. The simulation results were compared to measurement in waveguide setup in order to validate the code and to find a relationship between the carrier densities employed in the simulation and optical power in the measurement. It was concluded that for the carrier densities in excess of 10^{17} (cm^{-3}), the photoinduced plasma behaves almost as a perfect conductor.

Two novels photonically controlled reflectarray with single and multi-layers configurations were simulated, fabricated and tested. The simulation results show the single layer configuration suffers from some drawbacks such as high loss and low isolation between the optical source and RF signal.

An optically controlled three-layer reflectarray was designed and fabricated. This reflectarray has better phase variation and RF and optics isolation in comparison to the single layer reflectarray (see Fig. 6-4). The measurement setup for the measurement of the radiation pattern of this antenna was described. This measurement setup has the capability of measuring the radiation pattern of the reflectarray antenna as it is illuminated by an optical pulse excitation. The fabrication process of this antenna was presented and the sources of phase error and loss in the efficiency were studied. The measurement result shows that the antenna has the capability of collimating the beam. However, more works is required to improve the efficiency and bandwidth of the antenna.

7.2 Directions for future research

An optical pulse source has been utilized for the generation of photoinduced plasma inside the silicon wafer of the optically controlled reflectarray antenna presented in this dissertation. As it was shown in chapter 6 the reflectarray can collimate the beam only during the optical excitation and the reflectarray can not collimate the beam in the absence of the optical pulse. To use this reflectarray as an antenna, a continuous wave optical excitation should be used to generate a time independent plasma profile inside the silicon and generate a desired radiation pattern. Several different continuous wave optical source can be used as an alternative optical source for this antenna. LED array, halogen

lamp, continuous wave Xenon lamp and laser diodes are some of the sources that can be studied as the optical source for this antenna. Note the maximum absorption coefficient of silicon, around 900 nm, sets a criterion for the selection of the optical source.

The reflectarray that was described in this dissertation can be used to collimate the beam in the desire angle by changing the pattern of the photoinduced plasma inside the silicon. In the prototype presented in this dissertation the pattern on the photoinduced plasma can be controlled by using a glass mask beneath the reflectarray. The pattern of glass mask can not be changed dynamically. Further research is required as to the alternatives for the dynamic variation of the pattern of photoinduced plasma. Using an addressable optical mask is one possibility. Spatial light modulator (SLM) is a method to accomplish this objective. These devices can be addressed optically or electronically. Using an LED array or optical fibers illuminated with a laser diode to control the array elements by changing the status of elements (ON/OFF) are other alternatives for the dynamic control of the pattern of photoinduced plasma inside the semiconductor.

The efficiency of this reflectarray is fairly low. Various possibilities to raise the efficiency have been listed below:

1) As noted before, the loss inside the silicon decreases the antenna efficiency. This loss has an inverse relationship with carrier density of plasma. The carrier density is a function of optical characteristics of semiconductor such as carrier lifetime, carrier recombination velocity and absorption coefficient. One way to increase the efficiency is changing these characteristics to get higher carrier densities or use semiconductor materials that are better suited to the generation higher carrier density of

photoinduced plasma. Cadmium sulfide is an alternative to silicon that can be studied in the future.

2) Increasing the optical power is another way to increase the carrier density. The size of a high gain reflectarray antenna is usually large and to shine the surface of the reflectarray a high power optical source is required which might be infeasible in most cases. Decreasing the size of reflectarray and therefore increasing the optical power density is one way to overcome this problem. A method to achieve this goal is using the optically controlled reflectarray as a sub-reflector for another reflectarray or reflector. By changing the phase distribution of the sub-reflector through optical illumination, the phase distribution on the surface of the main reflectarray or reflector can be controlled. Since the size of the sub-reflector can be rather small, higher power density and efficiency can be achieved for this configuration.

3) Two technologies have been used in the past to excite plasma inside the semiconductor: photo-injection and injection through electrode [62]. In this dissertation the first technique was utilized to generate the photoinduced plasma inside the silicon. The other method uses carrier injection via electrodes to generate excess carrier density. This method is based on using lateral p-i-n devices as conductive radiating elements. These p-i-n devices act as plasma islands when injected by carriers (DC voltage). This innovative plasma concept can be used in the reflectarray presented in this dissertation to change the slot size by designing the p-i-n devices inside the silicon beneath the slot with identical size. This method has the potential of being more compact, with lower power requirements, lower cost, and fully compatible with MMIC processing.

REFERENCES

1) Daryoush, K. Bontzos and P. Herczfeld, " Optically tuned patch antenna for phase array application, "IEEE. AP-S International symposium Digest, 1986. Philadelphia, PA, pp. 361-364.

2) D.A. Cohen, Y. Chang, A.F.J. Levi, H. R. Fetterman, "Optically Controlled Serially Fed Phased array sensor," IEEE. Photonics technology letters, Vol. 8, No. 12, Dec. 1996. pp. 1683-1685.

4) M. Y. Frankel, and R.D. Esman, "Reconfigurable time-steered array-antenna beam former," Appl. Optics, Vol. 36, pp. 9261-9268, 1997.

4) Vilf F., Manasson V., Sadovnic L., " Beam-steering control plasma-grating antennas," SPIE Vol. 3795, July 1999, pp. 441-445.

5) Manasson V., Sadovnic L., Shnister PI., Mino R., " MMW optically scanning antenna based on plasma-induced grating," SPIE Vol. 2532, pp. 290-299.

6) G. F. Brand, " Remote Millimeter-Wave Beam Control by the Illumination of a Semiconductor," IEEE. Trans. on Microwave Theory and Techniques, Vol. 48, No. 5, May 2000, pp. 855-857.

7) G. W. Webb, W. Vernon, M. S. Sanchez, S. C. Rose, S. Angello , "Optically Controlled Millimeter Wave Antenna," Microwave Photonics, 1999. MWP 99, pp. 275- 278.

8) G. W. Webb, W. Vernon, M. S. Sanchez, S. C. Rose , "Novel Photonically Controlled Antenna for MMW Communications," Microwave Photonics, 2000 MWP 2000, pp. 97- 100.

9) D. Liu, D. Charett, M. Bergeron, H. Karwacki, S. Adam, B. Lanning and F. Kustas, " Structurally embedded photoconductive silicon bowtie antenna," IEEE. Photonics Tech. Lett., Vol. 10, No. 5, May 1998, pp.716-718

10) A. Alphones, M. Tsutsuni, " Leaky wave radiation of millimeter wave by photoinduced plasma grating in semiconductor slab," IEE. Proc. Microwave Antennas Propag. Vol. 146, No. 1, Feb. 1999. pp. 77- 83.

11) V. Manasson, L. Sadovnik V.A. Yepishin and D. Marker, " An optically controlled MMW beam-steering antenna based on a novel architecture," IEEE. Trans on Microwave theory and Tech., Vol. 45, No. 8, Aug. 1997, pp. 1497- 1450.

12) A. Alphones and M. Tsutsumi, " Leaky wave radiation from a periodically photoinduced semiconductor slab waveguide," IEEE Trans. on Microwave Theory and tech. Vol. 43, No. 9, Sep. 1995, pp. 2435-2441.

13) V.A. Manason, V.A. Yepishin, D. Eliyahu, L.S. Sadovnik, V. Rubstov, " Photoinduced plasma grating technology for X-and W-band beam steering antennas," Proceeding of SPIE, Vol. 4042 (2000) pp. 156-159.

14) V.A. Manason, L. S. Sadovnik and V.A. Yepishin, " New architectures of light controlled MMW steering antennas," SPIE Vol. 3160, pp. 80-88.

15) V.A. Manasson, L.S. Sadovik, P.I. Shniter,R. Mino, "Millimeter-wave optically scanning antenna based on photoinduced plasma grating ," Optical Engineering, Vol. 35, Feb. 1996, pp. 357-361.

16) G. F. Brand, " Diffraction of millimeter waves by projecting a shadow pattern onto a semiconductor," International Journal of Infrared and Millimeter Wave, Vol. 17, No. 7, 1996, pp. 1253-1262.

17) K. Nishimura, M. Tsutsumi, " Scattering of millimeter waves by metallic strip gratings on an optically plasma-induced semiconductor slab," IEEE Trans. on Microwave Theory and Tech., Vol. 44, Vol. 44, No. 12, Dec. 1996.

18) R.N. Edward and W.C. Nunnally, "Investigation of photoconductive silicon as a reconfigurable antenna," SPIE, Vol. 1918 Smart sensing, Processing, and instrumentation (1993), pp. 344-352.

19) M.R. Chaharmir, J. Shaker, M. Cuaci , A. Sebak, " Novel photonically controlled reflectarray antenna for beam-steering in MMW application" , US patent filing is in process.

20) D.G. Berry, R.G. Malech, and W.A. Kennedy, " The Reflectarray antenna," IEEE. Trans. Antennas Propagat., Vol. AP-11, pp. 655-651, Nov. 1963.

21) R.W. Munson, H. Haddad, and J. Hanlen, "Microstrip reflectarray antenna for satellite communication and RCS enhancement," US patent 4684952, Aug. 1987.

22) J.C. Vardaxoglou, " Frequency selective surfaces," John Wiley & sons Inc. 1997.

23) J. P. Montgomery, " Scattering by an infinite periodic array on thin conductors on a dielectric sheet," IEEE. Trans. Antennas Propagat., Vol. 23, No. 1, Jan1975, pp. 70-75.

24) J. Jin and J. Volakis, " Electromagnetic scattering by a perfectly conducting patch array on a dielectric slab," IEEE. Trans. Antennas Propagat. Vol. 38, No. 4, Apr. 1990, pp. 556-563.

25) R. Mittra, C.H. Chan, T. Cwik, " Techniques for analyzing frequency selective surface- A review," Proc. Of IEEE, Vol. 76, No. 12, Dec. 1988.

26) D.M. Pozar," Finite phase array of rectangular microstrip patches," IEEE. Trans. Antenna propagat., Vol. 34, pp. 658-665, 1987.

27) A. Ishimaru, R. Coe, G. Miller and P. Geren, " Finite periodic structure approach to large scanning array problems," IEEE. Trans. Antennas Propagat., Vol 33, pp. 1213-1220, 1985.

28) A. H. Tsao and R. Mittra, " Spectral-domain analysis of frequency selective surfaces comprised of periodic arrays of cross dipoles and Jerusalem crosses," IEEE. Trans. Antennas Propagat., Vol. AP32, No. 5, pp. 478-486, May 1984.

29) R. Mittra, R. C. Hall, C. H. Tsao, " Spectral-domain analysis of circular patch frequency selective surfaces," IEEE. Trans. Antennas Propagat., Vol. Ap32, No. 5, pp. 533-536, May 1984.

30) J. Bayard and D. Schaubert, "Finite difference solution of infinite arrays of two dimensional microstrip structures," Computer Physics Communication, No. 68 (1991) pp. 366-392.

31) Taflove, " Advances in computational electromagnetics. The finite-difference time-domain method," Artech House Inc. 1998.

32) A S. H. Lou, L. Tsang, C. H. Chan, A. Ishimaru, " Application of the finite element method to Monte Carlo simulation of scattering of waves by random rough surfaces

with the periodic boundary condition," Electromag. Waves Appl., 1991, 5, pp. 835-885.

33) G. Pelosi, A. Freni, R. Coccioli, "Hybrid technique for analyzing scattering from periodic structures," IEE. Proceeding-H, Vol. 140, No. 2, pp.65-70, April 1993.

34) N. C. Karmakar and M. E. Bialowski, " A modal expansion method analysis for rectangular electromagnetically coupled microstrip patch antennas in waveguides," Proc. Asia-Pacific Microwave Conference, Taiwan, R.O.C. 18-21 Oct. 1993.

35) Ansoft HFSS™, The 3D, electromagnetic, finite-element simulation tools for high-frequency design, http://www.ansoft.com.

36) J. 36. J. Huang, "Microstrip Reflectarray ," IEEE AP-S/URSI symposium, London, Ontario, Canada, pp. 612-615, June 1991.

37) J. Huang, "The finite ground plane effect on microstrip antenna radiation patterns", IEEE. Trans. on Antenna and Prop. Vol. AP-31, July 1983, pp. 649-653.

38) Reference 38- A.G. Derneryd, " Linearly polarized microstrip antennas," IEEE. Trans. Antennas Propagat. , Vol. AP-24, No. 6, pp. 846-850, Nov. 1976.

39) F.J. Harackiewicz, " Electromagnetic radiation and scattering from microstrip antennas on anisotropic substrates," Ph.D. thesis, Univ. Massachusetts, Amherst, 1990.

40) R.D. Javor, X.D. Wu and K. Chang, " Design and Performance of a Microstrip Reflectarray Antenna," IEEE Trans. Antennas Propagat., Vol. 43, No. 9, Sep. 1995, pp. 932-939.

41) D.M. Pozar and T.A. Metzler, "Analysis of reflectarray antenna using microstrip patches of variable size", Elec. Letters 15th Apr. 1993, Vol.29, No. 8, pp. 657-658.

42) J. Huang, R.J. Pogorzelski, " A Ka-band Microstrip Reflectarray with Elements Having Variable Rotation Angles," IEEE Trans. Of Antennas Propagat., Vol. 46, No. 5, May 1998 pp 650-656.

43) M.G. Keller, M. Cuhaci, J. Shaker, A. Petosa, A. Ittipiboon, Y.M.M. Antar, "Investigation of Novel Reflectarray Configurations," ANTEM 2000, pp.299-302.

44) M.R. Chaharmir, J. Shaker, M. Cuhaci, A. Sebak , "Reflectarray with variable slots on ground plane," Received acceptance to publish in IEE proceeding of microwave, antenna and propagat.

45) M.R. Chaharmir, J. Shaker, M. Cuhaci, A. Sebak, "Novel mechanically controlled reflectarray antenna for beam switching and beam shaping in millimeter wave applications", Electronics Letters 3rd April 2003, Vol.39, No. 7, pp. 591-592

46) Dieter K. Schroder, " Semiconductor Material and Device Characterization", New York: Wiley, 1998.

47) G. Streetman, Sanjay Banerjee, "Solid state Electronic Devices", Fifth, edition,1998.

48) G. Duggan and G.B. Scott, " The efficiency of photoluminescence of thin epitaxial semiconductors," J. Applied Phys. 52, 407-411, Jan. 1981.

49) Platte, W., " Spectral dependence of microwave power transmission in laser-controlled solid state microstrip switches," IEE. Proc. I, 1978,2,(4),pp. 97-103.

50) M.R. Chaharmir, J. shaker, M. Cuhaci, A. Sebak, "Analysis of plasma profile in a semiconductor under quasi-CW laser illumination for application in millimeter wave band antennas", IEEE CCECE02 Vol. 1, pp. 333-335.

51) W. Platte, "Effective photoconductivity and plasma depth in optically quasi-CW controlled microwave switching device", IEE. Proceedings, Vol. 135, Pt. J, No. 3, June 1988.

52) Lee, C.H." Picosecond Opto-electronic device," (Academic Press, London, 1984).

53) J. M. Borrego, R. J. Gutmann, N. Jenes, " Non- destructive lifetime measurement in silicon wafer by microwave reflection", Solid-state electronics, Vol. 30, No. 2, pp. 195-203, 1987.

54) M.R. Chaharmir, J. Shaker, M. Cuhaci, A. Sebak, "Application of waveguide technology for calculating the profile of photoinduced plasma," ICEAA03, Torino, Italy, Sep. 8-12, 2003, pp.21-24.

55) Platte, W., "Spectral dependence of microwave power transmission in laser-controlled solid state microstrip switches", Solid-State and Electron Devices, July, 1978,2,(4), pp. 97-103.

56) J.C. Vardaxoglou, P. K. Lau, and M. J. Kearney, " Frequency selective surface from optically excited semiconductor on a substrate," Electron. Lett., Vol. 34, pp. 570-571, 1998.

57) EMPiCASSO, EMAG Technologies Inc., http://www.emagtechnologies.com.

58) 3 Inch collimated output Flash Photolysis System, Cairn Research Limited, http://www.cairnweb.com

59) D.R. Raguin, " Subwavelength structured surfaces: theory and applications," Ph.D. dissertation, University of Rochester, 1993.

60) V. Cracium, D. Cracium, C. Chen, J. Hwang, R.K. Singh, " Room temperature growth tin oxide film by ultraviolet-assisted pulsed laser deposition," Mat. Res. Soc. Symp. Vol. 617 © 2000 Material Research Society.

61) X.W. Sun, H.C. Huang and H.S. Kwok, " On the initial growth of indium tin oxide on glass," © 1996, American Institute of physics, pp. 2663-2665.

62) Aly E. Fathy, A.R. Rosen, H.S. Owen, F.McGinty, D.J. McGee, G.C. Taylor, R. Amantea, P.K. Swain, S.M. Perlow, M. ElSherbiny, " Silicon-Based Reconfigurable Antenna-Concept, analysis, Implementation, and Feasibility." IEEE. Trans. on Microwave Theory and Technology, vol. 51, No. 6, June 2003.